An Integrated Sediment Budget for the Le Sueur River Basin

Final Report
June 2011

With primary contributions from

Karen Gran[1,2], Patrick Belmont[1,3], Stephanie Day[1,4], Carrie Jennings[4,7], J. Wesley Lauer[5], Enrica Viparelli[1,8], Peter Wilcock[1,9], Gary Parker[1,8]

[1]*National Center for Earth-surface Dynamics*
[2]*University of Minnesota, Duluth*
[3]*Utah State University*
[4]*University of Minnesota*
[5]*Seattle University*
[6]*University of California, Santa Cruz*
[7]*Minnesota Geological Survey*
[8]*University of Illinois, Urbana-Champaign*
[9]*Johns Hopkins University*
[10]*Minnesota State University, Mankato*
[11]*Florida International University*

and additional assistance from

Luam Azmera[11], Caitlyn Etcherling[5], Noah Finnegan[1,6],Andrea Johnson[2], Fukhrudin Khalif Maalim[11], Scott Matteson[10], Assefa Melesse[11], Tammy Rittenour[3], Ashley Thomas[11], Barbara Utley[1,3]

Table of Contents

Executive Summary

This is the final report of a four-year project intended to develop a sediment budget for the Le Sueur River watershed in southern Minnesota. Primary funding for the work was provided by the Minnesota Pollution Control Agency (MPCA) with additional funding from the National Center for Earth-surface Dynamics, a Science and Technology Center funded by the National Science Foundation and housed at the St. Anthony Falls Laboratory of the University of Minnesota. The motivation for the work arises from the need to address elevated levels of suspended solids in the Minnesota River and related water quality problems and infilling of Lake Pepin on the Mississippi River, although this research project focuses specifically on sediment in the Le Sueur River watershed. A recent summary of the sedimentation and turbidity issues in the Minnesota River Basin is provided by Wilcock (2009), available from the MPCA.

The Le Sueur watershed is large (2,880 km^2) and a prolific source of sediment. Sediment is produced via a large variety of different mechanisms whose rates vary broadly across both time and space. To develop reliability in our estimates of erosion, we rely on multiple methods and work to corroborate different, independent lines of evidence. A powerful tool for constraining our understanding of many, varied sources is a sediment budget. This is a mass balance in which the difference between inputs and outputs must equal any changes in storage. In general, we try to bring as many lines of evidence together as possible – in effect, closing the budget for any time-period or watershed scale for which sediment information is available. The evidence varies from the very large scale (e.g. evacuation of sediment from the Le Sueur watershed over the last 13,400 years) to much smaller scales (e.g. the increase in sediment loading over a storm between two gauges along a stream).

This report documents the different methods used to understand and constrain sediment from all significant sources. We begin with the geologic setting and geomorphic history of the Le Sueur River (Chapter 1) and then discuss how sediment sources in the Le Sueur River watershed have changed since the initial carving of the Minnesota River valley (Chapter 2). This deep time perspective helps to understand pre-settlement erosion rates in the Le Sueur River watershed, thereby providing an estimate of background conditions prior to agricultural development. A brief overview of sediment gauging records in the area is covered in Chapter 3. Section II covers the sediment budget in detail, first through an overview, and then with each individual sediment source covered in its own chapter (uplands (4), ravines (5), bluffs (6), and floodplains (7)). The budget is followed by a discussion of a morphodynamic sediment routing model (Section III), which was developed to better understand how changes in input conditions affect the geomorphic response of the system.

Summary of Findings

The Le Sueur River watershed is geologically primed to produce large amounts of sediment as the river, a tributary of the Minnesota River, incises through glacial tills in response to the initial carving of the Minnesota River valley over 13,000 years before present. This event established the template on which modern land use activity and climate occur, causing a steep, deeply-incised valley near the mouth of the river in an otherwise low-gradient landscape. Even before settlement and land-use conversion, this incised reach, comprising ~40 km along each of the three main branches of the Le Sueur River, was a large contributor of suspended sediment to the mainstem Minnesota River. Using constraints on the timing of incision, high-resolution

topography, dating of river terraces, and numerical modeling of river incision and valley excavation, we have determined that long-term valley excavation before the time of European settlement contributed 50,000 Mg/yr of fine-grained sediment to the mouth of the Le Sueur River. An additional 10,000 Mg/yr came from ravine excavation, with minimal sediment derived from the low-gradient uplands.

The nearly complete transformation of the land surface, vegetation, and hydrology over the past two centuries has increased these already large sediment loadings by a factor of four to five. The average total suspended solids (TSS) load at the mouth of the Le Sueur River during the monitoring season from 2000-2010 was 225,000 Mg/yr (WRC and MPCA, 2009; MPCA, unpublished data), which is 4 to 5 times higher than the amount estimated from pre-settlement valley excavation. The increased delivery of water, sediment, and nutrients to the Minnesota River from the Le Sueur and nearby watersheds now represents an important water quality problem that the State of Minnesota is addressing.

Using multiple lines of evidence, we have demonstrated that, under current conditions, the largest sediment sources remain near-channel sources (erosion of bluffs and channel widening and incision) within the incised portion of "knick zone" of the Le Sueur watershed. Current erosion from bluffs is producing the majority of the fine-grained sediment. Net contributions from the channel and floodplain adds an additional 8%, with most of that sediment coming from channel widening. The other main sources of sediment, ravines and uplands, contribute approximately 9% and 27% of the annual sediment load on average in the modern time period (2000-2010) (Figure ES.1). These values will fluctuate from year to year given annual hydrologic conditions and represent average annual contributions as percentages of sediment at the mouth of the Le Sueur River.

These rates have changed through time. As mentioned above, valley excavation accounted for 50,000 Mg/yr of fine-grained sediment to the Le Sueur River. This can be compared with modern bluff and channel erosion, now estimated to be 152,000 Mg/yr. Ravines contributed 10,000 Mg/yr, with modern rates estimated at 20,000 mg/yr. Although agricultural uplands account for only one quarter of the suspended sediment currently exported from the Le Sueur watershed, upland sediment represents the source which has experienced the largest percentage increase in erosion rates and is the dominant source above the incised reach.

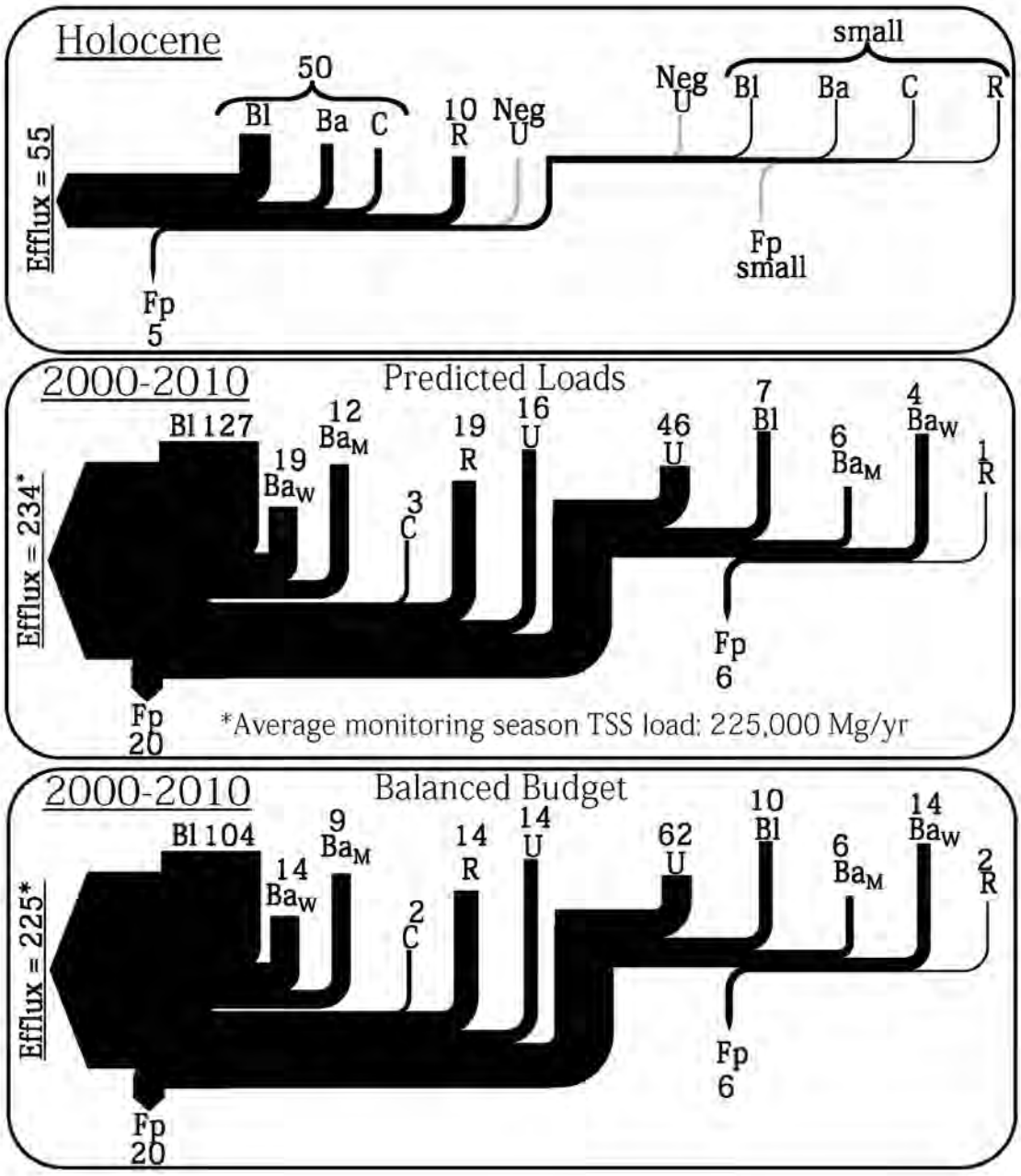

Figure ES-1: Predicted average annual fine sediment loads (silt and clay), by source, for two time periods: the Holocene (top), which represents pre-settlement conditions, and 2000-2010 (middle). Sources are calculated separately above and below the knick point on all three channels (combined here). This budget is compared with average TSS loads for the monitoring season from 2000-2010. (Bl=Bluffs; R=Ravines; U=Uplands; C=Channel incision; Ba_M=Bank contributions from meandering; Ba_W=Bank contributions from widening; Fp=Floodplain deposition). At the bottom, the budget has been balanced, so that inputs and outputs match both at the upper gauges and at the Red Jacket gauge near the mouth of the Le Sueur.

Bluff retreat rates were determined over decadal time scales using repeat aerial photography and over annual time scales using ground-based terrestrial LiDAR (Light Detection and Ranging) technology. Airborne lidar data were used to map the extent and area of bluffs adjacent to active channels, thus turning retreat rates into erosion volumes. Multiple methods were used to up-scale measurements to cover all bluffs within the watershed in order to derive a total mass of sediment associated with bluff retreat in the entire watershed. Ravine erosion rates were determined from direct monitoring of four ravines in the lower Le Sueur watershed for up to three years. Resulting loads were up-scaled to the entire watershed using airborne lidar data and compared with loads on the mainstem Le Sueur to determine percent contributions. Upland yields were calculated as a percent of the sediment arriving at stream gauges above the knick zone as determined from sediment fingerprinting using meteoric ^{10}Be and ^{210}Pb isotopic tracers. Channel contributions were calculated as a combined sum including cutbank erosion, floodplain deposition, channel incision, and channel widening.

The sediment budget is organized spatially, with separate budgets compiled at each of two gauges on the Maple River, the Big and Little Cobb Rivers, and the Le Sueur River. The upper gauges give a measure of the volume of sediment leaving the vast area of watershed above the knick zone, and the comparison between the upper and lower gauges give a measure of the increase in sediment loading as the river passes through the high-relief knick zone. Figure ES.1 summarizes the changes in sediment sources as the river moves through the knick zone, showing the vast increases in near-channel sediment sources as the river flows downstream. In addition, the modern budget is compared to the pre-settlement budget, showing increases in all sources over pre-settlement conditions. More details on individual elements of the sediment budget, including uncertainties associated with each element of the budget, are given in Section II.

Figure ES.1 includes both the predicted budgets for the Holocene and the modern budget (2000-2010). At the bottom the modern budget has been balanced so that inputs and outputs match at both the upper gauges and at the Red Jacket gauge near the mouth of the Le Sueur River. This balancing was done by raising or lowering all sediment inputs by a set percentage of their uncertainty above and below the upper gauges. The process of balancing the budget is described more in Section II. It is worth noting that the initial, unbalanced budget actually does a very good job of predicting the sediment loads at Red Jacket, within 5% of the average annual load for the decade, but it underestimates sediment loads at the upper gauges.

Because of the geologic history and setting, the near-channel areas are vulnerable to accelerated erosion, and hydrologic changes in the upper watershed have had large impacts on sediment loading. Any further increases in intense rainfall events over the next century in the upper Midwest are likely to further accelerate sediment supply through hydrologic amplification of naturally-sensitive channel reaches.

Management Implications

In order to define management actions to reduce sediment loading, it is necessary to identify the location and rates of erosion, as well as the erosion mechanisms and their controls. Our work provides information to help identify the location and magnitude of sediment sources within the Le Sueur watershed and indicates that a combination of hydrologic and sediment measures need to be considered in reducing nonpoint sediment loading.

Effective management will require a combination of actions to reduce erosion at its source and more effectively control the physical drivers of erosion, requiring management of peak flows. If only sediment sources are addressed, management actions will risk addressing the symptom but not a dominant causal factor. As high flows in the river are the underlying, systemic driver of near-channel erosion, increased water retention in uplands will reduce sediment loads over the long-term and can help mitigate on-going and future changes in precipitation. In key locations, vulnerable areas along the mainstem channels should have stronger protections, in terms of setbacks, mechanical armoring, limiting direct discharge from tile lines or pipes, or ensuring adequate buffers. The contribution of ravines to the total sediment loading is smaller than bluffs due to their much smaller spatial extent. Nonetheless, some ravines can deliver sediment to the river channel at very large rates, and these sediment hot-spots can represent good initial management opportunities for sediment reduction.

Future Information Needs

Improved Methods for Identifying Local Sediment Hot Spots

Although the dominance of sediment loading from bluff and ravine erosion in the knick zone has been demonstrated, management actions require specific identification of sites for prioritized action. Which bluffs produce the most sediment? Which ravines are hotspots? Air photo analysis has identified bluffs that have eroded rapidly over the past 60 years, although this is not a guarantee that these bluffs will continue to erode at a high rate in the future (the large erosion observed over decades may result from one or two large events). Further analysis is needed to indicate the combination of bluff composition, geometry, and aspect that are most likely to produce large erosion rates in the future as well as the hydrologic (seepage and undercutting) and thermal (freeze-thaw) conditions that accelerate bluff failure.

Although their limited aerial extent means that the cumulative sediment loading from ravines is much smaller than bluffs, individual ravines can produce large sediment supplies. Hence, some ravines can provide good candidates for management action. Active ravines can be identified by a sequence of terraces, indicating episodic periods of filling and cutting. A period of filling stores sediment and reduces sediment delivery to the river. A period of cutting evacuates stored sediment and accelerates delivery of sediment to the river network. Ravines that are in the process of reconnecting to the main stem river through incision across a terrace have the highest potential of producing abundant sediment in the near future.

Identification of bluffs and ravines subject to accelerated sediment supply can be usefully presented in terms of erosion hazard maps. These would combine historical erosion rates, bluff geometry, and erosion potential in a highly valuable resource for local planners and for prioritizing erosion mitigation. Such maps could be used by county and township officials to restrict practices (farming; tile discharge; home, bridge and road construction) in those locations.

Extrapolating sediment budget results to other Minnesota River Basin subwatersheds

We have developed a sediment budget for the Le Sueur watershed, one of the most prolific sources of sediment in the Minnesota River Basin (MRB). Many methods and results from this study are likely transferrable to similar watersheds (especially the Blue Earth) along the Minnesota River, but verification of this extrapolation is needed. Verification would entail

measurement of the extent of river channel, ravines, and bluffs and comparison of computed loads against observations using gauging and sediment fingerprinting. Once verified, it will be possible to develop a sediment simulation model for the Greater Blue Earth system (Blue Earth, Watonwan, Le Sueur) that responds to changes in land use, climate, and conservation/restoration practices.

The mix of erosion mechanisms and rates will differ in other subwatersheds with less severe incision and fewer bluffs and ravines. The existing work supports development of sediment hypotheses that can be tested in other watersheds. The new state-wide lidar dataset currently in progress will make the necessary topographic analysis especially tractable.

Predicting hydrologic change and its effect on sediment supply

Multiple factors have acted to increase river discharge and erosion of near-channel sediment sources. An extensive tile and ditch network has increased connectivity between uplands and the channel network, effectively increasing both the drainage area and the efficiency of drainage. In addition, mean precipitation has increased in Minnesota, along with an increase in the frequency and magnitude of extreme events, exacerbating these land use-driven hydrologic alterations.

The long-term geomorphic effect of increased runoff has been and will continue to be larger stream channels and more rapid stream channel migration. Both processes increase sediment supply. Over a period of decades, channel enlargement in response to an increase in runoff may be self-limiting; the channels gradually adjust their size to a regime of larger floods. The extent of channel enlargement and the period of adjustment currently are not known. Increases in stream channel migration rate may also produce increased sediment supply from bluffs and ravines in the knick zones of MRB tributaries. Given the large size of the drainage network and erodible glacial material in the deeply incised valley walls (bluffs) of the tributary knick zones, this represents a potentially enormous amount of sediment. Controlling peak discharges in the river networks is imperative.

Better information is needed to identify the relative roles of changing land use and drainage patterns vs. changing climate in controlling water runoff and sediment delivery from bluffs and ravines. An effective first step in evaluating the effect of changed drainage on sediment yield is to develop a reliable estimate of pre-settlement hydrology. We have developed good evidence of pre-settlement sediment sources and yields. By combining this information with the hydrology of the past 150 years, we will have a stronger basis for forecasting future changes and for testing management alternatives for controlling peak flows.

The role of tile and ditch drainage in changing stream hydrology and the erosive potential of Minnesota River tributaries must be studied further. Debate continues regarding the effects of tile drainage on high flows in the spring, summer, and fall. While tile drainage inevitably increases the rate at which water is conveyed to the channel, the magnitude of this effect on peak and total runoff is poorly understood in large watersheds. Furthermore, accelerated drainage of the uplands reduces soil moisture and therefore increases infiltration capacity in the upper soil horizons, which likely reduces highly erosive surface runoff. In this way, the drain tiles likely have a beneficial influence in reducing upland erosion.

The hydrology used in our modeling is based primarily on the MPCA HSPF model and represents existing conditions. For these conditions, we see similar flow-duration relationships across a range of drainage areas within the Le Sueur basin. We know that discharge on the

Minnesota River at Mankato has increased since the end of the 19th century. However, we do not know if a similar increase is observed on smaller channels higher in the watershed. Because changes in the sediment budget appear to be driven by increased runoff, it would be helpful to develop a rainfall-runoff model that accounts for changes in the surface and sub-surface drainage network, vegetation type, as well as changes in precipitation frequency and magnitude everywhere in the basin. Such a model is necessary to appropriately represent historic spatial and temporal variability. On-going work analyzing changes in runoff ratios is a good start in this direction.

Management actions to control peak flows will require a means to store water in the low-gradient headwaters of the basin. Efforts to restore wetlands and lakes will be needed. This work can be supported by the development of maps for natural water-storage potential, indicating favorable locations for surface storage in closed depressions (or formerly closed depressions).

Monitoring

Management actions to reduce sediment loading will be expensive. Given the large number of sediment sources and the episodic and contingent nature of erosion, documenting success in reducing erosion will not be simple. In order to implement a successful, adaptable management program, it is essential that monitoring be developed that documents not only management actions, but system response. Two monitoring techniques provide good reliability at reasonable cost.

Stream gauging provides the most direct and reliable evidence of erosion rates from a watershed. Although gauging requires effort and expense, much of what we know about sediment sources in the MRB comes from stream gauging. Of particular value are streams with a gauge located above and below the tributary knick zones. Comparison of the loads at the upstream and downstream gauges helps differentiate between sediment delivered from the vast uplands versus near-channel sources in the knick zone and also allows us to track the sensitivity of near-channel sources to future changes in hydrology.

A suite of sediment fingerprinting methods (^{10}Be, ^{210}Pb, and ^{137}Cs) have been demonstrated to provide a robust monitoring tool that very effectively supplements stream gauging. It is important to collect fingerprinting samples within a nested, synchronous scheme that allows the source apportionment to distinguish source location (upland vs. incised knick zone) and seasonality (spring vs. fall). The power of interpretation increases significantly when all three tracers are measured, as described in Chapter 4.

Gauging provides a direct measure of sediment load. Fingerprinting provides an estimate of the proportion coming from upland fields. Gauges and fingerprint samples located above and below the knick zones measure the sediment increase from predominantly bluffs and ravines. Combining this information, a monitoring program can provide reliable, corroborating evidence of the system response to management actions.

Implementation Strategy

Implementation of a successful sediment-reduction strategy will require collaboration among a large and diverse group of stakeholders. Although the available information is improving rapidly, it will never be perfect. Identification, funding, and implementation of

management strategies will require a decision analysis system in which the costs and benefits of management alternatives can be evaluated in a consistent and transparent fashion, incorporating the best available scientific information and accounting for uncertainty. Within the Greater Blue Earth watershed, the sediment budget developed for the Le Sueur can be used to develop and test a simulation model that allows effects on sediment reduction of different management actions to be evaluated, incorporates uncertainty in supporting information, and is accessible to those making management decisions.

Lower Minnesota River

Based on stream gauging results, more sediment is delivered to the Minnesota River from its tributaries than is discharged to the Mississippi and Lake Pepin, indicating that sediment storage occurs along the Minnesota River and its wide valley bottom. In some years, this storage may approach half of the sediment supplied from Minnesota River tributaries (Wilcock, 2009). This is significant for Lake Pepin restoration for two reasons. First, reductions in loading in the tributaries will be proportionally reduced by the amount of sediment stored along the Minnesota River. Second, factors that influence changes in sediment storage along the Minnesota River valley bottom will play a dominant role in determining sediment supply to Lake Pepin. The role of floodplain storage on the Minnesota River and of net changes in the channel cross-section associated with changes in water and sand loads and dredging require a much better understanding. It will be difficult to link changes in sediment sources in the Mankato area to reductions in turbidity and infilling at Lake Pepin without accounting for potential changes in floodplain storage in the Lower Minnesota. It is necessary to develop a sediment budget for the Minnesota River mainstem in order to identify the magnitude of sediment storage and the factors that control changes in sediment storage. This will provide a basis for evaluating possible management actions along the mainstem that may alter the proportion of sediment stored in the river floodplain.

Acknowledgements

In a large and long-term project such as this, it is inevitable that essential assistance was provided by a very large number of people. It would be excessive (and inevitably incomplete) to attempt to acknowledge all of them here. At the same time, we would be remiss if we did not recognize the exceptional contribution of three people, Pat Baskfield and Chuck Regan of the Minnesota Pollution Control Agency, and Scott Matteson, formerly at Minnesota State University at Mankato and now at the Minnesota Department of Agriculture. Without their extraordinary dedication to designing, maintaining, conducting, and analyzing stream monitoring information, our understanding of the Le Sueur River watershed would be far poorer.

Section I: Introduction

1. Overview:

The Le Sueur River drains 2,880 km^2 of primarily agricultural land (84%), the vast majority of which is in row crops (Kudelka, 2010). There are no major urban areas, although the municipality of Mankato is expanding into the northern portion of the watershed. There are three major branches of the Le Sueur River with the Big Cobb and Maple tributaries entering the Le Sueur within 10 km of its confluence with the Blue Earth River (Figure 1.1). The Le Sueur flows into the Blue Earth River 5km above its confluence with the Minnesota River.

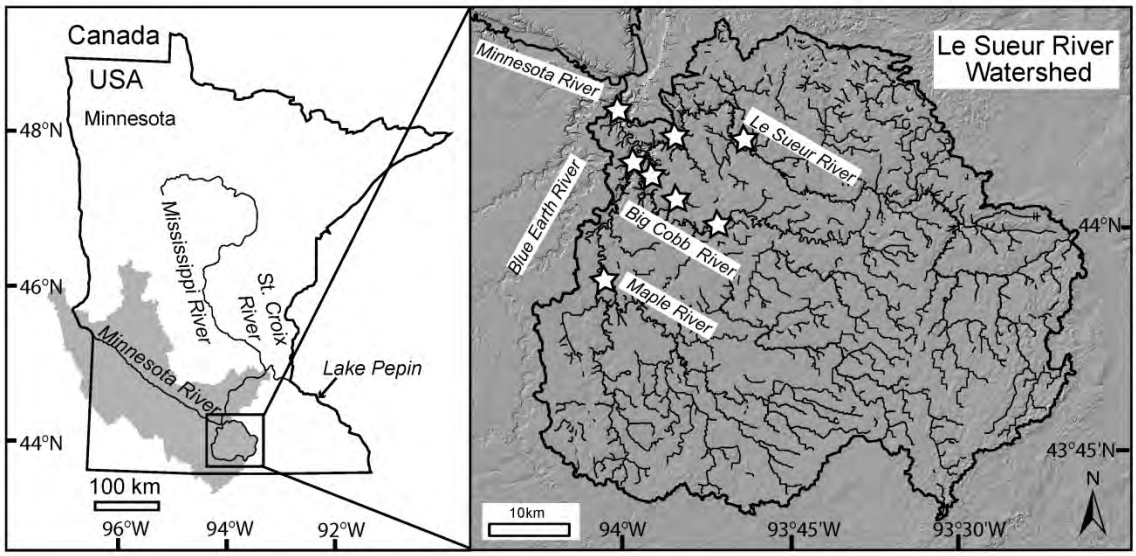

Figure 1.1: Location of Le Sueur River and its major tributaries (adapted from Gran et al., (2009).

The Le Sueur River is one of the heaviest contributors of sediment to the Minnesota River. Monitoring during the time period of 2000 – 2005 showed that 24-30% of the total suspended solids (TSS) load entering the Minnesota River came from the Le Sueur River watershed (MPCA et al., 2007), despite it containing only 7% of the watershed area. The Minnesota River provides 85-90% of the sediment load to Lake Pepin (Kelley and Nater, 2000), which has seen a ten-fold increase in sedimentation rates from pre-settlement to the present (Engstrom et al., 2008). Both the Le Sueur and Minnesota Rivers have multiple reaches listed as impaired for turbidity under section 303d of the Clean Water Act. Most of that turbidity comes from high suspended sediment loads. Although some portion of that high suspended sediment load is very likely due to land use management in the watershed, the Le Sueur also appears to be naturally predisposed to relatively high sediment loads due to its fine-grained substrate and ongoing vertical incision in the lower 35 km of the river network, which has resulted in an anomalously steep gradient, or knick zone, in the lower reaches of the river.

Our efforts have focused on understanding sediment sources to the Le Sueur River over multiple spatial and temporal scales, in particular over annual and decadal scales as well as how sediment sources have changed over the past 13,400 years. We are also investigating how sediment cycles through the Le Sueur River floodplain. Our efforts have involved various types of field surveys, water quality monitoring on the mainstem Le Sueur River and on ravines, GIS

analyses of airborne lidar data, numerical modeling of the mainstem channel, and sediment fingerprinting.

We address zones below and above the knick zone separately because different geomorphic processes dominate in each zone. This report covers long-term evolution of the drainage basin, upland erosion, erosion of high bluffs, streambank and floodplain processes, and ravines. We have sought to measure and define sources independently from one another. They are compiled together on the spreadsheet we are providing and compared with gauging results from a series of paired gauges. It is important to recognize that the processes operating in the Le Sueur today and the modern sediment budget are fundamentally controlled by the geomorphology of the system and that alterations made by humans appear to have altered the efficiency of water and sediment transport in the system leading to the particularly high loads we have today.

Background:

Geomorphic History:

The Le Sueur River watershed is comprised of a relatively low-relief upper watershed, with high-relief ravines and bluffs along the lower river corridor. The high relief in the lower 35 km of the Le Sueur, Big Cobb, and Maple River valleys is the result of knickpoint migration through the basin (Gran et al., 2009). These knickpoints originated from a sharp drop in base level on the mainstem Minnesota River during the catastrophic draining of glacial Lake Agassiz. As the Laurentide ice sheet retreated from the mid-continent at the end of the last glaciation, meltwater from the wasting ice was impounded by a low moraine dam in western Minnesota and formed glacial Lake Agassiz. It eventually covered much of western Minnesota, eastern North Dakota, Manitoba, and western Ontario (Upham, 1890, 1895; Matsch, 1972). The only outlet for much of this time was to the south through glacial River Warren, the valley now occupied by the Minnesota River. River Warren incised older tills, saprolites and bedrock in the valley floor (Matsch, 1983), creating a valley that was 45 m deep at its mouth and 70 m deep near Mankato, 300 km downstream.

The initial incision was around 11,500 radiocarbon years before present (rcbp) (Clayton and Moran, 1982; Matsch, 1983) (~13,400 calendar BP). The valley was occupied until about 10,900 rcbp. Two other outlets were used between 10,900 - 10,300 (Thorleifson, 1996) and 10,000 - 9,600 rcbp (Lowell et al., 2005) during which time the southern outlet was not used. River Warren was reoccupied after 9,600 rcbp and finally lost glacial lake discharge by 8,200 rcbp. Pre-existing tributaries like the Blue Earth and Le Sueur rivers were low-gradient streams of glacial meltwater origin that were stranded above the master stream when the initial incision occurred. Knickpoint migration continues today, driven by hydrology and sediment transport. Through most of the knick zone the river is incising through fine-grained till substrate. Bedrock waterfalls occur where the channel incises through limestone on several tributaries in the lowermost river valley. In the Le Sueur River, the record of incision following glacial River Warren is manifest in over 400 terrace surfaces spread throughout the lower basin. Knickpoints are expressed as slope discontinuities evident on all three major branches of the river, and they have propagated approximately 35-40 km upstream from the Minnesota River on each branch (Gran et al., 2009).

The surficial geology of the central Le Sueur watershed is dominated by a low relief loamy glacial till with a minimum age of 12,000 rcbp by an unnamed phase of the Des Moines lobe that is younger than the Algona moraine in Iowa (Ruhe and Scholtes, 1959). The till is

mantled by up to 3 m of alternating beds of glaciolacustrine silt and clay that were deposited in glacial Lake Minnesota as this phase of the ice lobe stagnated. Low-relief ice-walled lake plains rise above the general elevation of lake sediment in the basin. The lake lacks clear shorelines and is enclosed on the eastern and southern headwater areas by higher relief, ice-marginal, stagnant-ice deposits and thrust moraines. This leads to the interpretation that the lake initially began on the wasting ice surface in isolated ice-walled depressions that gradually deepened and broadened as the ice wasted. It is sandier in the western part of the Le Sueur watershed, where south-east-trending ice-marginal streams flowed along another unnamed margin of the Des Moines lobe aligned with the modern Cottonwood River and formed a delta as it entered the lake. The river is currently incising through the most recent glacial deposits as well as underlying early- to mid-Pleistocene glacial sediment and in places has reached the underlying Cambrian Jordan sandstone. Bedrock crops out along the lower Maple, Le Sueur and Cobb rivers within 15 km of the mouth. As part of this project, the surficial geology of the Le Sueur watershed was mapped in detail (Figure 1.2) and is available through the Minnesota Geological Survey (Jennings, 2010).

Land Use/Land Cover History:

The dominant land cover before the influence of humans was prairie and wet prairie (Marschner, 1930, Minnesota Department of Natural Resources, 2007). Hardwood forests were limited to river corridors and the northeastern portion of the watershed (Marschner, 1930). The two main changes that resulted from Euro-American settlement beginning in the mid-1800s were the conversion of original prairie to agricultural fields and the alteration to the hydrology through artificial drainage. Hydrology changes included draining of the wetlands, creating a large public and private ditch network, and the installation of tile drainage systems. In addition, the conversion from perennial grasses to annual crops also constitutes a major change in hydrology, as evapotranspiration rates have changed dramatically, particularly in the spring and early summer. Approximately 84% of the basin is now cropland (Kudelka, 2010), primarily row crops such as corn and soybeans, and according the Water Resources Center (2000) of Minnesota State University in Mankato, Minnesota, almost all of the farm fields have artificial drainage which has increased the depth, density, and capacity over time.

Superimposed on this direct manipulation of the drainage system are indirect changes imposed by climate change in the last ~50 years. Trends show a statewide increase in mean annual precipitation, the number of days with precipitation, and the number of intense rainfall events per year (Novotny and Stefan, 2007). To compound the complexity of the system, these changes to land use, hydrology, and climate, affect a geomorphically young, evolving channel network in the Le Sueur River watershed.

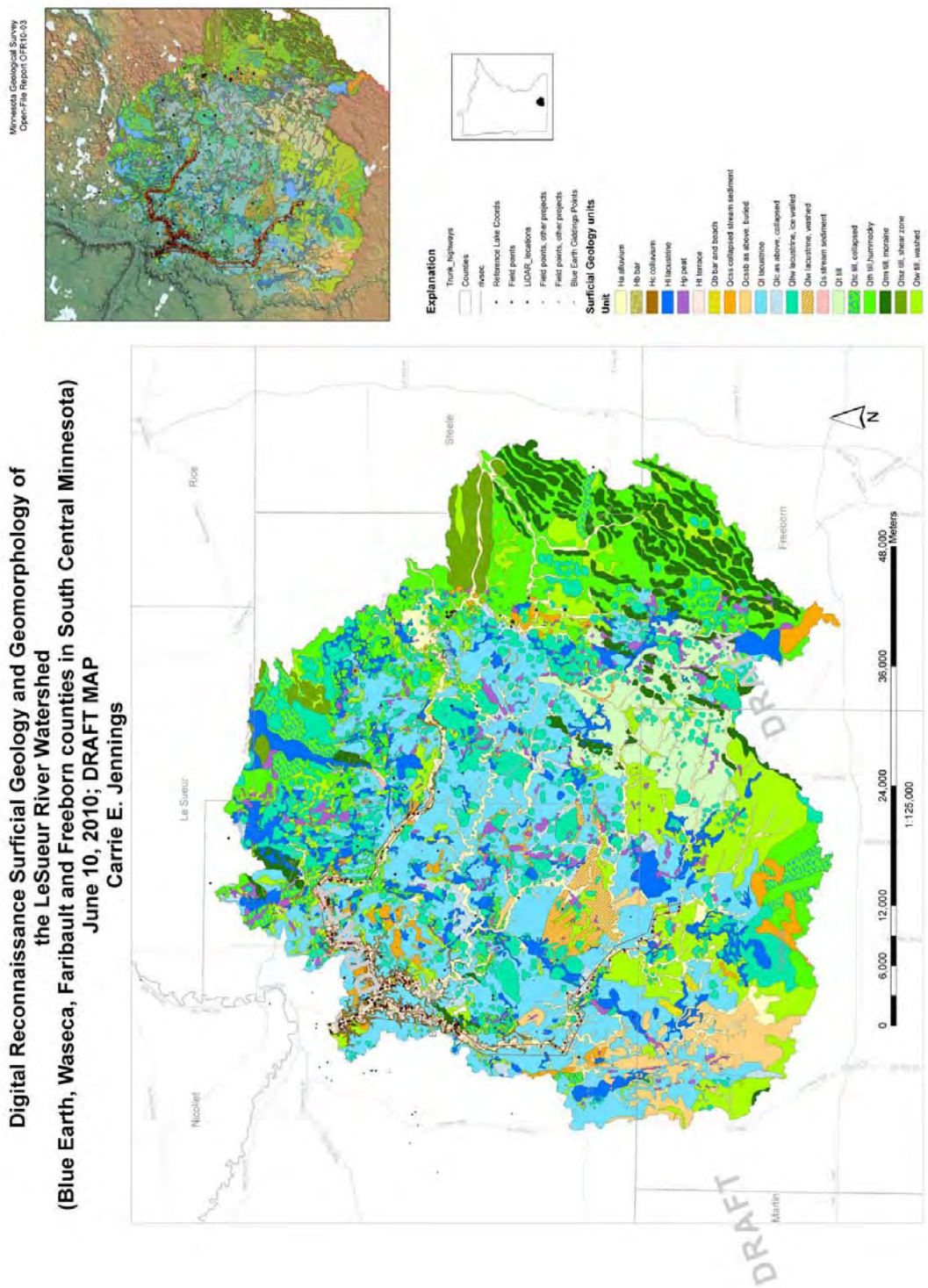

Figure 1.2: Surficial geologic map of Le Sueur River watershed (Jennings, 2010).

2. Constraining pre-settlement erosion rates

Introduction

The Le Sueur River offers a well-constrained example of landscape evolution following base level fall in a low-gradient landscape. The initial base level fall event is well-timed to 13,400 BP. The modern longitudinal profile shows clearly where the knickpoint is today, and hundreds of terraces throughout the knick zone record the history of river incision. These terraces are strath terraces, carved into glacial till with a thin cap of alluvium on top. We used terrace ages and locations, as well as modern conditions and the timing of initial base level fall to constrain a 1D numerical model of channel incision. The resulting best-fit 1D model was used to determine inputs to a 2D model which incorporated meandering and the effects of valley widening. The results of the 1D model show us how river incision rates have changed through time, and the results from the 2D model show us how sediment export volumes changed through time. Modeling was completed on the Le Sueur River only, but volumes of sediment removed were up-scaled to the entire watershed using airborne lidar data to determine total volume of sediment removed over the past 13,400 years and assuming that patterns of sediment evacuation on the Maple and Big Cobb tributaries were the same as on the Le Sueur River. By understanding how valley excavation proceeded during the Holocene, we are able to estimate a "pre-settlement" erosion rate that can then be compared with modern erosion rates and sediment loads.

Methods

GIS Analyses

Over 500 terraces were identified on a hillslope image created from the 1m lidar DEM (Figure 2.1). Terraces were defined as flat surfaces with no surface undulations > 5m, bearing one side with a steeper slope, and located within the river valley but above the geomorphic floodplain (1-2 meters above the river). A subset of mapped terraces was confirmed by field-checking.

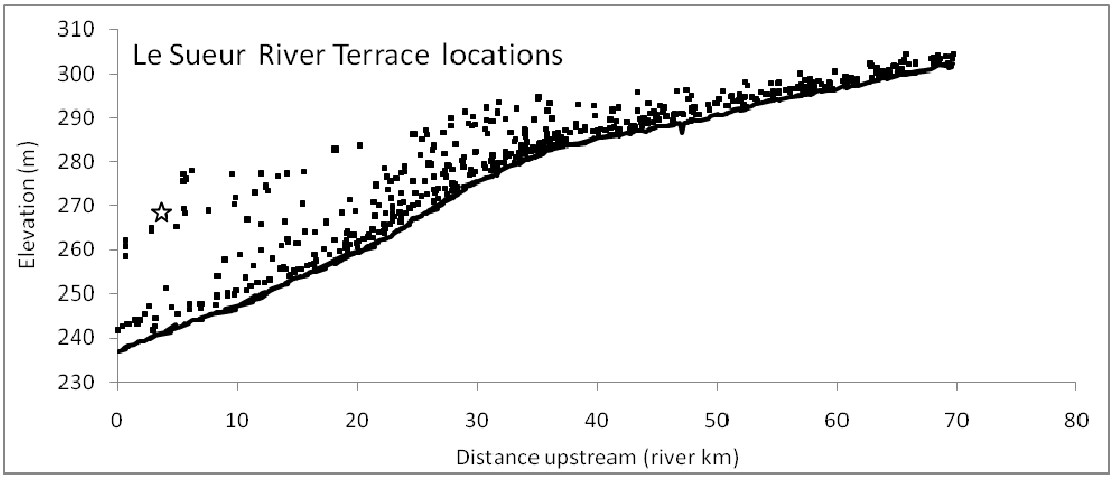

Figure 2.1: Location and elevation of terraces along the Le Sueur River. River elevations are shown in the solid line, with the knickpoint visible as a change in slope at 35km upstream of the mouth of the Le Sueur River. The star marks the oldest dated terrace at 13.04 ± 0.94 ka BP.

Because most of the Le Sueur River watershed was covered by glacial Lake Minnesota prior to valley incision, we assume the flat upland surface extended across the top of the river valley prior to valley excavation. The current valley topography was subtracted from this initial surface in 5 km increments going up each tributary. This sets a maximum bound for the volume of sediment excavated from the valley since base level fall. This sediment was eroded through bluff and bank erosion and incision of the channel bed. A closer inspection of the terrace data reveals a gap between the upper surface and the highest terrace of approximately 20 meters near the mouth and 13 meters along the upper reaches of the mainstem Le Sueur River. Without any direct physical evidence the river occupied that area after the time of initial base level fall, we calculate a second valley volume from the surface of the highest terraces down to the valley floor. This sets a minimum bound for the valley volume excavated in the past 13,400 years. There is a high terrace near the mouth with a depositional age of 13,040 BP ± 940, giving some evidence that the channel was at this elevation fairly early in its incision history (Figure 2.1). The valley volumes were converted in mass (Mg) and are summarized in Table 2.1.

Table 2.1: Mass excavated from valleys since base level fall (from Gran et al., 2009).

	Min valley mass (Mg)	**Max valley mass (Mg)**
Le Sueur	5.92×10^8	1.32×10^9
Big Cobb	1.57×10^8	4.29×10^8
Maple	2.61×10^8	6.42×10^8
Total	1.01×10^9	2.40×10^9

Within each 5 km reach on the Le Sueur River, the valley was further subdivided into vertical subsections aligning with terraces. An age model was developed for incision based on height above the bed, and used to determine the age of each terrace layer. Volumes were derived from subtraction of underlying topography below each terrace layer. These volumes represent the volume of sediment eroded during a given time period. One complication with this method of volume quantification is that as rivers meander into high bluffs along valley walls, valleys widen. The method we used to calculate valley volumes in each time interval would assign that later erosion to an earlier time period than when it actually occurred. To compensate for this, we width-corrected the valleys, using the assumption that active floodplain width should not change through time. The width-corrected volumes were binned into 1000-year increments and summed along the entire Le Sueur River valley to get the total volume of sediment removed during that interval.

Field Work

Nineteen terraces were dated using optically-stimulated luminescence (OSL) dating of alluvial sands and radiocarbon dating of shells within the alluvial sands. Sampled terraces were chosen to obtain A) a series of terraces of varying heights in the same area and B) a suite of samples at the same elevation above the channel but at different distances upstream. Nine sites were sampled for OSL dating at Utah State University's Luminesence Lab in Logan, Utah. OSL is a technique that measures a buried quartz- or feldspar-grain's last exposure to sunlight, thus providing a depositional age. It can be used on fluvial materials where there is insufficient material for other dating techniques. A major assumption is that the luminescence signal gets reset to zero by an appropriate period of exposure to light prior to deposition (Wallinga, 2002). This may not always be achieved in some fluvial deposits because grains are exposed to varying amounts of light during transport (Wallinga, 2002). If the sediment has incomplete zeroing,

referred to as “partial bleaching”, then the age may be overestimated. The effects of partial bleaching were minimized by using the single-aliquot regenerative-dose procedure (Murray and Wintle, 2000, 2003; Wintle and Murray, 2006). An additional thirteen samples of shells were collected and dated using standard AMS radiocarbon techniques at Beta Analytic laboratory. Figure 2.2 shows the location of terraces where samples were collected for either OSL, radiocarbon, or grain size distribution data. Figure 2.3 shows the general stratigraphy of terraces and sampling locations within that.

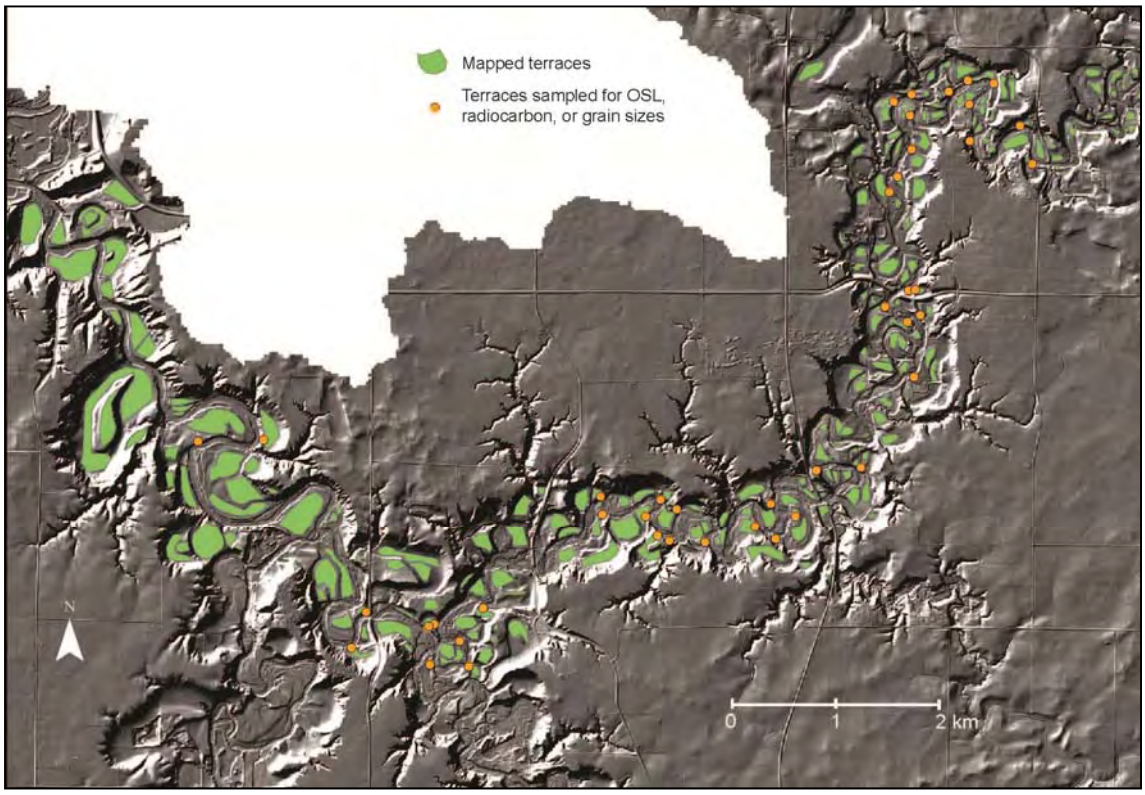

Figure 2.2. A sampling of mapped terraces for about 35 km of the Le Sueur River. The green shapes represent mapped terraces. The orange dots indicate locations that were sampled for OSL, radiocarbon, grain size distributions, or a combination.

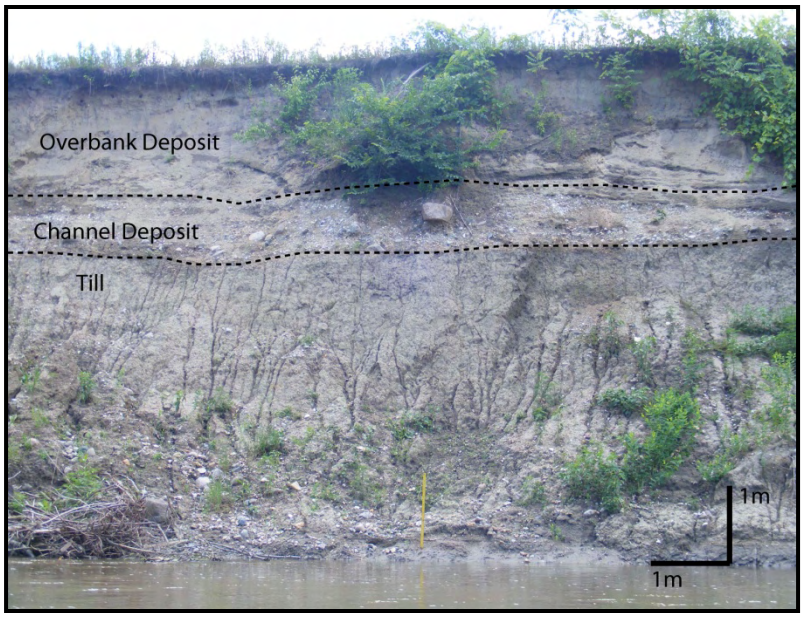

Figure 2.3. Example of strath terrace stratigraphy along the river. Samples for dating were taken either right above the channel deposit (OSL), or within the upper portion of the channel deposit (radiocarbon).

Modeling:

A 1D kinematic numerical model of river incision was used to determine river profile evolution for the Le Sueur River through time (Finnegan et al., 2010). Two potential models were used. The first is a transport-limited model where sediment transport is a function of flux divergence. The general form of the model is $dz/dt = i(dQ_t/dx)$ with sediment transport (Q_t) based on Fernandez-Luque and van Beek (1976) and *i* an intermittency factor to account for the fact that bedload transport only occurs during a small fraction of each year. Here, z is the channel elevation as a function of distance upstream, x. The second model is a detachment-limited model based on Howard and Kerby (1983) of the form: $dz/dt = k(\tau^*-\tau^*_c)$, $\tau^* > \tau^*_c$ where *k* is a rate constant, τ^* is the Shields stress, and τ^*_c is the critical Shields stress. The transport-limited model is most appropriate for an alluvial channel and the detachment-limited model is more applicable to incision in a bedrock channel. Although the Le Sueur River has an alluvial floodplain, it is incising through till, which acts like bedrock and can lead to behavior more appropriate to a bedrock or semi-alluvial channel.

Each model was run under two grain size scenarios. Under scenario 1, grain size was held fixed at 0.01 m, the average D_{50} (median grain size) for the Le Sueur River as measured in the field. Under scenario 2, grain size was allowed to vary downstream. The primary source of coarse material (gravel to boulders) in the Le Sueur River is the stacked tills and glaciofluvial sediments. As the Le Sueur River incises, it accesses a greater volume of coarse material. This leads to downstream coarsening. Thus, scenario 2 was run to allow for increasing downstream coarsening as incision progressed. For both scenarios, hydraulic geometry of channels were based on measured channel cross-sections for the Le Sueur River, with width (w) and depth (d) as functions of Area (A): $w=1.02A^{0.50}$ and $d=0.53A^{0.21}$. Runs were conducted using a Monte Carlo approach, simulating a hundred runs for each scenario.

Four combinations of scenarios were run with a single base level fall event at 13,400 yBP. The best scenario was determined both through a match of final long profile to the modern long profile and through a match of terrace ages with predicted ages based on the 1D model.

The results from the 1D modeling tell us which kinematic model best describes the incision and evolution of the Le Sueur River. The results can be used to look at the incisional history of the mainstem channel in 1D.

The best fit kinematic model was used to run two alternate scenarios. The first tested the sensitivity of the model to a change in climate, simulating the mid-Holocene dry period. The second tested a two-phase incision model, with the first step occurring at 13.5 ka BP and the second occurring at 10.3 ka BP, after a potential stream capture event of the lower Le Sueur River by the Blue Earth River (Meixell et al., 2009; Wittkop, personal communication).

Although 1D modeling can tell us how incision has changed through time, we need the full three dimensions to determine how volumes of sediment evacuated through time has changed. Because the channel meanders as it incises, and the bluffs increase in height as incision progresses, a decrease in incision through time does not necessarily translate into a decrease in erosional volume through time. Lateral migration into increasingly taller bluffs could lead to an increase in sediment volumes removed through time, even if incision rates decrease.

A 2D kinematic model for river meandering (Howard and Knutson, 1984) was run with the best fit 1D incision model. The goal here was to constrain how sediment volumes derived from river meandering into increasingly high bluffs change through time. Two runs have been conducted to determine how sediment volumes exported out of the Le Sueur River change through time. To change from dimensionless volumes to actual sediment loads, the total volume removed in the model was scaled to the total volume of sediment removed (on all three main rivers) since the initial base level fall 13,400 yBP as determined through lidar analyses. Total volumes were converted into Mg of silt and clay to compare with modern TSS loads.

Results/Discussion

Incision History:

Nineteen terraces were sampled to determine depositional ages. These terraces ranged from 2.0 to 25.9 m above the modern channel, with ages ranging from 1.54 ± 0.23 ka BP to 13.04 ± 0.94 ka BP, covering most of the time of incision. All dates are listed in Table 2.2. There were three sets of terraces that fell at different elevations but within a short reach of channel. These were used to look at incision patterns through time. Figure 2.4 shows these terrace sets, plotted as elevation above the channel vs. age. In all three sets, incision could be modeled as constant through time, but a model with faster incision rate followed by a slowing of incision also fits the data. Taking all terrace height and age data together, an age model was developed that relates height above the bed to depositional age.

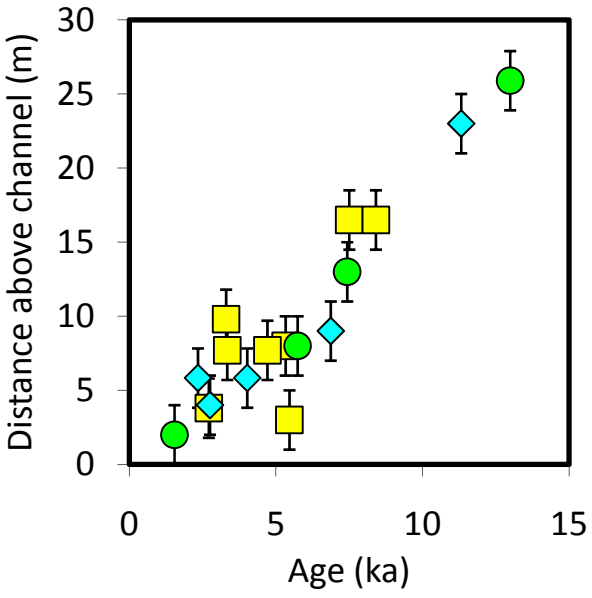

Figure 2.4: Terrace sets in three reaches along Le Sueur River, showing relatively linear increase in elevation above bed with age.

Table 2.2. Terrace depositional ages (from Johnson, in prep).

Terrace name	Terrace Height (m)	Terrace elevation (m)	Distance Upstream (km)	Sample Type	[1]OSL Age (cal ka BP)	[2]Conventional Radiocarbon Age (rc ka BP)	[2]Calibrated Age (cal ka BP)	[3]Average Date (ka BP)
C*	25.9	267.4	4.35	OSL	13.04±0.94			
Y	3.8	257.7	15.55	OSL	2.17±0.38			
X	9.8	264.2	16.05	OSL	3.3±0.49			
K*	13.86	288.6	29.73	OSL	5.01±0.44			
L*	15.21	290.3	30.1	OSL	6.35±0.48			
P	7.54	279.1	28.18	C^{14}		4.33±0.04	4.91±0.065	
R*	16.5	270.5	15.95	OSL, C^{14}	7.48±0.5	7.63±0.05	8.45±0.08	7.95±0.5
V†*	7.7	261.5	15.42	OSL, C^{14}	4.57±0.43	3.09±0.04	3.31±0.09	3.94±0.6
W†	5.83	270.8	24.38	OSL, C^{14}	4.02±0.86	2.33±0.04	2.34±0.02	3.18±0.8
Z	2.0	251.3	11.53	OSL	1.54±0.23			
LS-90-03	11.71	276.1	23.69	C^{14}		6.86±0.07	6.85±0.07	
LS-08-01	9.90	259.8	12.43	C^{14}		6.51±0.05	7.41±0.09	
LS-16-00	9.10	256.9	9.74	C^{14}		5.03±0.05	5.78±0.13	
LS-22-04	5.30	262.4	18.08	C^{14}		4.58±0.05	5.26±0.20	
LS-22-06	2.30	256.4	16	C^{14}		4.71±0.05	5.46±0.14	
LS-41-01	15.21	290.3	30.1	C^{14}		5.26±0.07	6.08±0.18	
LS-41-10	10.19	279.4	26.63	C^{14}		4.57±0.05	5.25±0.2	
LS-90-01	3.89	268.6	23.92	C^{14}		2.62±0.05	2.75±0.04	
LS-90-05	24.06	283.8	20.73	C^{14}		9.95±0.06	11.46±0.23	

[1] *OSL = Optically stimulated luminescence ages*

[2] *Conventional and calibrated radiocarbon ages are reported with 2 sigma uncertainty.*

[3] *Average between OSL and C^{14} ages.*

[*] *Terraces high potential for partial bleaching resulting in an overestimation in age.*

[†] *Terraces 'V' and 'W' had two units dated using the radiocarbon technique. The upper unit was used to assign a terrace age.*

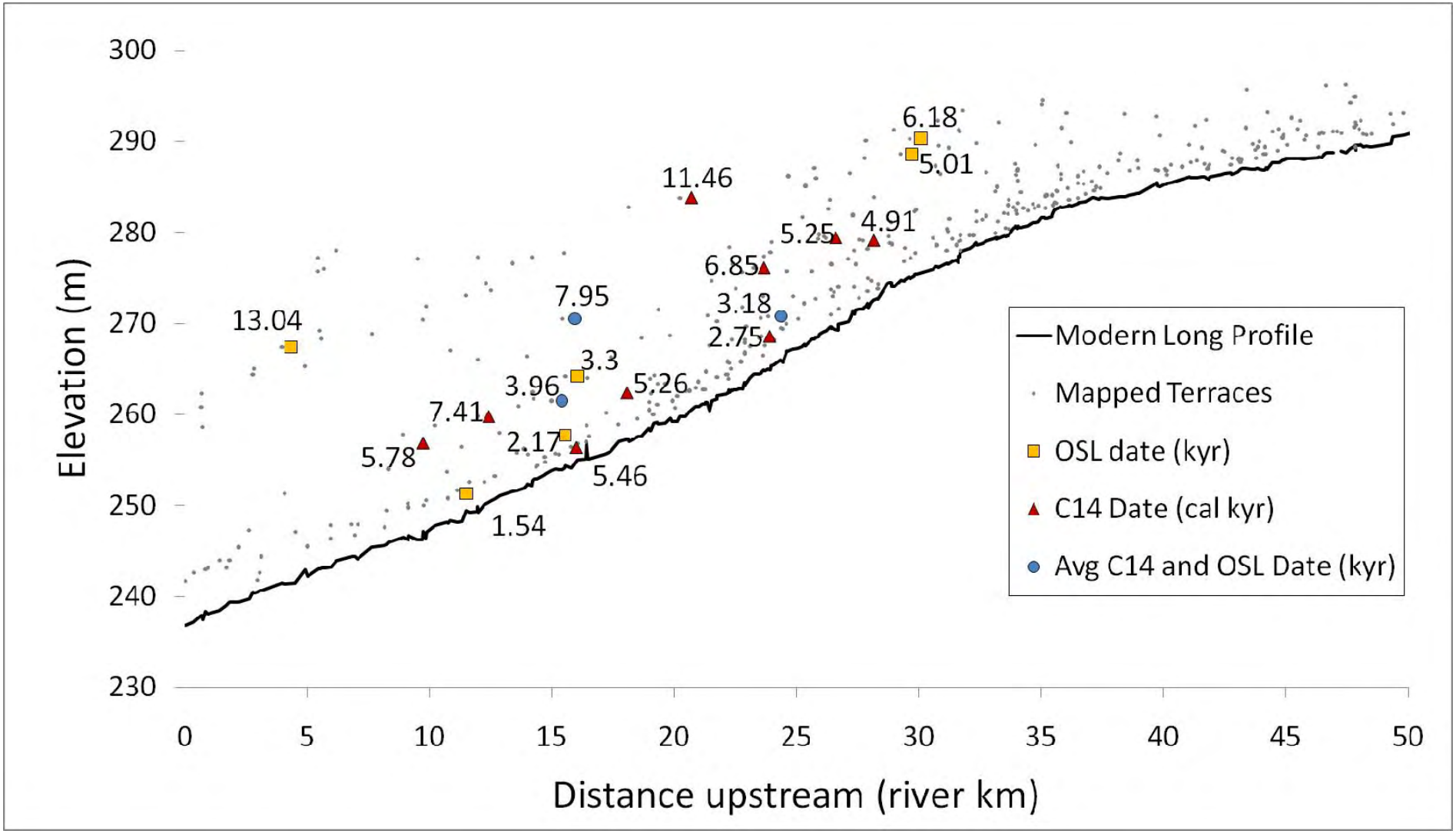
300
290
280
270
260
250
240
230
Elevation (m)
0
5
10
15
20
25
30
35
40
45
50
Distance upstream (river km)
6.18
5.01
11.46
5.25
4.91
6.85
7.95
3.18
13.04
2.75
3.3
3.96
5.26
7.41
5.78
2.17
5.46
1.54
Modern Long Profile
Mapped Terraces
OSL date (kyr)
C14 Date (cal kyr)
Avg C14 and OSL Date (kyr)

Figure 2.5 (previous page). Terraces mapped from 1 m airborne lidar on the Le Sueur River. Dated terraces are noted in squares (OSL), triangles (C14) and circles (both). Uncertainties are given in Table 2.2. Adapted from Belmont et al., in press.

The 1D modeling provides another route to determine the incision history. For each run, the root mean square errors (RMSE) associated with comparing the final channel profile to the modern long profile and comparing the measured terrace ages to the modeled ages are shown. The best fit scenario for both criteria was the detachment-limited run with downstream coarsening. Although the long profile was also well-predicted by the downstream coarsening, detachment-limited system with a mid-Holocene dry period signal superimposed on it, the terrace ages were a better match under the scenario with one base level fall. Figure 2.6 shows the results from the best-fit model run.

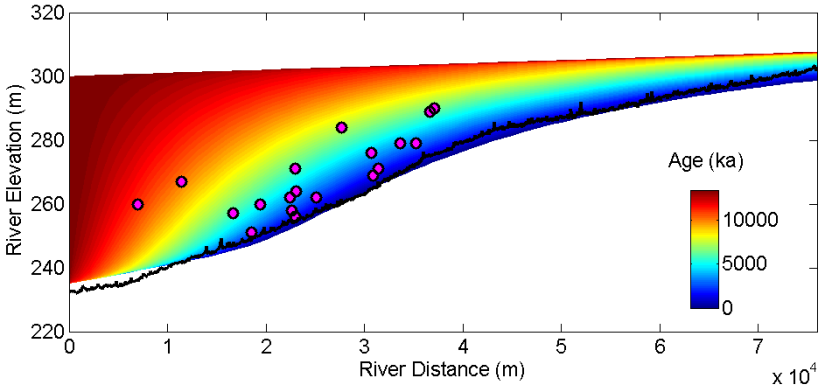

Figure 2.6: Results from best-fit model of detachment-limited with downstream coarsening (from Finnegan et al., 2010).

The incision history associated with the best-fit model is shown in Figure 2.7. This incision rate is an average covering the lower 80 km of river, combining area above and below the knick zone. The plot shows that the incision rate was initially quite high (~8 mm/yr), decreasing within the first few hundred years to half its initial value and then slowly declining through time for the next 13,000 years to an average rate of 1.3 mm/yr today.

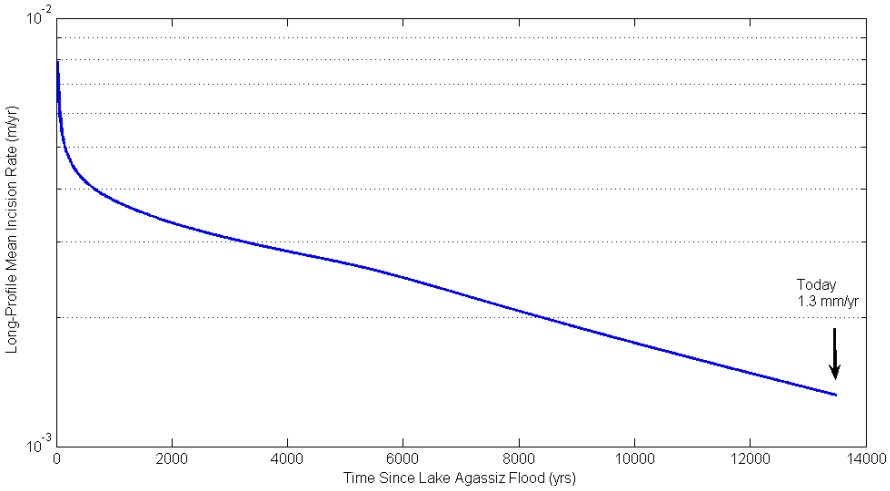

Figure 2.7: Incision history from the detachment-limited model with downstream coarsening following one base level fall (from Finnegan et al., 2010).

Erosional volume history:

Two approaches were taken to determine erosional volume through time. The first used the age model developed from the terrace data where age is a function of elevation above the modern river. These ages were assigned to the width-corrected volumes as computed from subtraction of vertical subsections every 5 km along the channel, and volumes were binned into 1000-year increments and summed along the length of the Le Sueur River (Figure 2.8). These results show a relatively constant sediment export through time, with a dip in volume near the mid-Holocene and a rise in sediment export afterwards. These fluctuations may not be statistically significant, given the large error associated with this methodology, but the results show that it is more likely that sediment volumes were fairly constant through time, rather than exponentially increasing or decreasing.

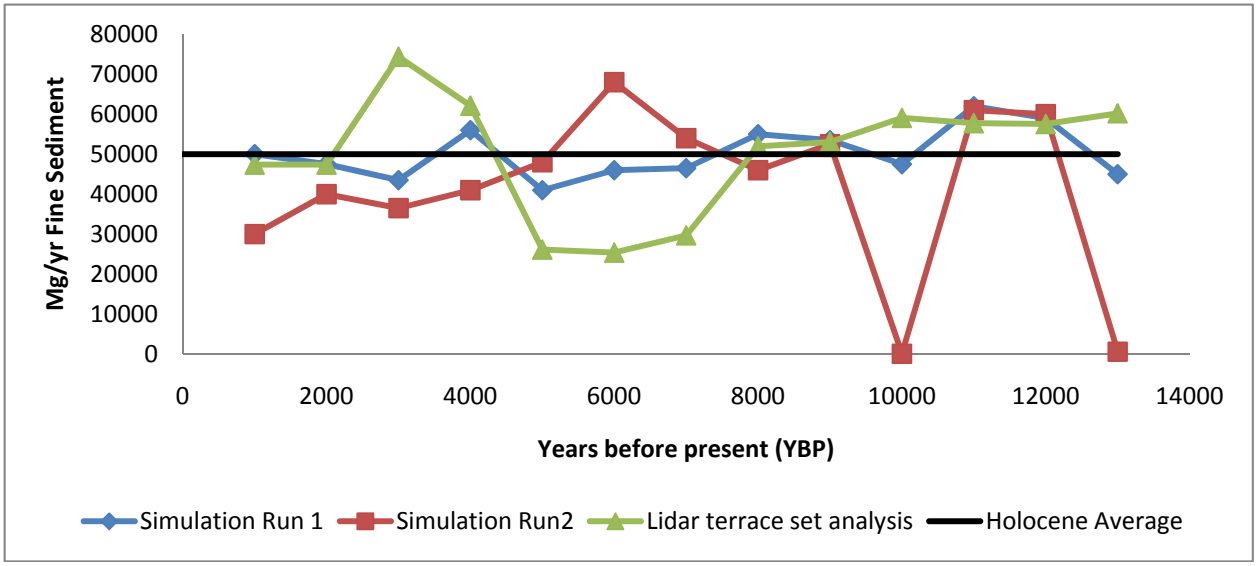

Figure 2.8: Sediment export using width-corrected valley volumes and age model developed from terrace ages and elevations above channel (lidar terrace set analysis) compared with the pattern of valley excavation from two 2D numerical model runs (2D model run 1 and 2). The lidar terrace set analysis was done for the Le Sueur River branch only and scaled up for the entire basin. The 2D numerical model was scaled so that the average volume excavated matched the average Le Sueur River excavation volume. Holocene average fine sediment load is shown in black. The modern TSS load is 225,000 Mg/yr, which is off the chart.

The 2D modeling using the best fit kinematic model from the 1D modeling (detachment-limited with downstream coarsening) was also used to look at volume exports out through time (Figure 2.8). Like the age model-volume approach, these runs indicate that the average sediment export was fairly steady during the Holocene, although fluctuations around the mean were high. If we assume a stationary mean, the standard deviations around the mean are ± 13% and 22%. This is compared with a standard deviation of ± 30% in the age model-volume approach.

Given that the simplest model, of steady sediment export through time, is supported by both approaches, we calculated the mean annual sediment export through the Holocene by a simple volumetric analysis (see Table 2.1). We feel the minimum value is more defendable, since our age control on the highest terrace measured shows it was 13.04 ka BP, only 400 years

after the initial base level fall. Translating the volume into a silt and clay load gives 50,000 ± 15,000 Mg/yr at the mouth of the Le Sueur River.

Conclusions and Implications:

The Holocene and late Pleistocene history is very well-constrained, allowing us to model the kinematics of incision on the mainstem Le Sueur River. We found that the Le Sueur River is best modeled as a detachment-limited system. In this case, the bedrock is actually glacial till, so incision rates are high compared to other forms of bedrock, but incision into till is still more comparable to incision into bedrock than into alluvium. The modeling work shows the importance of downstream coarsening on essentially pinning the toe of the knick zone in place making it harder to erode, and thus leading to the modern geometry we see today.

Both approaches to determine sediment volumes exported through time came to the same conclusion that sediment export has fluctuated around a steady mean throughout the Holocene. Those fluctuations can be quite significant, and lead to rather large uncertainty on pre-settlement erosion rates. These fluctuations are driven by internal dynamics of meander cutoffs and ensuing slope adjustments rather than externally-forced, for instance, through climate changes. When taken on a single channel, like the Le Sueur River branch modeled here, the pre-settlement erosion rates could vary by a factor of 2. As more channels come together, however, it is unlikely the internally-generated dynamics would align all high or all low, and thus the uncertainty declines through spatial averaging. The end result is that although the fluctuations may be high on one branch of the Le Sueur, these fluctuations would diminish as more and more channels are added, and when considered over the scale of the entire Minnesota River, would likely trend towards the mean with much less internally-generated variability.

Overall, the Holocene average load is 50,000 ± 15,000 Mg/year of silt and clay, derived primarily from bluff and bank erosion as well as channel incision. This is our best pre-settlement erosion estimate. It is a factor of 4-5 lower than the modern total load on the Le Sueur River from 2000-2010 (225,000 Mg/yr).

Valley excavation should be compared with the modern erosion from bluffs, banks, and the channel bed, as these are the primary processes by which valley excavation proceeds. Bluff erosion alone is estimated at 134,000 +/- 50,000 Mg/yr depending on the up-scaling method used. This is 2-3 times higher than pre-settlement erosion rates, indicating that bluff erosion must have increased in modern times. The management implication is not that we use the pre-settlement erosion rate as a target, which is likely unattainable, but rather that we recognize that bluff erosion has been accelerated in recent times over pre-settlement rates.

3. Gauging Record

The gauging network currently in place in the Le Sueur River basin has allowed us to put bounds on suspended sediment loads at several points in the system. On each of the three major tributaries, there are now gauges both above the knick zone and near the mouth of the tributary. The existing network thus helps constrain the relative importance of sources above vs. below the knickpoint and also provides estimates for sediment flux from each major tributary and at the mouth of the Le Sueur River. Comparisons between the two gauges on each channel show a dramatic increase in sediment load (most of TSS is suspended sediment) as the rivers flow through the knick zone (Table 3.1, Figure 3.1). The differences in load can be attributed primarily to the relief in the lower basin, where high bluffs and steep ravines provide additional sources of sediment that are only minimally present above the upper gauges. Also, greater relief between field and stream can accelerate runoff and its associated erosion. In our efforts to draw up a sediment budget, we will continually refer back to the increase in sediment from the upper to the lower gauges.

On the Maple River, there are paired gauge measurements for 2006-2009. The Big Cobb-Little Cobb paired gauges have data from 2006-2009, and the Le Sueur River has paired gauge data from 2007-2009 (Table 3.1). Loads were computed using the Army Corps of Engineers FLUX program, which takes a tiered statistical approach to computing loads rather than a standard rating curve approach. Gauges with continuous turbidity sensors had loads computed directly. The Blue Earth County Soil & Water Conservation District runs the Maple River gauge, and Minnesota State University at Mankato has been responsible for sampling and load calculations for the Cobb and Le Sueur River gauges.

Table 3.1: Paired gauging stations in the Le Sueur River watershed.

Basin	Upstream Area (km^2)	TSS Loads* (Mg/yr)				
		2006	**2007**	**2008**	**2009**	**2010**
Upper Maple	800	7874	13285	6060	3452	
Lower Maple	880	22326	37909	22326	4916	
Little Cobb	335	3966	4415	3061	1564	
Big Cobb	735	33391	21829	14632	6312	48904
Upper Le Sueur	870		42214	22400	4289	
Lower Le Sueur	1210	86558	74645	42786	13404	126986
Le Sueur mouth (Red Jacket)	2880	135362	136439	86285	26303	543981

*Data from 2006-2009 come from Blue Earth County SWCD and MSU-Mankato, pers. comm.

The Le Sueur River is not the only river in the Minnesota River basin to have paired gauges (Table 3.2). Data are available for seven rivers with period of record ranging from one to six years (Table 3.2). In all cases, the increase in TSS load exceeds the increase in drainage area from the upper to lower gauges. Between 30% to 95% of the sediment yield is picked up in the knick zone, even though the increase in contributing area is generally much smaller. The increase in loading through the incised reaches is particularly large in smaller watersheds entering the Minnesota River from its left bank (Seven Mile Ck, Rush River, High Island Creek), but also quite large in the Maple and Cobb Rivers. Without any additional analysis or

assumptions, these data demonstrate that a large portion of the TSS derives from the steeper terrain between the gauges.

Table 3.2

River	# Years Record	Gauges used	% increase upper to lower gauge Drainage area	TSS
Cottonwood R	3	Upper: PLC010 + PLS005 Lower: PLC001	12.0	30.5
Maple R	2	Upper Maple Lower Maple	9.7	64.8
Cobb R	2	Upper: Beauford + Little Cobb Lower: Big Cobb	51.3	83.1
Le Sueur R	1	Upper: LES 35 Lower: LES 11.3	20.9	43.4
Seven Mile Ck	6	Upper: SMC1 + SMC2 Lower: SMC3	19.0	80.4
Rush R	3	Upper: 2RP + 3RP+ 4RP + 5RP Lower 1RP	16.2	90.3
High Island Ck	5	Upper HI-5P Lower: HI-10P	32.5	94.8

Gauges used in evaluating TSS contribution in knick zone

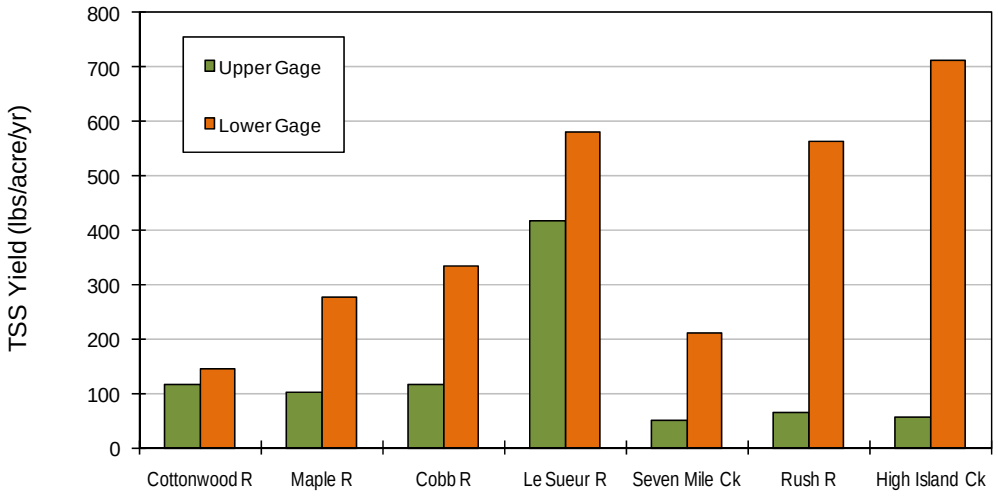

Figure 3.1. Annual TSS yield at upper and lower gauges in seven watersheds tributary to the Minnesota River. The gauges are located above and below the incised lower portions of the river valleys. Increases in TSS yield are generally much larger than the corresponding increase in drainage area, indicating that disproportionately large amounts of sediment are supplied in the incised reaches between each pair of gauges.

Many of the upstream/downstream gauge pairs have been located on rivers with relatively large TSS yield (Wilcock, 2009). The comparison of upstream/ downstream gauges clearly indicates that much of the loading occurs as the rivers move through the incised portions of the watershed. The stream gauging provides a direct confirmation of increased loading in these reaches and provides estimates of not just relative contributions, but the sediment delivery rates.

Section II: Sediment sources, sinks, and budget

Summary of sediment budget:

The sediment budget was compiled over multiple temporal and spatial scales. Background information on individual sources is given in chapters 4 (uplands), 5 (ravines), 6 (bluffs), and 7 (channels and floodplains) with an overview of the total budget in the "Summary of Findings" section at the beginning of the report. Data on ravine and bluff inventories and channel location and migration information are summarized in attribute tables of accompanying GIS shapefiles. Chapter 8 focuses on the morphodynamic model that allows one to investigate channel adjustment and time periods of adjustment due to changing input conditions. It incorporates inputs from ravines, bluffs, and uplands explicitly, and then allows the channel and floodplain to adjust dynamically.

The sediment budget is organized by tributary (Maple, Big Cobb, and Le Sueur), and within each tributary, by reach. Paired gauges on the Maple, Le Sueur, and Big Cobb-Little Cobb systems allow for spatial organization of the basin into zones above the upper gauge (above the knick zone), zones between gauges (within the knick zone), and zones below the lower gauge but above the mouth (within and below the knick zone). The modern sediment budget at the mouth is summarized in the "Summary of Findings" section at the beginning of this document and in Table II.1 and compared with gauging data from 2000-2010, a time period which encompasses a range of hydrologic conditions. Because most gauges were not active during that entire time period, the existing gauge records (Table 3.1) were scaled based on the relationship between the gauging time period and 2000-2010 at the Red Jacket gauge.

At each gauging station, there is a predicted load, based off of independent measures of each sediment source, and a measured load, based on TSS loads as determined by FLUX at each of the gauging stations. The FLUX loads were compiled by staff at the Water Resources Center at the Minnesota State University at Mankato and the Blue Earth County Soil and Water Conservation District. Measured loads reported here are monitoring season loads. At Red Jacket, from 2000-2010 the predicted fine sediment load was 234,000 Mg/yr and the measured monitoring season TSS load was 225,000 Mg/yr. Table II.1 shows the predicted and measured average annual TSS loads at each gauge, with uncertainty, for the time period 2000-2010.

Sediment budgets represent a compilation of many different components, each with uncertainty. A mass balance (inputs, storage changes, and outputs must balance) provides a strong constraint for evaluating these uncertainties. Subject to this constraint, different assumptions and scenarios can be evaluated in determining the most plausible combination. To allow the reader to evaluate the sediment budget, it is presented in a spreadsheet, which allows the user to explore the sediment balance for different assumptions, time scales, and sediment reduction scenarios. Below is a brief outline of how we compiled the budget and how it could be used to look at different temporal scales and under different scenarios. We also discuss how the budget can be balanced both above and knick zone and at mouth of the Le Sueur River at the Red Jacket gauge.

Table II.1: Predicted average annual fine sediment loads, by source and by reach, from 2000-2010.

A. Maple River Annual Mud Loads (Mg/yr)					
Source	Above Upper Gauge	Between Gauges	Below Lower Gauge	Sum at Lower Gauge	Sum at confluence
Upland	12,500 ± 3,700	1,200 ± 400	200 ± 60	13,700 ± 4,100	13,900 ± 4,200
Ravine	1,300 ± 700	3,600 ± 1,800	500 ± 260	4,900 ± 2,500	5,500 ± 2,700
Bluff	2,300 ± 800	19,200 ± 6,500	8,800 ± 3,000	21,600 ± 7,300	42,200 ± 10,200
Streambank	1,500 ± 3,000	5,000 ± 2,500	(4,900) ± 2,400	6,600 ± 2,500	200 ± 2,400
Total Predicted	**17,700** ± 9,200	29,100 ± 11,200	4,600 ± 5,700	**46,800** ± 16,400	**51,400** ± 19,500
Total Measured	**17,820**			**64,741**	

B. Big Cobb River Annual Mud Loads (Mg/yr)					
Source	Above Upper Gauge	Between Gauges	Below Lower Gauge	Sum at Lower Gauge	Sum at confluence
Upland	4,900 ±1,5 00	5,900 ± 1,800	200 ± 60	10,800 ± 3,200	11,000 ± 3,300
Ravine	--	2,900 ± 1,400	2,100 ± 1,000	2,900 ± 1,400	5,000 ± 2,500
Bluff	300 ± 100	27,500 ± 10,600	16,000 ± 6,800	38,100 ± 10,700	54,100 ±17,500
Streambank	800 ± 1,600	12,300 ± 6,200	(5,200) ± 2,600	12,300 ± 6,200	7,100 ± 3,900
Total Predicted	**6,000** ± 3,200	48,500 ± 19,900	10,900 ± 10,500	**64,100** ± 21,500	**77,200** ± 27,200
Total Measured	**7,040**			**30,200**	

C. Le Sueur River Annual Mud Loads (Mg/yr)					
Source	Above Upper Gauge	Between Gauges	Below Lower Gauge	Sum at Lower Gauge	Sum at Red Jacket
Upland	28,800 ± 8,600	7,500 ± 2,300	1,000 ± 300	36,300 ± 10,900	62,300 ± 20,000
Ravine	--	5,100 ±2,500	4,400 ± 2,200	5,100 ± 2,600	20,000 ± 10,000
Bluff	4,700 ± 1,900	21,400 ± 8,400	31,900 ± 13,100	26,100 ±10,400	134,400 ± 23,400
Streambank	2,000 ± 4,000	7,900 ± 3,900	(1,800) ± 900	9,900 ± 3,900	17,800 ± 10,900
Total Predicted	**35,500** ± 14,600	41,900 ± 17,200	35,600 ±16,500	**77,400** ± 27,700	**234,400** ± 64,100
Total Measured	**63,900**			**83,200**	**224,900**

In the sediment budget, four major sediment sources were delineated: bluffs, ravines, streambanks, and uplands. To accommodate the local and episodic nature of bluff erosion, we use two different time and spatial scales to estimate sediment supply from bluffs. Bluff erosion rates over 67 years were calculated by measuring bluff crest retreat from aerial photographs. Retreat rates were measured for roughly half (243) of all 480 mapped bluffs in the watershed. Measured retreat rates were applied to un-measured bluffs using two up-scaling methods and accounting for bluff size, bluff location, channel migration rates, the presence of active toe erosion, aspect, and vegetation cover. Bluff retreat rates were converted to volumes using geometric data derived from airborne lidar DEMs. Locations and accompanying data on each bluff are in the bluff shapefile attribute table. At a local spatial scale and shorter time scale, we measured erosion rates for four years on a subset of bluffs using a high-resolution ground-based lidar scanner. Although highly accurate, these local measurements are more difficult to up-scale to the entire basin. Methods and estimates of uncertainty are discussed in chapter 6. Annual bluff sediment supply associated with each of the three methods (Table 6.3) is available in the sediment budget spreadsheet. The budget summarized in Table II.1 takes the average of the three predicted loads for each reach in the watershed. The average annual predicted sediment load from bluffs was 134,000 Mg/yr at the Red Jacket gauge.

Loads from ravines were calculated from direct monitoring of four ravines for up to three years each. Measured ravine loads scaled well with incised ravine area, both over the course of a monitoring season and within a single storm event. Thus, loads from each ravine monitoring season were up-scaled to the entire watershed based on incised ravine area as measured from airborne lidar data. Locations and accompanying data for all ravines are in the ravine shapefile attribute tables. Because ravines were not monitored for the same time period as the mainstem Le Sueur River, loads on the Le Sueur River were recalculated for the same monitoring period as the ravines, and the percent load attributed to ravines was determined. We applied the average percent load to the average total load at Red Jacket from 2000-2010 to determine a ravine load for the sediment budget and apportioned it to different reaches based on incised ravine area within each reach. The average annual predicted sediment load from ravines was 20,000 Mg/yr.

Channel and floodplain contributions are calculated as the sum of four components. Three of the components are sources: channel widening, channel incision, and channel migration (eroding banks tend to be taller than depositing banks and the difference represents a sediment source). The last component of the channel/floodplain balance is a sink: sediment deposited on top of floodplains (treated as a negative source). The source from meandering was determined from migration rates determined from 1938 and 2005 aerial photographs coupled with bank elevation data from the lidar DEM, so that only the portion of the cutbank higher than the point bar side of the channel is added as a source. Floodplains are small and scarce in the knick zone and floodplain deposition occurs primarily in the upper and lower channel segments in each watershed. Channel widening estimates were based on aerial photograph measurements throughout the Le Sueur and neighboring basins as well as the lower Minnesota River. Percentage widening rates were developed for each reach of the Le Sueur and multiplied by channel area to estimate the volume sediment source. Details are given in Chapter 7. Sediment derived from channel incision was estimated using the average incision rate from our hydraulic modeling of the Le Sueur River. Sediment sources from incision were added only within the knick zone. Net average annual contributions of fine sediment from channel and floodplain processes is estimated at 17,800 Mg/yr.

The upland sediment source is determined as a percentage of the upper gauge load, with the balance derived from channel/floodplain contributions, bluffs, and ravines. Sediment fingerprinting using a combination of ^{210}Pb, ^{137}Cs, and meteoric ^{10}Be on storm samples is used to estimate the percentage of the load at the upper gauges that derives from upland fields. Samples were collected from the Maple and Le Sueur Rivers. The Little Cobb River is assigned the same upland percentage as the Maple River due to similar surficial geology and upland relief. An option is included on the spreadsheet to assign the entire upper gauge load to uplands or to calculate the upland supply as the difference between at the load at the upper gauge less bluff, ravine, and channel inputs above the gauge. More information on upland sources can be found in chapter 4. The budget presented in Table II.1 uses sediment fingerprinting results to determine upland sediment loads. The average annual sediment load from the uplands is predicted to be 62,300 Mg/yr.

Gauging data with TSS loads are available from 2000-2010 on the Le Sueur River at Red Jacket. Gauging records for the remaining gauges cover shorter periods, with gauges coming on line in 2006 and 2007. One option for estimated loads is to use records in overlapping years to scale all gauging records to the 2000-2010 loads at Red Jacket. This period gives a wide range of conditions, including both dry and wet years, but requires the assumption that the proportional relation among sediment loads in the overlap period also holds for the remainder of the 11-year

record. A second option is to restrict the estimate of gauge loads to 2006-2009, the period for which we have direct measurements on all gauges except for the upper Le Sueur (St Clair) gauge, which was installed in 2007. Unfortunately, the 2006-2009 period is much drier than normal and cannot be used to represent mean loads under present conditions. A third option is to use the five-yr period 2006-2010, which includes the wet year, 2010. Not all of the 2010 loads have been calculated (as of June 30, 2011), so this is currently incomplete. Either 2000-2010 and 2006-2009 periods can be selected on the spreadsheet on the main worksheet ('Combo' page). The period selection does not change sediment supply for ravines, bluffs, and streambanks, but will change upland supply, which is calculated as a percent of the upper gauge loads. Thus, the "predicted loads" will change slightly, in addition to changing the "observed loads" to cover the time period of interest.

The spreadsheet also allows calculation of a sediment budget for the Holocene and late Pleistocene (ca. 13,400 years BP), in which sediment supply is calculated for pre-settlement conditions. Instead of anchoring the sediment sources to gauge records, the budget is compared to the estimated evacuation of sediment over the Holocene. This allows the user to compare modern to pre-settlement conditions. There is a larger uncertainty on these measurements that is not incorporated into the spreadsheet.

For all source estimates, there is uncertainty associated with the values used in the sediment budget. These are discussed in more detail in each chapter, but in the spreadsheet they are incorporated in order to allow the user to see the full range of possible loads. The user is able to set the load estimates to be the maximum or minimum based on the uncertainties specified, or to specify lowering or raising all sources by a fraction of the uncertainty (i.e. lower all sources within the knick zone by 10% of their respective uncertainties). This latter option was used to create the balanced budget seen in the initial 'Summary of Findings' section.

Lastly, the budget is set up to evaluate scenarios related to source reductions. Individual sources (ravines, bluffs, etc.) can be reduced by a user-specified amount and the change in total sediment yield is calculated. For example, what is the effect of reducing ravine erosion by 50% or bluff erosion by 25%? Reductions can be assigned to individual river segments.

The spreadsheet includes both numerical load predictions and a series of pie charts showing the break-down of total load by source for each tributary. Both sets of data are important to compare, and both can change with various adjustments. For example, Figure II.1 shows the results for the default case, with all sources set to 100% of their estimated value over the 2000-2010 time period. Note that the budget over-predicts the load at Red Jacket by 4% (pred/obs values). This budget was not created by attempting to balance sources off of each other, but simply to come up with the best estimates of "average" conditions in the modern environment for each source separately.

If a balanced budget is desired for this time period, then balancing can occur by reducing the predicted sources by a set percentage of their uncertainty. If all sources throughout the watershed are reduced by 9% of 1 standard deviation uncertainty (0.09σ), then the loads at Red Jacket balance (Figure II.2). Alternatively, the loads can be balanced both above and below the knick zone. This might be desirable because although the predicted load is within 5% of the measured monitoring season loads, there is a substantial underestimation of sediment loading at the upper gauges, particularly on the upper Le Sueur River gauge at St. Clair. Because loads were underpredicted at the upper gauges, this balance requires increasing load estimates by 1.12 σ above the knick zone (heavily dominated by upland sediment) and reducing load estimates by 0.47 σ within and below the knick zone (heavily dominated by bluff erosion). The end result is an increase in the percent upland and a decrease in the percent bluff (see Figure II.3).

The last example we put forth involves a scenario where funding can be allocated either towards lowering ravine loads 75% or lowering bluff loads just in the lower valley below the gauges by 25%. Which will have the greatest impact on loads at Red Jacket? These scenarios can be examined by simply changing the total load, by source, on the spreadsheet. In the first scenario, we enter 0.25 in the ravine cells in rows 61, 67 and 73. In the second scenario, we return the ravine cells to "1" (100%) and change the bluff cells in row 62, 68, and 74 to 0.75. Lowering ravine loads by 75% throughout the entire basin will drop the load at Red Jacket from 234,000 to 219,000 Mg/yr. Lowering bluff loads by 25% below the gauges has a similar effect, dropping loads to 220,000 Mg/yr.

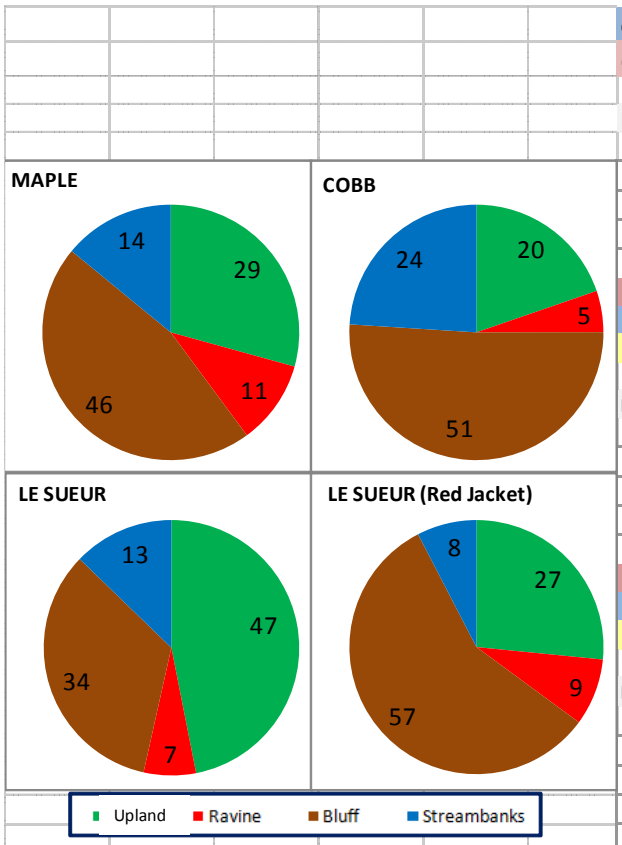

Cells in blus are observed monitoring season loads

Cells in pink are predicted annual loads.

Maple River Annual Mud Loads (Mg/yr)

AB UG	BTWN Gages	BL LG	SUM @ LG	SUM @ conf	
12,478	1,221	214	13,699	13,913	U
1,338	3,610	517	4,947	5,464	R
2,320	19,233	8,773	21,553	30,327	B
1,516	5,065	(4,865)	6,581	1,716	S
17,651	29,129	4,640	**46,780**	**51,420**	
17,826	obs	obs	64,761		
0.99	pred/obs	pred/obs	0.72		

Big Cobb River Annual Mud Loads (Mg/yr)

AB UG	BTWN Gages	BL LG	SUM @ LG	SUM @ conf	
4,929	5,865	213	10,795	11,008	U
-	2,883	2,093	2,883	4,977	R
277	27,667	18,167	27,943	46,110	B
811	12,329	(5,195)	13,140	7,945	S
6,017	48,744	15,278	**54,761**	**70,039**	
7,042	obs	obs	30,210		
0.85	pred/obs	pred/obs	1.81		

Le Sueur River Annual Mud Loads (Mg/yr)

AB UG	BTWN Gages	BL LG	SUM @ LG	SUM @ Rd Jckt	
28,766	7,533	1,043	36,299	62,262	U
29	5,073	4,434	5,102	19,977	R
4,743	21,367	31,867	26,110	134,413	B
1,996	7,881	(1,752)	9,877	17,786	S
35,535	41,853	35,591	**77,388**	**234,439**	
63,924	obs	obs	83,190	224,932	
0.56	pred/obs	pred/obs	0.93	1.04	

Figure II.1. Default conditions for sediment budget. All sources include full estimated values. Observations come from gauging records from 2000-2010, or records scaled to 2000-2010. (On the far right, U = Upland; R = Ravine; B = Bluff; and S = Streambank and Floodplain combined.)

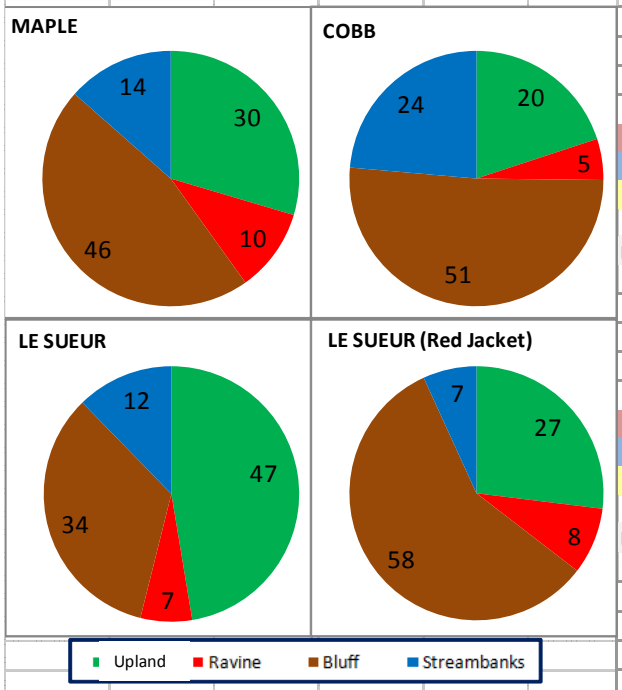

Cells in blus are observed monitoring season loads

Cells in pink are predicted annual loads.

Maple River Annual Mud Loads (Mg/yr)

AB UG	BTWN Gages	BL LG	SUM @ LG	SUM @ conf	
12,141	1,188	208	13,329	13,537	U
1,278	3,447	494	4,725	5,218	R
2,249	18,651	8,507	20,900	29,407	B
1,246	4,837	(5,084)	6,083	999	S
16,914	28,123	4,125	**45,037**	**49,162**	
17,826	obs	obs	64,761		
0.95	pred/obs	pred/obs	0.70		

Big Cobb River Annual Mud Loads (Mg/yr)

AB UG	BTWN Gages	BL LG	SUM @ LG	SUM @ conf	
4,796	5,707	207	10,503	10,710	U
-	2,754	1,999	2,754	4,753	R
267	26,715	17,552	26,982	44,533	B
667	11,774	(5,429)	12,441	7,012	S
5,730	46,950	14,329	**52,680**	**67,009**	
7,042	obs	obs	30,210		
0.81	pred/obs	pred/obs	1.74		

Le Sueur River Annual Mud Loads (Mg/yr)

AB UG	BTWN Gages	BL LG	SUM @ LG	SUM @ Rd Jckt	
27,990	7,330	1,014	35,319	60,582	U
28	4,844	4,234	4,872	19,078	R
4,571	20,606	30,692	25,177	129,809	B
1,636	7,526	(1,830)	9,162	15,344	S
34,225	40,306	34,110	**74,531**	**224,812**	
63,924	obs	obs	83,190	224,932	
0.54	pred/obs	pred/obs	0.90	1.00	

Figure II.2. The same budget as in Figure II.1, although all sources in the knick zone (below the upper gauge) have been reduced by 9% of their one sigma uncertainty. Note that the loads at Red Jacket now match, although the source allocation by percent has not changed substantially.

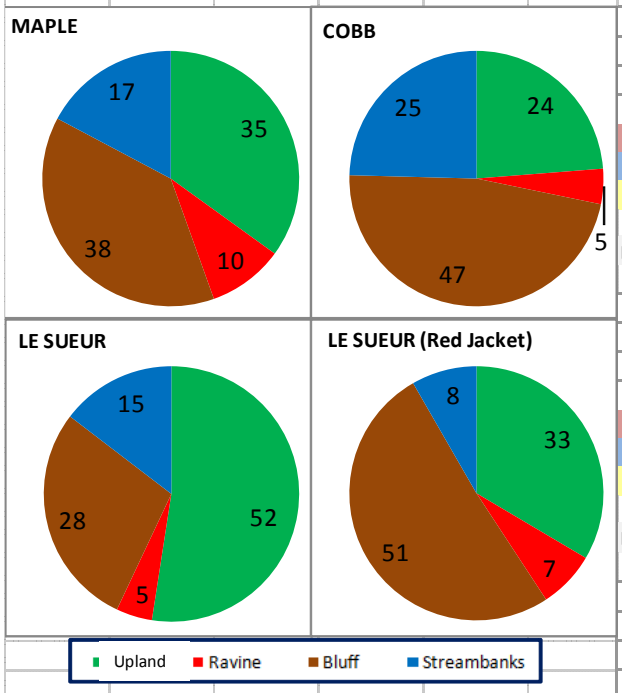

Cells in blus are observed monitoring season loads

Cells in pink are predicted annual loads.

Maple River Annual Mud Loads (Mg/yr)

AB UG	BTWN Gages	BL LG	SUM @ LG	SUM @ conf	
16,669	1,049	184	17,718	17,902	U
2,087	2,762	395	4,848	5,244	R
3,198	16,191	7,381	19,389	26,770	B
4,876	3,875	(6,008)	8,750	2,743	S
26,830	23,876	1,953	**50,706**	**52,659**	
17,826	obs	obs	64,761		
1.51	pred/obs	pred/obs	0.78		

Big Cobb River Annual Mud Loads (Mg/yr)

AB UG	BTWN Gages	BL LG	SUM @ LG	SUM @ conf	
6,585	5,038	183	11,624	11,807	U
-	2,206	1,602	2,206	3,808	R
398	22,695	14,954	23,093	38,047	B
2,603	9,432	(6,416)	12,035	5,619	S
9,586	39,372	10,323	**48,957**	**59,280**	
7,042	obs	obs	30,210		
1.36	pred/obs	pred/obs	1.62		

Le Sueur River Annual Mud Loads (Mg/yr)

AB UG	BTWN Gages	BL LG	SUM @ LG	SUM @ Rd Jckt	
38,428	6,471	896	44,900	75,504	U
46	3,881	3,392	3,927	16,370	R
6,888	17,393	25,732	24,281	114,831	B
6,476	6,029	(2,163)	12,505	18,703	S
51,838	33,774	27,856	**85,613**	**225,408**	
63,924	obs	obs	83,190	224,932	
0.81	pred/obs	pred/obs	1.03	1.00	

Figure II.3. The same budget as in Figure II.1, although now the sources have been balanced at both the upper gauges (in sum) and at Red Jacket. Because loads were underpredicted at the upper gauges, this balance requires increasing load estimates by 1.12 σ above the knick zone (heavily dominated by upland sediment) and reducing load estimates by 0.47 σ within and below the knick zone (heavily dominated by bluff erosion). The end result is an increase in the percent upland and a decrease in the percent bluff.

4. Uplands

Background:

The Le Sueur River covers 2,880 km^2 of primarily agricultural land use (84%) (Kudelka, 2010), the vast majority of which is in row crops. There are no major urban areas, although the municipality of Mankato is expanding into the northern portion of the watershed. Two major changes to the landscape have occurred in the last 200 years: conversion of original prairie to agriculture and alterations to the basin hydrology (see Section 1 for more details).

The role of tile drainage in altering the hydrology of a large basin is still poorly understood (Blann et al., 2009). Most studies occur at the plot scale, and translating the results up to the scale of a large basin is more complex. At the plot scale, tile drainage tends to increase rapid drainage during storm events through surface inlets and macropores in the unsaturated soil zone (Magdalene, 2004; Chapman et al., 2005). Magdalene (2004) found that drainage responded to precipitation events within minutes to hours, even in areas without surface inlets. In addition, surface inlets provide a direct route for surface runoff to reach tile drains. Although tile drains do decrease surface runoff, many are installed in areas that would have poor drainage (and thus little surface runoff) anyway. Tile drainage thus decreases surface runoff but increases the rapidity with which flow reaches channels. Research on similar streams in Iowa found that storm flows, annual baseflows, and minimum flows have commonly increased over the second half of the 20^{th} century, and the increase is more than can be accounted for by climatic changes. The hydrologic change has been attributed to artificial drainage and incision and widening of streams (Schilling and Libra, 2003; Zhang and Schilling, 2006; Schilling and Helmers, 2008).

The role of tile drainage on sediment yields coming from the uplands depends quite heavily on the type of tile drainage installed. Surface inlets carry a disproportionate amount of sediment into tile lines. In Magdalene's (2004) study, subsurface drainage carried 90% of the water but only 60% of the sediment while surface runoff into tile inlets carried 10% of the water but 40% of the sediment load. Most of the annual sediment (77-92%) and water discharge came from storm events (Magdalene, 2004). Sediment enters tile drains through inlets or settles in pipes and is flushed during the next storm event (Schilling and Helmers, 2008). Stone and Krishnappan (2002) found that tile drains contributed 18% of the total sediment load. Two studies in the United Kingdom found that 27-55% and 25-55% of the basin sediment yield could be attributed to tile drainage (Chapman et al., 2005, Russell et al. 2001). Other studies have found very little sediment coming from tile drains (i.e., on-going MDA study). These variable rates of sediment flux from tile drains, including subsurface tiles, could have a large effect on both the sediment budget for the watershed and interpretation of sediment fingerprinting results.

Upland erosion comes from a combination of erosion from direct precipitation and overland flow, erosion from concentrated flow in rills or gullies, and wind-blown erosion. Tile drains also contribute both surface sediment produced by the above processes and sediment entering the pipeline in the subsurface. Agricultural ditches in the uplands connect upland fields to the stream network, but we treat them as upland sediment sources here. Ditches are periodically cleaned out, with sediment from the ditches returning to the fields.

Much of the sediment eroded from upland sources is deposited nearby and never reaches the channel network. Thus, it is not just the erosion rate that is of prime importance, it is also the sediment delivery ratio (SDR), calculated as the ratio between the mass of sediment transported past a given point in the river and the total mass of sediment eroded in the landscape. Fields adjacent to channels will have a higher SDR and contribute more to the sediment load in the

mainstem channel than similar fields not adjacent to a channel. Ditch cleaning is another process that reduces the SDR from uplands to mainstem channel, though the amount of sediment removed from the ditches as a result of the cleaning process is not documented. It is likely that the upland/ditch SDR would differ for sand versus mud.

Methods:

To address upland erosion, we are using a multi-prong approach to get spatially-averaged erosion rates for the uplands that combine all of the above-mentioned sediment erosion and delivery mechanisms. The simplest method we have used to determine upland sediment yields is simply to look at sediment loads delivered to upstream gauges. This essentially provides an upper bound on the sediment delivered from uplands to the mainstem channel, although the upland yield could increase further downstream as relief increases.

A second measure of upland erosion comes from ravine gauging. In 2008, we installed 3 ISCO autosamplers on ravines in the lower Le Sueur valley. This work was conducted with Scott Matteson at Minnesota State University at Mankato. On one of the ravines, samplers were installed at both the top and the bottom of the ravine. The upper sampler (RavU90) had only 10 meters of relief (compared with 40 m of relief at the lower samplers), and we have used it as a proxy for sediment coming from the uplands being delivered to ravines. This ravineshed has no surface tile inlets, which should be taken into consideration when comparing the rates of upland erosion and sediment delivery there to other measures. We have upland sediment yields for that ravineshed in 2008, 2009, and 2010. In 2009, two more samplers were installed, with one of them placed near the top of a second ravine (Rav22S). Thus, we have two more years of yield from that upper ravine sampler.

We also used sediment fingerprinting to determine the amount of sediment derived from uplands versus non-upland sources over the course of individual storm events. We used natural geochemical tracers Beryllium-10 (^{10}Be), Lead-210 (^{210}Pb), and Cesium-137 (^{137}Cs). Beryllium-10 and ^{210}Pb are both perpetually produced in the atmosphere, delivered via dry deposition and/or during rain events, and adsorb tightly to soil particles within the top 5-10 and 150 cm of the soil profile for ^{210}Pb and ^{10}Be, respectively. Cesium-137 was delivered primarily as a result of nuclear bomb testing ~ 1955 to 1963 (Robbins et al. 2000). The primary benefit to using this suite of tracers is that they have well constrained production rates and disparate radioactive decay rates (22.3, 30, and 1,400,000 years for ^{210}Pb, ^{137}Cs, and ^{10}Be, respectively), allowing us to use them to study both erosional and depositional processes. For more detailed discussion of sediment fingerprinting using ^{210}Pb and ^{137}Cs the reader should be directed to Schottler et al. (2010). For detailed explanation of ^{10}Be systematics the reader is directed to Willenbring and VonBlanckenburg (2010).

Results:

The upper gauge TSS data suggest an upland yield of 4.3 – 16.6 Mg/km^2 in the Maple, 4.7-13.2 Mg/km^2 in the Little Cobb, and 4.9-48.5 Mg/km^2 in the upper Le Sueur above St. Clair (see Table 4.1). The yields calculated from the RavU90 sampler were the lowest of all, ranging from 0.7 – 21.1 Mg/km^2. All yields in 2009 were low due to the dry conditions that year. At the time of writing the only upland yields we have come from the upper ravine samplers, which were substantially higher in 2010 than in 2009.

Table 4.1: Upland yields in the Le Sueur River basin from gauging

Basin	Upstream Area (km^2)	Sediment Yields (Mg/km^2)				
		2006	2007	2008	2009	2010
Upper Maple	800	9.8	16.6	7.5	4.3	
Little Cobb	335	11.8	13.2	9.1	4.7	
Upper Le Sueur	870	N/A	48.5	25.7	4.9	
RavU90*	2.7	N/A	N/A	5.1	0.7	21.1
Rav22S*	2.4	N/A	N/A	N/A	0.04*	96.5

**RavU90 and Rav22S yields come from upper samplers in ravines, with 10-13 m of relief, so they contain some "ravine" sediment in addition to upland sediment. In addition, Rav22S was not operational until June 2009.*

The lowest measure of upland sediment yield came from the ravines in 2008 and 2009. RavU90 did not have any surface tile inlets, so water running into the ravine from tile lines was likely low in sediment. Research done on sediment loads in tile lines has found significantly higher sediment loads in tile lines with surface inlets when compared with those that only have subsurface drainage (i.e. Magdalene 2004). In 2009, we set up a sampler high in a second ravine (Rav22S), giving it a similar amount of relief as compared with the RavU90. If we make the assumption that all sediment measured at the gauge in the upper end of that ravine was derived from uplands, the "upland" sediment yield is 0.04 Mg/km^2 in 2009 and 96.5 Mg/km^2 in 2010. The 2009 data started in June 2009, missing the spring runoff. This accounts for the exceedingly low yield in 2009.

The upstream gauges on the Le Sueur, Maple, and Little Cobb show that sediment yield from the upper Le Sueur is high compared to the Maple and Cobb data. The eastern part of the basin has a different underlying geology (tills instead of glaciolacustrine deposits) and more hummocky topography (see Figure 4.1).

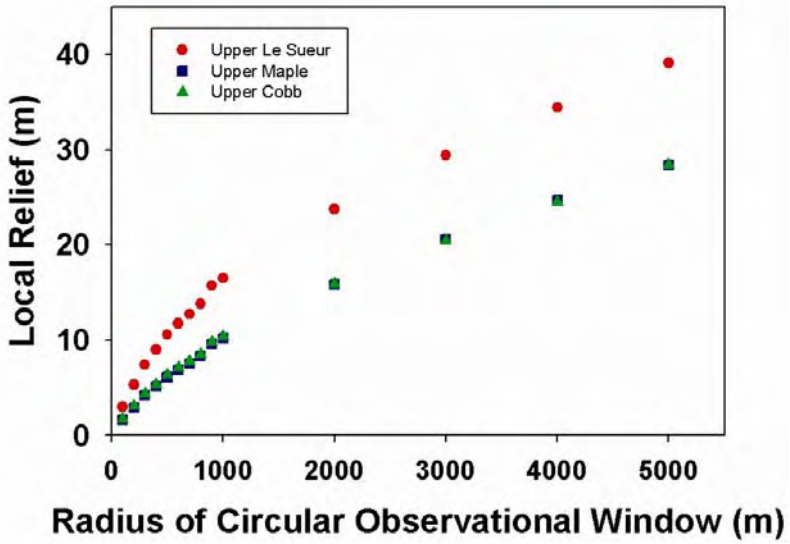

Figure 4.1: Local relief in the Le Sueur, Maple, and Little Cobb, upstream of the upper gauges in each basin. We used an increasing window of observation to see if relief was scale dependent, and at all spatial scales, the Upper Le Sueur had higher relief than the Little Cobb or Upper Maple.

Using the upland yields presented here, we can derive what percentage of total sediment load is derived from upland sources vs. other sources in the Le Sueur. If we take the upper

gauge to be 100% upland sediment (clearly an upper bound only) and apply that sediment yield to the basin area at the lower gauge, we get an upper bound for the percentage upland sediment. This measurement is sensitive to the assumption that all of the sediment entering the upper sampler is derived from the uplands, not from ravines, bluffs, or streambanks, and this assumption is clearly not accurate for all basins. In addition, it assumes that the sediment delivery ratio does not increase when the mainstem channels enter the knick zone and relief increases.

The percent upland derived from this calculation and applied to the lower gauges using 2006-2009 data gives upland % contributions of 17% on the Maple, 12% on the Cobb, and 44% on the Le Sueur, with 20% upland contribution at Red Jacket. Using gauging records extrapolated out to cover 2000-2010 (using Red Jacket record for scaling loads) gives higher upper gauge loads and thus higher upland contributions: 32% on the Maple, 22% on the Cobb, and 64% on the Le Sueur, with an integrated upland contribution of 36% at Red Jacket. The same analysis applied to several other Minnesota River tributaries shows that the percent estimated to be coming from the uplands is lower in Seven Mile Creek, High Island Creek, and Rush Creek and much higher (70%) on the Cottonwood River, relative to the proportion derived from uplands in the Le Sueur (see chapter 3).

The estimates generated from this yield extrapolation exercise are generally higher than those determined through sediment fingerprinting by Schottler et al., (2010), which shows fairly consistent percent upland contributions ranging from 15%-40% across the Minnesota River basin (see Figure A.9 in Appendix A). These differing results indicate that either there are significant net contributions from streambanks, ravines, or bluffs above the upper gauges and thus our upper bound estimate of 100% upper gauge sediment is indeed too high, or that there are inherent biases in the sediment fingerprinting work that must be quantified and corrected. Thus, we use multiple sediment fingerprinting tracers to better constrain this % upland term (see below).

One potential source of bias in the ^{210}Pb and ^{137}Cs fingerprinting estimates is exchange of sediment between the channel and floodplains. Figure 4.2 shows a simple example of how channel-floodplain exchange can bias estimates of sediment apportionment when two conditions are met a) some significant portion of the sediment in transport is temporarily stored (and released) from floodplains, and b) the half-life of the tracer is much shorter than the average residence time of sediment in the floodplain. The scenario in the figure depicts a case in which 100 units (e.g., Mg) of sediment are contributed to a stream, derived entirely from uplands, which have a tracer concentration of 10 (e.g., 10 atoms of our tracer per gram of sediment). During channel transport, X units of that sediment are deposited in floodplains. Assuming this is a steady state process (i.e., 100 units with a concentration of 10 are contributed to the channel every year and X units are transferred to the floodplain, the concentration of the tracer in the floodplains goes to zero if the half-life of the tracer is much shorter than the average residence time of sediment in the floodplain (as is the case for ^{210}Pb and ^{137}Cs). Again, for the sake of simplicity, we assume that the same amount of sediment (X units) is contributed back from the floodplains to the channel, restoring our total load of 100 units measured at a gauging station. In this scenario, the sediment apportionment would be based on the concentration equation in the blue box to the right (at the gauge) and is entirely dependent on X, the channel-floodplain exchange amount.

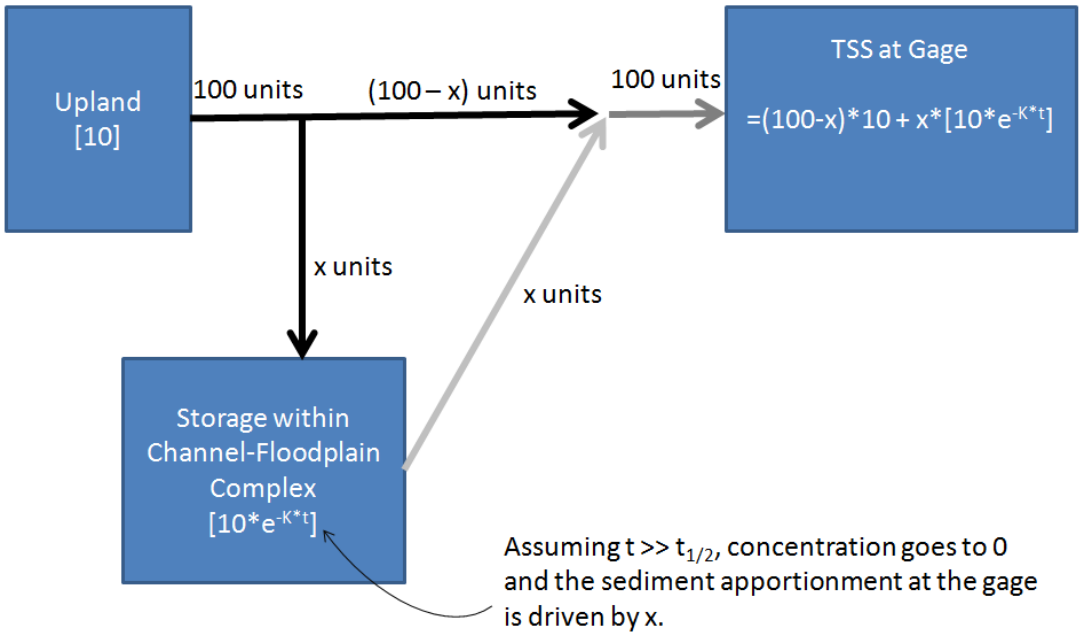

Figure 4.2. Simple scenario depicting the potential dilution effect that occurs for short-lived radionuclide tracers in systems where the channel and floodplain actively exchange sediment.

Most real river systems have significantly more complexity in terms of additional sediment sources, spatial heterogeneity in source tracer concentrations, and unsteadiness in time. Nevertheless, Figure 4.2 demonstrates the potential for this bias. Using a radiogenic tracer that has a half-life that is much longer than the residence time of sediment in the floodplain circumvents this problem and for this reason we have chosen to use meteoric ^{10}Be as a sediment fingerprinting tracer (half-life 1.4 million years). However, long-lived tracers have a different set of caveats. First, the fact that ^{10}Be does not decay in the floodplains means that floodplain and upland sources have very similar concentrations, meaning they cannot be readily distinguished by ^{10}Be concentration alone (in contrast to bluffs and ravines, which have significantly lower concentrations). Second, production of ^{10}Be is perpetual, so the concentration of ^{10}Be will increase with storage time in floodplains. Both of these bias estimates toward the high end in contrast to the dilution effect of ^{210}Pb and ^{137}Cs, which tend to bias estimates to the low end. For this reason, it is most useful to use them in combination.

We built on the extensive ^{210}Pb and ^{137}Cs research that has been completed by Schottler et al., (2010) to determine source fingerprints for these tracers. To constrain the agricultural field fingerprint for ^{10}Be we collected sediment samples from agricultural fields and bluffs, which represent the end member source areas in terms of tracer concentrations. Consistent with expectations, bluffs have a very low concentration ([^{10}Be] = 0.07 (± .01) x 10^8 atoms g^{-1}; n =4) and agricultural fields have a high concentration ([^{10}Be] = 2.0 (± .36) x 10^8 atoms g^{-1} n = 5). From these two end members we can use the ^{10}Be concentration measured in suspended sediment samples collected during storm events to estimate the proportion of the suspended sediment that was derived from agricultural fields.

We collected a total of 28 suspended sediment samples during the 2009 field season, mostly from the Maple River. Stream flow during the 2009 season was among the lowest on record since 1938. The hydrograph and hyetograph for the monitoring season (March 27 – Nov 12) at the Lower Maple River gauge is shown in Figure 4.3 (top panel). Only one significant

runoff event occurred during the year, June 22-29. The portion of the annual hydrograph bounded by dashed lines is included in the lower two panels. We collected samples for ^{210}Pb and ^{10}Be analysis at the Upper Maple (UM) and Lower Maple (LM) gauging stations at each of the times indicated by triangles in the middle panel of Figure 4.3. The bottom panel shows TSS concentrations (data from Water Resources Center) and hourly suspended sediment loads throughout the event. Our samples cover the duration of the event that transported most of the suspended sediment.

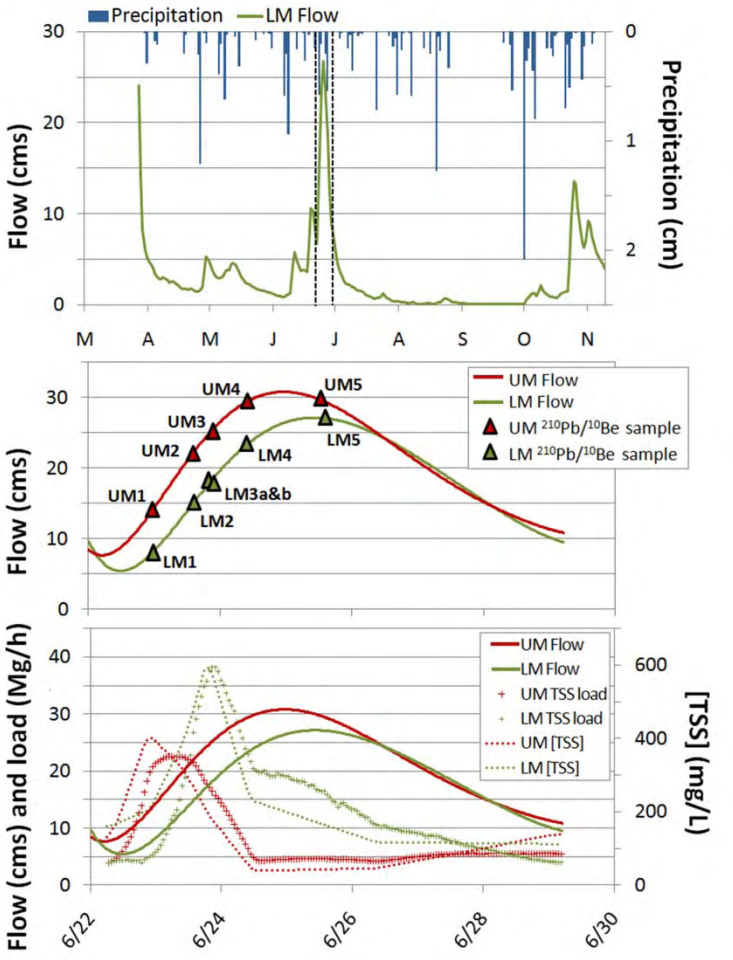

Figure 4.3. Flow (top), sample collection times (middle) and sediment concentration/load data (bottom) for the June 2009 event for which fingerprinting samples were collected. LM refers to Lower Maple gauge, and UM refers to the Upper Maple gauge.

We have plotted ^{10}Be and ^{210}Pb concentrations in Figure 4.4. Samples collected from the upper and lower sites show systematic differences in concentration of the two tracers. Using simple two end-member mixing models for each of the tracers independently we obtain slightly different estimates for the percentage of suspended sediment derived from fields (Figure 4.5). Three observations can be made from these two plots. First, the ^{10}Be concentrations uniformly suggest a higher concentration of field-derived sediment, indicating that channel-floodplain exchange is occurring (enriching ^{10}Be and diluting ^{210}Pb). Second, in general the concentrations measured at the Upper Maple gauge (above the knickpoint) relative to the Lower Maple gauge (within the knick zone) suggest a high proportion of field-derived sediment contributed above

the knickpoint. Third, low concentrations of both ^{210}Pb and ^{10}Be for the second and fifth samples collected at the Lower Maple gauge may indicate two pulses of bluff sediment contributed between the gauges. The disparity between ^{210}Pb and ^{10}Be for numerous samples indicates a significant contribution from banks during this particular event. These results represent the sediment dynamics for a single event during an anomalously dry year. Most of this work was funded by the Minnesota Department of Agriculture. Ongoing and future work will determine longer-term trends and variability of sediment sources in response to different stream flow events. Future modeling work will reconcile differences in ^{210}Pb and ^{10}Be percent-field estimates by accounting for tracer production and decay as well as exchange of tracers between the channel and floodplain (Viparelli et al., in review).

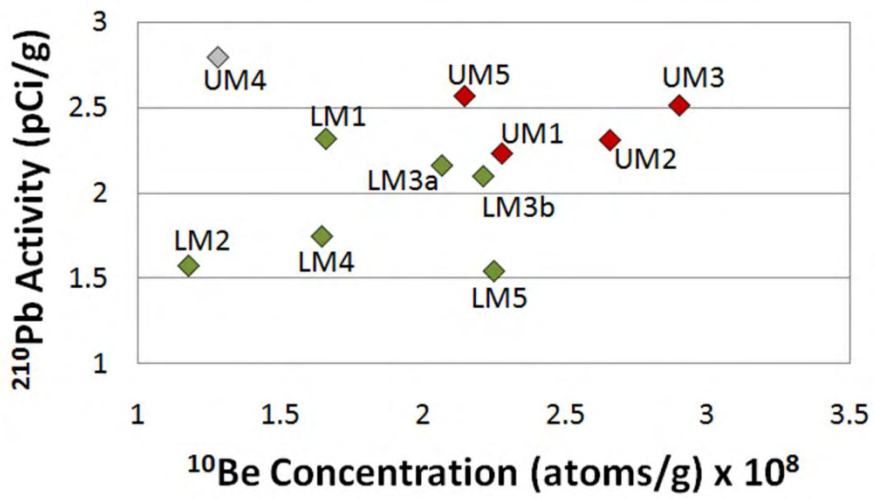

Figure 4.4. Beryllium-10 and ^{210}Pb concentrations measured in suspended sediment samples collected from the Upper Maple (UM) and Lower Maple (LM) gauging stations.

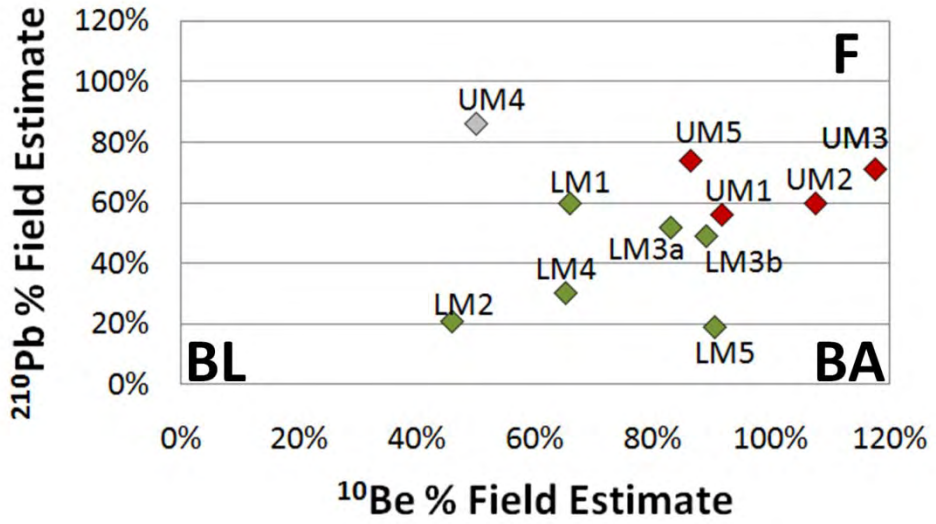

Figure 4.5. Estimates of percent field based on the ^{10}Be and ^{210}Pb fingerprints for in suspended sediment samples collected from the Upper Maple (UM) and Lower Maple (LM) gauging stations. The end-member sources, agricultural fields (F), bluffs (BL) and streambanks (BA) are labeled.

5. Ravines

Background:

Overland flow leads to erosion in the uplands, but the power of that overland flow increases when it concentrates into rills, gullies, and eventually large ravines. Ravines can erode rapidly, with steep, near vertical headcuts at the ravine tips. As ravines incise, hillslopes respond through erosion, widening the ravine. Many ravines in the Le Sueur River basin have threshold side slopes, meaning that incision or widening of the channel at the bottom of the ravine will lead to oversteepening of hillslopes and additional erosion as side slopes adjust.

Ravines not only act as sources of sediment, but they can also store sediment. One event may contribute large amounts of sediment to the river as it evacuates the stored sediment, while a later event of a similar magnitude may contribute far less sediment to the river, because less stored sediment is available. This storage can be temporary, lasting only from one event to the next, or more long-term tied to climate cycles rather than individual events. In the Le Sueur watershed, many episodes of ravine cut and fill appear to be tied to terrace formation at the mouth of ravines and subsequent incision through the terraces to reach the river below.

The timing of storm events plays an important role in ravine erosion. Freeze-thaw processes driven by temperature variations in the winter and spring disrupt the soil structure on the steep ravine hillslopes, which increases the probability of landslides. Once crops are up and the canopy is closed, not only is the surface less susceptible to erosion, but the crops evapotranspire a much greater percentage of total precipitation. Runoff rates drop substantially and ravines are often dry throughout late summer and early fall. Because ravine erosion and sediment transport is tightly coupled to hydrology in the ravines, there is concern that additional flow from subsurface drainage outlets that flow directly into ravines could increase the rate of erosion and sediment transport within these features. Our goal here was to determine how much suspended sediment is derived from ravines in the context of the Le Sueur River sediment budget.

Methods:

We employed three main approaches to studying ravines over different spatial and temporal scales. We used airborne lidar to map ravine locations throughout Blue Earth county and amass a database of ravine metrics. We then compared historical air photos from 1938 and 2005 to look for changes in ravine tip location over decadal scales. Finally, we monitored four ravines for up to three years to compute sediment loads during the ravine monitoring season. These loads are compared in a variety of ways to loads on the mainstem Le Sueur River to determine the overall contribution of ravine sediment.

The airborne lidar has proven very useful in mapping ravine locations. The change in slope between relatively flat uplands and the steep ravine walls is easy to delineate with high-resolution topographic data. Locations of major ravines were mapped throughout the entire basin and calculations made of incised ravine area, volume excavated, river kilometer location, relief, elevation, ravine channel length, and mean slope for all major ravines. It was also noted whether or not ravines cut all the way down to the mainstem river or ended on a higher terrace. This affects whether or not ravines are likely supplying sediment directly to the river, or depositing it in a fan on a terrace.

The total volume of material removed from ravines since the Le Sueur River valley first began to form was calculated from lidar inventories. The paleosurface elevation of each ravine

was determined using the average of 10 upland surface elevations surrounding the ravine, and the mass of material missing calculated through direct subtraction. These volumes were converted into mass using a till bulk density of 1.8 Mg m^{-3} (Thoma et al., 2005). To compare with TSS measurements, we assumed that only the silt and clay fractions (65% of the total mass based on till grain size analyses) move downstream as suspended load. This mass could then be compared to TSS loads from modern gauging efforts.

The second approach compared historical air photos to look for ravine elongation over a 67-year time period. We mapped 69 ravines in the Maple and Le Sueur Rivers and compared the location of ravine tips in 1938 and 2005. The 1938 photos were scanned in and georeferenced. The 2005 photos were already orthorectified and georeferenced. Georeferencing error is approximately ± 10 m, so ravine tip change needs to be greater than this to be measured using this technique. Given the error associated with georeferencing and the uncertainty identifying ravine tips, this analysis can only provide information on whether ravine tips had developed where there were none, expanded significantly, or reduced in size significantly. We did not assign quantitative measures of ravine change. In addition, this analysis looked at ravine tip changes only, not changes related to ravine incision or widening.

The third approach involved event monitoring of two ravines in 2008 and four ravines during 2009 and 2010 using ISCO and Sigma autosamplers. The four ravines are located about 6 kilometers south of the city of Mankato. The headcut of one of the study ravines is located south of Highway 90 (195th St., Hwy-90) and continues south parallel to State Route 22 (SR-22) to join the Le Sueur River. The second ravine starts few meters west of County Road- 8 (Monks Ave., CR-8) continues southwards and joins the Le Sueur River. In this report the ravine on Highway 90 is denoted as Rav90 and the second ravine as Rav8. The third and fourth ravines are located closer to SR-22, one on the north side of the Le Sueur River (Rav22N) along SR-22 and one of the south side (Rav22S) just to the west of SR-22.

We worked with Scott Matteson at Minnesota State University to install three ISCO and two Sigma autosamplers. Samplers were installed near the mouth of three ravines (Rav8, Rav22N, and Rav90). Rav22S had the sampler installed higher up in the ravine to measure contributions under conditions of low relief with a large drainage area. Rav90 had two samplers installed: one at the mouth (RavL90) and one near the top (RavU90). This paired installation allowed calculation of the percentage of sediment being picked up in the ravine itself vs. the percentage arriving from the uplands. The RavU90 sampler had about 10 m of relief and the lower samplers had 29-47 m of upstream relief. Table 5.1 summarizes physical characteristics of all five sites. Figure 5.1 shows locations of all ravine samplers.

Figure 5.1: Map showing general locations of all five samplers (image from Google Earth™).

Table 5.1: Sampler information

	RavU90	RavL90	Rav8	Rav22N	Rav22S
Drainage Area (ha)	274	400	436	97	235
Incised Ravine Area (ha)	4.7	31.2	47.1	13.7	3.6
Upland Area (ha)	270	369	389	84	231
Relief (m)	12	42	47	29	14

The initial sites, RavU90 and Rav8, were installed in late spring 2008 with ISCO 6712 samplers. The samplers were equipped with area-velocity meters and installed in culverts with a head drop at the outlet. They recorded 15-minute stage and velocity measurements that were converted to discharge measurements. The RavL90 site was also installed in late spring 2008, using an ISCO 6712 sampler without an area-velocity meter. In spring 2009 monitoring activities were expanded to two smaller nearby ravines, Rav22N and Rav22S, and Sigma 900 Max samplers were installed. Like the sampler on RavL90, the Sigma 900 Max samplers recorded level only and had to be calibrated for discharge using a rating curve developed at each

site. Table 5.2 provides the flow and water sample collection monitoring season for each of the sites.

Table 5.2: Monitoring seasons for ravines, 2008-2010.

Year	Type	RavU90	RavL90	Rav8	Rav22N	Rav22S
2008	Flow	4/21-9/30		5/9-9/30		
	Samples	5/29-9/30	5/29-9/30	5/29-9/30		
2009	Flow	3/25-10/31		3/23-10/31	4/8-10/31	4/9-10/31
	Samples	3/25-10/31	3/23-10/31	3/23-10/31	6/1-10/31	6/1-10/31
2010	Flow	3/22-8/31		3/9-8/31		3/22-8/31
	Samples	3/22-8/31	3/22-8/31	3/9-8/31		3/22-8/31

Ravine monitoring stations were set to trigger when the water level rose 2.4 cm (0.1 feet) above base flow. Water samples were collected throughout the hydrograph, usually in one hour intervals for a 24 hour period. Samples were analyzed for total suspended solids (TSS) using standard laboratory techniques at Minnesota Valley Testing Laboratory (MVTL) in New Ulm, Minnesota. A subset were also analyzed for turbidity, TSVS, TP, PO_4, and Nitrate at MVTL.

Seasonal and storm event TSS loads during the monitoring season were calculated for each site using discharge and TSS concentrations with an assumed background TSS concentration of 5 mg/l. Loads from ravines were compared with loads calculated on the mainstem Le Sueur River for the same monitoring periods. Since ravines were only significantly turbid (>20 mg/L TSS) during and immediately following snowmelt and storm event periods, we also compared the TSS load on the mainstem Le Sueur River at times when ravines were actively turbid vs. times when ravines were flowing relatively clear or not actively flowing. Comparisons between ravine monitoring stations were done to assess which ravine metrics were most closely correlated with the mass of sediment exported over storms and over the monitoring season. An additional comparison was made between the paired samples on Rav90 to determine what percentage of sediment was derived from the uplands vs. what percentage was picked up within the incised ravine itself.

In 2009, we monitored four different ravines, of varying size and relief. We compared the total drainage area, relief, incised ravine area, and average slope with computed sediment loads over the time period when all monitoring stations were operational and over an individual storm event on June 8, 2009. The strongest correlation with TSS load was incised ravine area (R^2=0.98). Watershed area was more weakly correlated with sediment loads (R^2=0.69 for monitoring season and 0.78 for the 6/8/09 storm). Thus, to extrapolate loads measured on the monitored ravines up to the scale of the entire watershed, we used incised ravine area.

Results:

lidar mapping:

From the lidar DEM data, we mapped ravine locations and calculated ravine area, volume, steepness, river kilometer location, relief, elevation, channel lengths, and mean slopes for ravines within the Le Sueur watershed, with the most extensive data collection on the Maple and subsets of attributes collected on the Cobb and Le Sueur. We found relationships between location (distance upstream) and total relief (Figure 5.2), maximum ravine tip length (Figure 5.2), mean slope (Figure 5.3), and ravine volume (Figure 5.3). The longest and most developed ravines are closest to the outlet and experienced base level fall first and most dramatically. The

average tip migration rate is 0.15 m/yr based on maximum ravine tip length and distance upstream.

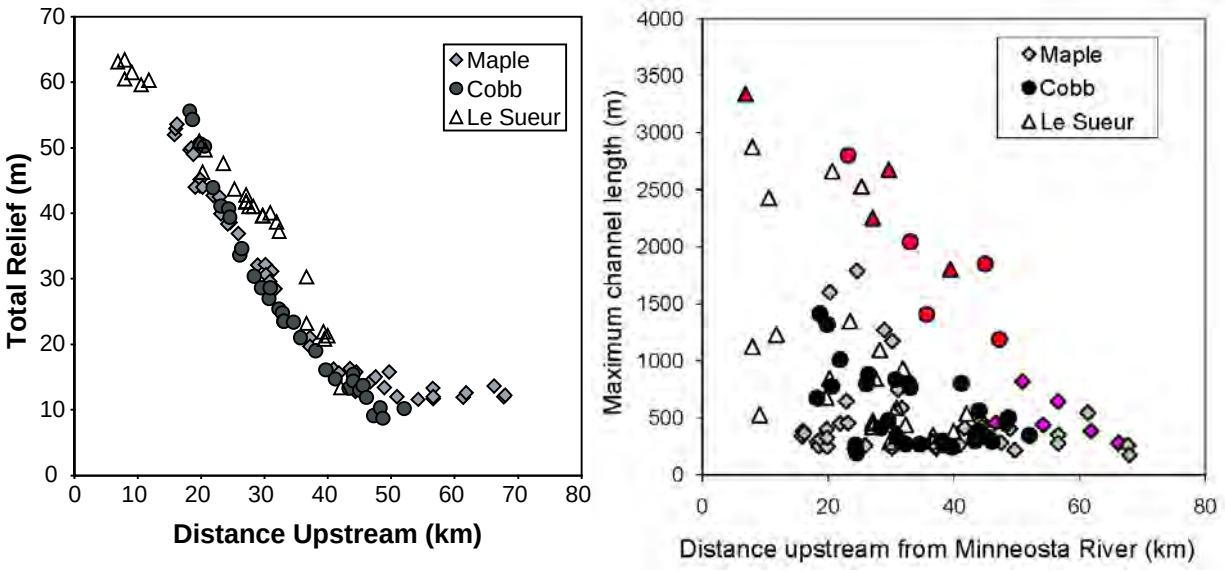

Figure 5.2: Total ravine relief (left) and maximum channel length (right) in ravines on the Maple, Cobb and Le Sueur Rivers. Maximum ravine length decreases with distance upstream. The longest ravines are closest to the mouth of the basin. Red symbols indicate ravines with ditches that drain directly into the ravine tip.

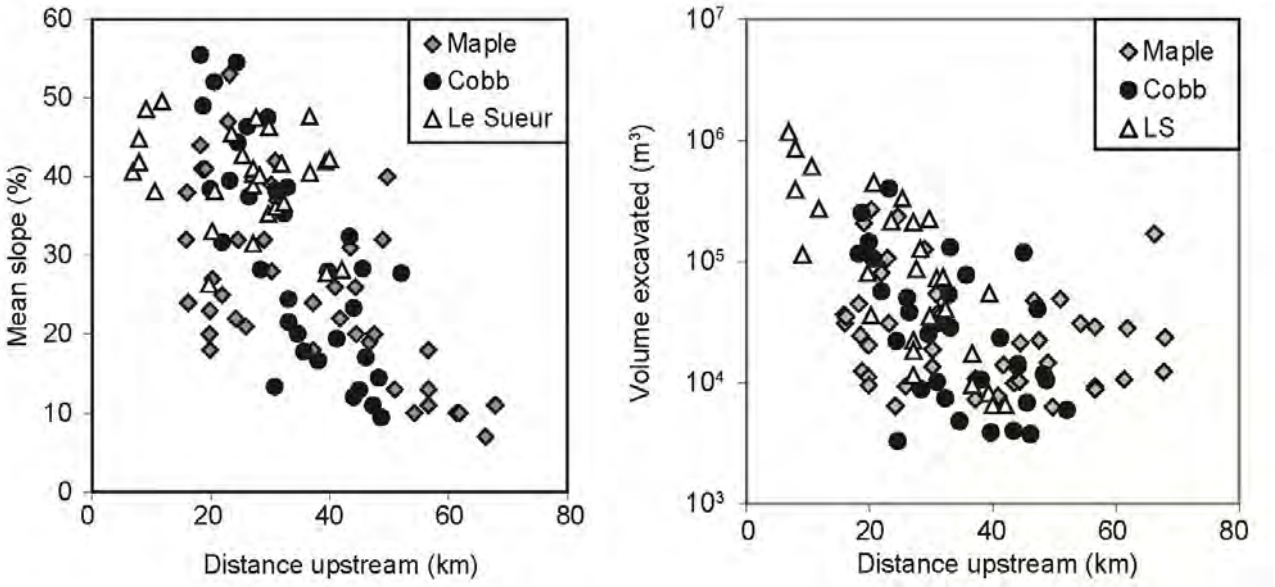

Figure 5.3: Mean ravine slope (left) and volume excavated (right) on Maple, Big Cobb, and Le Sueur Rivers.

Over the course of the Holocene, major ravines contributed a total volume of 1.1×10^8 m^3, or 2.0×10^8 Mg of sediment. Averaging over 13,400 years, this represents an average flux of 1.5×10^4 Mg/yr. Converting this mass into mass of silt and clay gives 1.0×10^4 Mg/yr of silt and

clay. This is a minimum estimate for the total volume of material removed by ravines because as the valley widens, portions of ravines are converted into valley. The Holocene-average ravine erosion rate is far lower than the Holocene-average valley erosion rate, and represents only ~10% of the total mass removed.

The incised ravine area compiled here covers only major ravines in Blue Earth County. A second inventory of ravines was done on the Le Sueur River branch only to include smaller ravines as well and determine the uncertainty associated with only digitizing in major ravines. Including all ravines >1 ha in area increases the ravine area in the Le Sueur River branch by 13%, including ravines down to 0.3 ha increases ravine area by 16%. To compensate for this, the total area in mapped ravines was increased from 898 ha to 970 ± 80 ha. This incised ravine area is used to determine annual ravine loads.

Field and remote observations:

Ravines often grade to terraces rather than to the mainstem channel, and fan deposits can be seen on these terraces. In some cases, ravines eventually connected back up to the river, re-incising to grade to a new baselevel and stranding fill terraces in the process. In our survey of ravines, half graded to a terrace, with most of those located below the knickpoint. Below the knickpoint, more terraces were present, with 59 out of the 74 ravines crossing at least one terrace, and 7 crossing at least three. Ravine metrics are compiled in the attribute tables of the accompanying shapefiles. The presence of these terraces leads to the rather complicated histories in many ravines.

Within individual ravines, sources of sediment include incision through fill terraces, eroding side slopes, headward erosion, and eroding ravine-wall bluffs. Attempts have been made in some places to arrest headward erosion through installation of berms. In other places, subsurface drainage tile outlets can be found entering ravine tips, enhancing erosion locally.

An assessment of ravine tip growth on 69 ravines from paired aerial photographs in 1938 and 2005 showed that only 9 showed significant change, with 5 showing elongation and 4 showing shortening (Figure 5.4). Meanwhile, 42 showed no significant change and 14 showed changes that were difficult to interpret (i.e. the tip was difficult to locate or some portions of the ravine were elongating while other portions showed retreat). This work was not able to assess ravine incision or widening. Ravines that elongated or shortened significantly were field-checked, and no common ravine morphometries were found associated with ravines that showed significant decadal-scale change. The main conclusion from this approach is that there is no evidence of systematic ravine lengthening over the past seven decades within the margin of error associated with georeferencing and delineating ravine tips from air photos. This error is estimated at ± 10 m. Given the average extension rate of 0.15 m/yr, ravine tips migrating at this rate would have progressed only 10.4 m in 69 years.

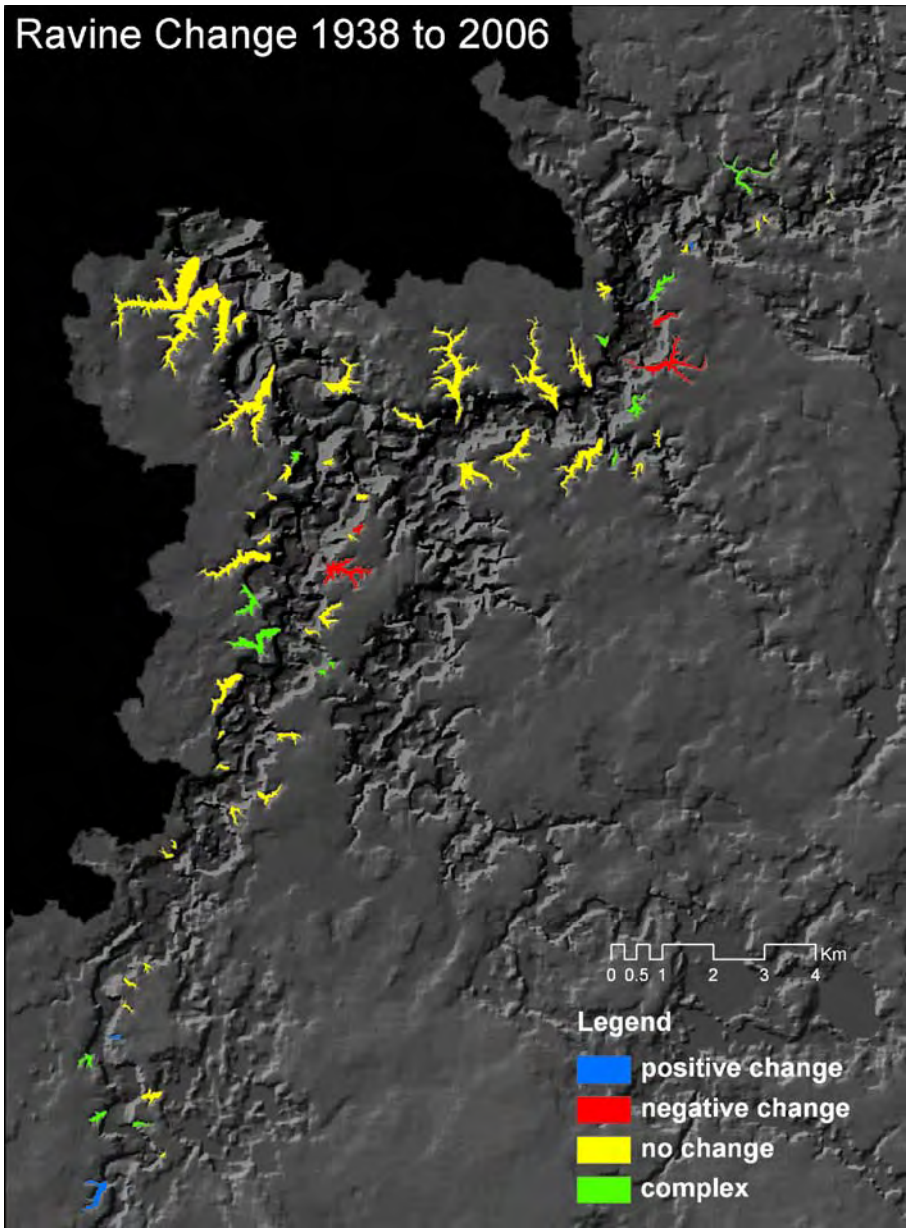

Figure 5.4. Results from comparisons of aerial photographs between 1938 and 2006, showing ravines with elongation (positive change), shortening (negative change), no change, or complex changes.

Ravine monitoring:

Four ravines were monitored with auto-samplers to capture sediment exported during storm events when the vast majority of sediment is evacuated from the ravines. Monitoring ravines is challenging, and we were unable to capture all storms for all years on all monitored ravines. In terms of runoff, 2008 was an average year, 2009 was lower than normal, and 2010 was higher. We ended our ravine monitoring program at the end of August 2010, and thus missed the big event in September 2010.

Because samples are only collected during storm events, base flow concentrations were estimated at 5 mg/L. Computed TSS loads for the duration of the monitoring season are shown in Table 5.3, compared with TSS loads for the Le Sueur River at the Red Jacket gauge (LES 1.3).

These loads were summed over the course of the ravine monitoring season to determine the % load in the Le Sueur River derived from these monitored ravines.

Table 5.3: Ravine monitoring season TSS loads

5/9/08 to 09/30/08	RavU90	RavL90	Rav8	Rav22N	Rav22S	LES 1.3
Runoff (inches)	3.68	3.68	2.48			3.22
TSS Load (kg)	8,985	148,178	159,612			38,010,906
TSS FWMC (mg/l)	38	396	583			162
TSS yield (Mg/km^2)	191	475	339			13

3/25/09-10/31/09	RavU90	RavL90	Rav8	Rav22N	Rav22S	LES 1.3
Runoff (inches)	2.59	2.59	2.52			2.18
TSS Load (kg)	2,405	9,370	9,791			22,433,214
TSS FWMC (mg/l)	13	36	35			149
TSS yield (Mg/km^2)	51	30	21			8

6/1/09-10/31/09	RavU90	RavL90	Rav8	Rav22N	Rav22S	LES 1.3
Runoff (inches)	1.41	1.41	1.92	1.70	0.06	1.1
TSS Load (kg)	1,890	8553	9,371	969	99	10,533,076
TSS FWMC (mg/l)	19	60	44	23	30	70
TSS yield (Mg/km^2)	40	27	20	7	3	4

3/9/10 to 8/31/10	RavU90	RavL90	Rav8	Rav22N	Rav22S	LES 1.3
Runoff (inches)			8.84			
TSS Load (kg)			1,096,678			
TSS FWMC (mg/l)			1,121			
TSS yield (Mg/km^2)			2,328			

3/22/10 to 8/31/10	RavU90	RavL90	Rav8	Rav22N	Rav22S	LES 1.3
Runoff (inches)	6.57	6.57	5.29		3.78	7.61
TSS Load (kg)	58,020	806,592	816,916		226,685	142,614,176
TSS FWMC (mg/l)	127	1,208	1,396		1,004	234
TSS yield (Mg/km^2)	1,234	2,585	1,734		6,297	50

TSS loads for individual storm events and flow weighted mean concentrations (FWMC) for the same events are shown in Table 5.4. Only one storm was captured by all five samplers, on 6/8/09. The Rav22S sampler was lost shortly thereafter. The loads for this storm event and for all three annual monitoring seasons were compared with incised area and relief, with the strongest relationship found between incised area and TSS load (R^2 values between 0.87 and 0.90). Relief also correlated well with TSS loads in 2008 and 2010, but was a poorer fit to 2009 TSS loads. We used incised ravine area in extrapolating from measured loads to estimated loads from ravines for the entire watershed.

Table 5.4: Storm event TSS loads and FWMC.

Storm Event TSS Load (kg) Comparison					
Date	RavU90	RavL90	Rav8	Rav22N	Rav22S
5/30/2008	3,907	69,559	71,768		
6/6/2008	514	12,497	15,237		
6/7/2008	675	9,865	16,197		
6/8/2008	865	14,181	18,980		
7/17/2008	974	24,755	23,209		
3/23/2009			76,774		
6/8/2009	1,095	4,137	4,948	188	26
5/13/2010	213	7,302	2,356		22
6/17/2010	15,669	156,191	164,968		22,789
6/25/2010	22,954	309,097	463,305		65,726
6/26/2010	16,317	268,258	173,574		84,410

Storm Event - TSS FWMC (mg/l) Comparison					
Date	RavU90	RavL90	Rav8	Rav22N	Rav22S
5/30/2008	335	4,093	3,158		
6/6/2008	34	573	732		
6/7/2008	54	545	786		
6/8/2008	50	562	856		
7/17/2008	149	2,593	1,797		
3/23/2009			1,267		
6/8/2009	127	329	318	249	47
5/13/2010	14	332	101		5
6/17/2010	200	1,370	1,867		696
6/25/2010	596	5,503	11,716		2,493
6/26/2010	212	2,397	2,452		2,235

The next analysis focused on the paired monitoring stations in Rav90. Sediment exported from the mouth of the ravine can either be sourced within the ravine or in the uplands with the ravines simply passing upland sediment through. The paired gauges on Rav90 were used to separate out those two components. The upper gauge was used to calculate an upland yield by assuming 100% of the sediment measured at the upper gauge was sourced in the uplands. That same upland yield was applied to the upland area above the lower gauge, and the remaining sediment load was used to derive an incised ravine load. The same upland yield was applied to all other monitored ravines over their upland areas to determine the % sediment sourced within the ravine vs. sourced in the uplands (Table 5.5). Rav22S was also located near the top of a ravine, so it likely did not have 78% of its sediment load sourced within the incised ravine, as implied in Table 5.5. Instead, this ravine likely had a much higher upland yield. Rav90 had an upland watershed without surface tile intakes which can lower the amount of sediment reaching the ravine from the uplands. Rav22S had surface inlets, and thus likely had a higher upland yield.

Table 5.5: Proportion of ravine TSS load sourced in ravines vs. sourced in uplands within ravine watershed using RavU90 as upland yield.

	Upland TSS load* (kg/ha)	RavU90*	RavL90	Rav8	Rav22N	Rav22S
2008	33	0%	92%	92%	N/A	N/A
2009	7	0%	70%	71%	41%	N/A
2010	211	0%	90%	90%	N/A	78%†

** RavU90 was set to 0% ravine, 100% upland and used to calculate the upland yield applied to other ravine upland areas during that monitoring season.*

†The Rav22S sampler was also near the top of the ravine. This % is using the RavU90 sampler as upland yield. It is likely the % sediment sourced within the ravine is much lower than 78%, and the upland yield in this ravine watershed much higher.

To extrapolate the monitored loads to the entire watershed, we calculated the total load of the monitored ravines and then scaled that up by area to cover all ravines in the Le Sueur watershed. This load was compared to the load at the mouth of the Le Sueur River during the same time period each year. In 2008, 9.7% of the total sediment load was derived from ravines. In 2009, it was 1.9%, and in 2010 it was 15%. The average % load derived from ravines was 8.9%. For the sediment budget, this % was applied to the average Le Sueur River TSS load from 2000 – 2010 to get a modern average sediment load derived from ravines of 20,000 Mg/yr.

To get an upper bound of the ravine load derived from ravines, we compiled the TSS load on the Le Sueur River during the 2008 to 2010 monitoring seasons time periods when ravines ran turbid. If the assumption is made that all suspended sediment in the Le Sueur River during this time period was derived from ravines, then the ravine contribution to the annual TSS load on the Le Sueur River was 21% and 3% during the 2008 and 2009 monitoring seasons, respectively. During the period when ravines were turbid other sources would also be contributing substantial sediment, thus the actually proportion of sediment load that came from ravines would be significantly less than 21% and 3% in 2008 and 2009. This is assuming the bulk of the sediment load from ravines that is delivered to the Le Sueur River is immediately exported (within hours) and is not deposited into the channel and slowly exported over an extended period (days/months). This value is approximately twice what was estimated by up-scaling from monitored ravines to the entire watershed, but is still a relatively low fraction of the total sediment budget.

Conclusions and Implications:

Ravines are the primary connection between the uplands and the main channel in the lower watershed of the Le Sueur River. They represent the newly emerging drainage network and increase connectivity in the lower basin. Although there are ravines above the knickpoint, they usually have less than 13 meters of relief and they are much less numerous than in and below the knick zone. Ravine length, area, volume, slope, and relief all increase with distance downstream in the knick zone, meaning that the importance of ravine sediment contributions to the sediment budget increase with distance downstream as well.

When ravines are transporting sediment, the concentrations can be very high. Concentrations as high as 67,000 mg/l were measured, with seasonal incised ravine yields as high as 6,000 Mg/km^2. However, because ravines occupy such a small area within the watershed (< 10 km^2 of incised ravine area), and flow for such a short time of the year, their contribution towards the overall sediment load is minimal. Our monitoring work showed that ravines contributed 1.9% of the TSS load in a dry year and 15% in a wet year, with an average

contribution from 2008-2010 of 8.9%. The maximum possible % sediment coming from ravines is about twice the amount determined from monitoring data, based on the total amount of TSS leaving the Le Sueur River on days when ravines are turbid. This is clearly an overestimation, but it sets a fairly rigid upper bound. Ravines contribute a relatively small percentage of the overall sediment load on the Le Sueur River, but it can still represent a large volume of sediment, compared with other tributary contributions in the Minnesota River watershed. The increase in % ravine contribution during the very wet 2010 monitoring season compared with the very low % during the dry 2009 season is also an indication that ravine contributions scale nonlinearly with precipitation. Years with more intense precipitation, particularly in the spring could lead to a higher % of the total sediment load coming from ravines.

Based on volumetric studies, ravines do not appear to have been a dominant source of sediment over the course of the Holocene. Over the past 13,400 years, ravines accounted for only about 10% of the total excavation volume, giving an annual excavation rate of 15,000 Mg/yr or 10,000 Mg/yr of silt and clay. Which is the proper comparison? The samples collected in ravines from 2008-2010 actually contain a lot of sand, much more so than grab samples taken on the mainstem Le Sueur River. Thus, comparing the mean excavation rate of 15,000 Mg/yr is most appropriate. This means that the modern ravine excavation rate is about 30% greater than the pre-settlement rate. By the same token, if we are sampling sand as well as fines, then we need to reduce the modern loads to remove the sand fraction from consideration, lowering their importance in the modern budget. Either way, ravines are a minor fraction in the modern budget and have changed by no more than a factor of 2 over pre-settlement erosion rates.

What are the management implications for ravines? No matter how we look at the data, ravines are a small portion of the total sediment load coming out of the Le Sueur River, but they can represent a high volume of sediment to the Minnesota River when compared to other low-producing tributaries. Ravines contribute heavily during spring storms, but then are relatively small contributors for the rest of the year. If the climate trends towards high frequency of intense storms or if land use changes lead to higher intensity flows in ravines, it could have a nonlinear affect on ravine contributions to the mainstem Le Sueur River, increasing both the volume of sediment coming from ravines and the % total load coming from ravines.

Even though they are a smaller fraction of the total budget, ravines should simply be neglected. Putting in erosional control mechanisms that slow ravine tip growth can be beneficial to landowners who are losing land to ravines while also lowering sediment loads to the mainstem channels. It is not likely that annual average ravine loads can be lowered by more than 50%, which is the Holocene-average erosion rate, and even that dramatic of a change would only reduce the annual sediment load on the Le Sueur River by a few %.

6. Bluffs

Bluff Types in the Le Sueur River Basin:

In the Le Sueur Basin bluffs can be divided into three types; normally-consolidated till bluffs, over-consolidated till bluffs, and terrace bluffs. Each bluff has unique characteristics that cause it to erode in different ways. Normally-consolidated till bluffs are the most common in the watershed. These bluffs have are composed of stacked tills with permeabilities consistent with the present day over-riding load. As described later in this report these bluffs primarily erode by undercutting due to the flow of the river. In some places seeps occur, but these tend to be localized at a contact with sand lenses or other stratigraphic change. We can identify that these seeps are not driving erosion because there is no evidence to show that erosion is higher where these seeps occur. Over-consolidated till bluffs occur less frequently in the watershed. These bluffs are again composed of stacked tills. After these tills were deposited a large load was placed on them likely due to a glacier re-advancing over them, forcing the moisture out. These bluffs have low permeabilities, are very steep, and have characteristic vertical joints. Bluff erosion appears to be highly episodic at these sites and is lower than on normally-consolidated till bluffs. While undercutting likely contributes to erosion at these sites, freeze-thaw processes may be the driving cause of erosion. Failure is common along vertical joints, which are likely conduits for water. As the water freezes and expands the joints become weaker, until the weight of the block ultimately overcomes any resisting forces and fails. The final bluff type, terrace bluffs, are normally-consolidated bluffs capped by alluvium. Terrace bluffs were banks at one point during the river evolution, but became stranded as the river incised. These bluffs often have a riverine gravel unit at the base of floodplain alluvium. This gravel unit is often a source of seeps. In this case seepage may be contributing to erosion, yet overwhelmingly field evidence suggests that these bluffs are also eroding primarily by undercutting. The absence of any obvious break in slope at these sites indicates that the lower till units are keeping pace with erosion in the overlying alluvium. While seepage erosion does occur at some of these sites, the long-term average rate of seepage erosion cannot be any greater than the long-term average rate of undercutting.

Bluff erosion Processes:

There are three primary causes for bluff erosion typically observed in the Minnesota River basin: sapping, undercutting, and freeze-thaw (Day et al., in review). Each of these processes leave different characteristic patterns of erosion, making it possible to determine which processes dominate erosion and which processes occur to a lesser degree. References in this section to the toe of the slope refer to the sediment deposited at the base of the bluff as opposed to the in-situ sediment which is referred to simply as the base of the bluff.

Typically undercutting is a result of shear stress imparted on the base of the bluff by the flow of the river. When the shear stress of the flow overwhelms the shear strength of the bluff, sediment is removed. Eventually enough sediment is removed that the weight of the overlying, now unsupported sediment is greater than the resisting forces. When this occurs the upper portion of the bluff will fail and deposit a toe at the base of the bluff. The bluff will not be undercut again until the toe is removed by the same fluid shear stress which causes undercutting to occur. This process is taking place in all rivers where flows are great enough to cause erosion.

In places where this process is dominant, the bluff faces are likely steep with an easily eroded toe sometimes present at the base. These bluffs maintain a steep face because over long time scales erosion is essentially equal at all portions of the bluff face. The constant removal of the toe reduces the ability of these bluffs to stabilize.

Sapping is the result of groundwater flow through the bluff, which seeps out along the face. As water infiltrates into the ground during a storm event, that water flows to areas of lower potential which may commonly be the river, or in agricultural areas, a tile drain or ditch. Sediment is eroded from the bluff face below the seep when the discharge of the seep is greater than the critical shear stress required to move sediment (Fox et al., 2007). Over-saturation from seeps may also weaken sediment in that location making the area more susceptible to mass failure (Lindow et al., 2009). Often seeps like these can be seen on the face of a bluff as an area of wet sediment, and sometimes water may be flowing in these areas. This form of erosion is often localized in non-homogeneous sediment such as tills, and may increase erosion in specific locations. In layered sediment a confining layer may reduce the risk of sapping below that layer and may cause erosion in only the upper, more permeable units (Fox et al., 2007). This is most common on terraces where alluvium capping the bluff is more permeable than the underlying till. If this occurs the upper unit can be seen to erode more rapidly than the underlying units. In homogeneous sediment, sapping occurs at the base of the bluff at the river water level elevation. When the water level is relatively constant this sapping does not dramatically increase erosion because the confining pressure of the river water helps to stabilize the slope (Jia et al., 2009). When the water elevation in the river drops quickly that confining pressure is removed and the resulting sapping can increase erosion along the base of the bluff. Similar to when traditional undercutting occurs the overlying unsupported portion of the bluff will fail and form a toe at the base of the bluff. With no other forces acting on the bluff that sediment will remain at the toe and the bluff will ultimately form a gentle slope at the angle of repose of the sediment. As the bluff slope lowers, vegetation will develop to further stabilize the bluff and will ultimately reduce sapping as the vegetation takes up the water.

Freeze-thaw events can also cause erosion. Even small amount of moisture in the sediment forming a bluff can freeze and expand 9% by volume (Liu, et al., 2008). As this happens that area of the bluff is weakened. Often water collects along conduits such as micro-fractures, joints or even along roots. This can focus the erosion to these areas and will likely result in localized erosion. In homogeneous sediment, freeze-thaw processes may be equally likely anywhere. When freeze-thaw processes result in erosion along the base of the bluff, the resulting undercutting can cause failure above. These failures will form a toe at the base of the bluff which will remain if there is no other force to remove the sediment. In many cases freeze-thaw events do not directly cause failure, and instead weaken sediment such that failure occurs as a result of spring storms (Thomas et al., 2009). Because freeze-thaw events are clearly seasonal one way to test their importance is to measure erosion in early spring and fall when there are the greatest number of freeze-thaw cycles.

While each of these processes are eroding bluffs in the Minnesota River basin, the absence of significant toe deposition and the presence of steep-faced bluffs suggest that undercutting is the dominant force of erosion. While sapping and freeze-thaw are both causing erosion these processes would likely lower the bluff slope if undercutting was not occurring. Undercutting will primarily occur when flows are high in the river, during spring or other flooding events throughout the year. This is not to suggest that undercutting cannot occur during normal flows, but the rate is lower.

Aerial Photograph Methods and Scaling:

Aerial photographs allow us to measure bluff erosion over large spatial scales and long time scales. In the Le Sueur Basin decadal aerial photographs are available starting in 1938. We aligned this earliest set of photographs to the 2005 photographs which accompany 2005 aerial lidar for Blue Earth County. The alignment and complete photographic analysis was done using ArcGIS.

Bluffs were automatically delineated on the 3m DEM using an algorithm that selected any feature with greater than three meters of relief in a 9 m^2 window. This algorithm was used to select all bluffs in the watershed, yet only the bluffs along the river were used to calculate the sediment load. Bluffs that have been stranded by terraces and are no longer connected to the river were excluded, because it is unlikely that the sediment eroded from these features enters the river through bluff erosion processes.

To track bluff retreat and estimate the long-term sediment contribution from these features, the bluff crest was traced in both the 1938 and the 2005 photographs. The average retreat rate was calculated by summing the area between the lines and dividing this area by the river length along the bluff and the time between the photographs (67 years). Where negative retreat was measured this area was subtracted from the total area, because there is no physical process which allows negative retreat to occur, and therefore must be a byproduct of error in the photograph alignment or tracing the bluff crest.

In addition to measuring bluff crest retreat, we also measured river migration. The river migration rate provides an estimate of the average retreat rate of the base of the bluff. By combining the migration rate with the crest retreat rate we can determine which bluffs are laying back and which are becoming steeper and refine our estimate of the total volume of sediment removed from bluffs. Where the river is migrating toward the bluff we use the measured rate as our migration rate at that site. Where the river appears to be migrating away from the bluff we assume zero migration. Field observations suggest that typically any deposition at the base of the bluff is quickly removed by the river. Also, migration away from the bluff may be artificial due to higher water levels when the 2005 photographs were taken. Where one edge of the river is lined by a bluff, higher water levels will cause the river's center line to appear closer to the opposite bank.

The 3m DEM was used to measure bluff height, *H*, allowing calculation of the total volume of sediment lost from each bluff, V_s :

$$V_s = \left[R + {}^1\!/_2\,(M - R)\right] * H * L \qquad (6.1)$$

where *R* is bluff retreat rate, *L* is river length along the bluff, and *M* is the river migration rate where *M* is zero in places where the river migrated away from the bluff.

All visible bluff crests were traced on the Maple, Big Cobb, and Le Sueur Rivers; of the 480 bluffs mapped, 243 were traced. In order to calculate the total sediment load from bluffs it was necessary to use the available information to scale to the remaining 237 bluffs. To interpolate the retreat rate for the non-traced bluffs, aspect and bluff vegetation were used for scaling. Both of these attributes are likely to have an effect on how bluffs erode. Bluff aspect may have an impact on the freeze-thaw cycles that a bluff face undergoes, while vegetation can increase soil strength and reduce the risk of erosion (Docker and Hubble, 2008). Parameters

including *H*, *L*, and *M* were all measured directly using the DEM and the aerial photographs for all mapped bluffs, leaving retreat rate as the only variable extrapolated from traced bluffs to non-traced bluffs.

To determine the retreat rate to be applied to each of the non-traced bluffs using aspect, the bluffs were separated into eight groups, each representing 45˚ (Table 6.1). Where the average aspect was north facing the bluff was assigned to either the 0-45˚ or 315-360˚ group. The average retreat rate was calculated for each group, and this rate was applied to all non-traced bluffs in the same aspect bin.

When vegetation was used as the primary attribute for scaling up the bluffs were separated into vegetated and non-vegetated groups (Table 6.2). For each traced vegetated bluff with positive retreat it was established that there was some time between 1938 and 2005 where the bluff was not vegetated, and was likely actively eroding. The bluffs were then separated again, this time geographically, based on where they are relative to the gauges (approximately marking the knick zone). For each of the six groups the average retreat rate was determined and applied to all non-traced bluffs in the same group.

Terrestrial Laser Mapping methods and Scaling:

Terrestrial Laser Mapping (TLM), also referred to as Terrestrial Laser Scanning (TLS) or ground-based or tripod-based lidar, is a laser-based topographic measuring system. Like aerial lidar, TLM relies on time-of-flight laser pulse returns to measure topography, but because TLM is tripod-based it can be used to measure vertical features like bluffs. For this project we used an Optech ILRIS 3_6D lidar system rented from the Lidar Lab now at Western State College of Colorado. This equipment has cm-scale resolution and can be used to measure small changes over sub-annual time scales (Day et al., in review; Wawrzyniec, 2007; Milan et al., 2007; Resop and Hession, 2010; Rosser et al., 2005; Lim et al., 2010; Gulyaev and Buckeridge, 2004). While this technique provides high-resolution data on the surveyed bluffs, significant data collection and processing time make it impossible to collect data at all the bluffs in the watershed.

TLM data were collected annually for four years at fifteen sites and processed based on the procedures outlined and validated in Day et al. (in review). Sites were selected to represent a range of stratigraphies and locations. Eight sites were scanned on the Le Sueur River, six within the knick zone and two upstream. On the Maple and Cobb River two and three sites, respectively, were scanned within the knick zone and zero and one upstream. The data from these fifteen sites were used to approximate bluff erosion throughout the basin. Four different scaling analyses were performed to show the range of possible sediment loads from bluffs over the past 4 years. For all scaling analyses, the height and length estimates of the bluffs were the same as those used for the aerial photograph analysis.

In addition to providing information about retreat rates, TLM data also provide information about bluff erosion processes. The high-resolution data give precise locations where erosion and deposition are taking place. This information can be used to interpolate what the most likely causes of erosion are at each of the scanned sites.

Results:

The aerial photograph results show a weak increasing trend, moving downstream, in the volume of sediment from each bluff (Fig. 6.1). On the Maple River this increase is more

pronounced. After passing the upper gauge and entering the knick zone (35 Km from the mouth) there are no bluffs which contribute less than 10 Mg/year of fine sediment. On the Le Sueur River there are bluffs with low erosion rates throughout the length of the river, yet those bluffs with the highest erosion rates (greater than 1000 Mg/yr) are all concentrated at the furthest downstream portions of the river (less than 25 Km from the mouth) in the lower portion of the knick zone and where the knickpoint has already passed.

The results for the Le Sueur River show a 27% difference in the total load depending on the aerial photograph scaling method used for measuring (Table 6.3). The Maple and Cobb Rivers have significantly less variability between the different methods 3% and 14% respectively (Table 6.3).

TLM data were collected annually from 2007- 2010 and two sets of scans were collected in 2008. During that time there was a wide range of seasonal variability. The data show that higher flow rates are well-correlated to higher average erosion rates measured on the bluffs (Day et al., in review).

The erosion rates measured using TLM range from 0.23 m/yr of deposition to 0.95 m/yr erosion with an average rate of 0.18 m/yr. Each of these extreme measurements was recorded over a short time period. In the case of the 0.23 m/yr deposition there were only 42 days between the scans. There was only one case where deposition was recorded where there was more than a year between the scans. At this site there was 0.09 m/yr of deposition measured over 374 days. This deposition took place between spring 2008 and spring 2009, at a site where erosion control structures had been put in place. The maximum erosion rate of 0.95 m/yr was recorded between 2009 and 2010 when the highest flow rate during this study was recorded. The three largest erosion rates measured were all measured during this time interval. The higher rates measured between 2009 and 2010 also raised the average erosion rate to one which more closely approximates the average retreat rate measured on the aerial photographs.

The average rate for all the scanned bluffs is 0.18 m/yr. Just applying this average rate to all the bluffs in the Le Sueur River watershed gives a total sediment load of 220,000 Mg/yr of fine sediment. Because TLM data were collected only from unvegetated bluffs and represent active erosion rates right now on unvegetated bluffs only, we chose to apply the TLM rates only to the unvegetated portions of bluffs. Using the average rate to unvegetated portions of bluffs gives a total load of 105,000 Mg/yr of fine sediment. Using the three different scaling methods, the total fine sediment load for the Le Sueur watershed ranges between 113,000 and 156,000 Mg/yr with an average of 134,000 Mg/yr.

Additional results based on analysis of the TLM data show that bluff erosion on all bluff types is highly episodic. Failed material that collects at the bluff toe is often quickly removed, and while net deposition was observed over short time scales, it was rare, and never occurred when measuring buff change over two or more years. Failure on normally-consolidated till bluffs did appear to be different than failure on over-consolidated till bluffs. Over-consolidated till bluffs tend to have very low erosion rates over long time scales, and they appear to fail along the vertical joints which define them.

In most cases, bluff erosion occurs along the entire bluff face when integrated over time. The only area where a rotational failure occurred near the top of the bluff and excluded the lower half of the bluff face was on a terrace bluff. At this site the failure occurred exclusively in the overlying alluvium. This only occurred at one time interval at one site. At all other bluffs failure was typically not predictable and was equally likely to occur at one portion of the bluff as it was to occur somewhere else both vertically and laterally across the bluff face.

Discussion:

The results of this study show that bluffs contribute a significant portion of the total sediment load in the Le Sueur River watershed, consistent with findings by other researchers (e.g. Sekely et al. 2002; Hansen et al. 2010). Regardless of the specific method used to measure bluff erosion, the loads could always account for as much as 100% of the total load measured at the gauging stations within uncertainty. Because these numbers do not account for deposition, and additional work has shown that there is some erosion from other sediment sources it is likely that bluff erosion actually accounts for approximately 50-60% of the total sediment budget. This result is unsurprising considering these features line 32% of the river in Blue Earth County and can be as much as 60 meters high. In addition, over decadal time scales bluffs are exclusively a source of sediment and typically any sediment deposited at the toe is only temporary, whereas both floodplains and ravines can store sediment.

One reassuring find from this study was that the results of both the TLM and the aerial photograph analyses were remarkably consistent. These two techniques measured bluff erosion over very different spatial and time scales yet the total volume of sediment estimated from each technique are within 32% of each other on average. This suggests that the four years we measured bluff erosion using TLM were representative of the range of conditions experienced over decadal time scale, and the fifteen bluffs sampled did a good job approximating average bluffs in the watershed. The results from the TLM were slightly higher than the aerial photograph results. This is likely because of both higher error due to up-scaling for the TLM results and may also be due to a bias toward bluffs with little vegetation. We know from the aerial photographs that vegetation does not stabilize bluffs over the long term, but over the short-term, vegetation can exert a stabilizing influence. For all bluffs that were vegetated in 2005 there was some period of time since 1938 where they were un-vegetated. Further evidence that vegetation does not play a significant role in the rate of longer-term bluff erosion are the similar retreat rates measured for the vegetated and non-vegetated bluffs. This result is contradictory to beliefs about bank erosion, but because bluffs are high features vegetation can be undercut and cannot stabilize the slope long-term (Docker and Hubble, 2008; Cancienne et al., 2008; Harden et al., 2009).

While vegetation didn't play as significant a role in bluff retreat as was expected aspect did appear to be an important variable. On both the Le Sueur and the Maple River north and west facing bluffs had the highest erosion rates, while on the Cobb east facing bluffs had the highest retreat rates. The result on the Maple and Le Sueur suggest that a high number of freeze-thaw cycles may contribute to higher erosion. The results on the Cobb appear to contradict this, but these results may be due to the low number of westward-facing bluffs traced. In Minnesota it is impossible to deny that freeze-thaw cycles contribute to erosion, yet it seems unlikely that this is the primary driving erosive force. The TLM data paired with field observation suggest that undercutting and toe erosion drive bluff retreat. This is supported by aerial photograph analyses which show that the river is migrating toward the bluff in many places over multi-decadal time scales. Further evidence that bluff retreat is driven by erosion at the toe of the bluff comes from the positive correlation between the peak flow between TLM scans and the average erosion rate between scans. High spring flows in 2010 caused erosion rates measured between 2009 and 2010 to be quite high (Day et al., in review). Relatively low flows for the three years previous

caused the four year average retreat rate to be much lower and more closely approximate the average retreat rate measured from the aerial photographs.

Evaluation of Aerial Photograph vs. TLM data:

When considering the pros and cons of aerial photograph and TLM data, it is important to consider cost, value of data, and confidence in the data. Many aerial photographs are freely available online, making the primary cost a person's time; the data collection and analysis can be learned quickly by personnel familiar with GIS. TLM is considerably more costly. In addition, effective data collection and proper processing requires more time to learn. The data generated with the aerial photographs provides long-term bluff retreat based on the bluff crest, yet provides little information about how the bluff is eroding. TLM data provides information over a much shorter time scale, and on fewer bluffs, yet the data are more detailed and can provide information about erosion processes. The confidence in the data is similar between each technique, yet the sources of error are different. The aerial photograph data have significant error due to tracing the bluff crest and georeferencing the photographs and little error due to up-scaling. TLM data have greater error due to up-scaling and a very low error associated with data collection and processing. In general aerial photograph data is a better choice to study all the bluffs in a watershed, or where the main interest is associated with finding the total load associated with bluff retreat. TLM data is more appropriate where a one or a small number of bluffs are of interest. The TLM data will provide a greater amount of information about these individual bluffs, including specific information about erosion processes.

Management Implications:

Bluffs are clearly a significant source of sediment along the Le Sueur River and any attempts to lower turbidity must include some form of bluff erosion mediation. The two main approaches are to focus on the problem at hand (bluff erosion) or to focus on the cause (increased flows). Addressing bluff erosion at the bluff scale requires an understanding of which bluffs are most likely to erode in the future, which is challenging given the episodic nature of bluff erosion (i.e. the high producers today may not erode much for the next few decades). In addition, while vegetation presence may be an indicator of recent activity, it does not necessarily lead to more stable bluffs. Vegetated bluffs were just as likely as non-vegetated bluffs to have migrated in the past 67 years. Stabilization must not rely upon vegetation, as roots may not penetrate to the depth of the failure plane, and undercutting by the channel can still proceed unabated. It is not known if riprap or other structures will work well to stabilize these features long-term, especially in the knick zone which is actively incising. Any work on bluffs should be accompanied by regulations to protect vulnerable sites (greater set-backs, stricter zoning, no direct drainpipes, etc.). In addition, to get at the source of the problem, high flows need to be addressed and mitigated. The best way to reduce bluff erosion throughout the entire watershed may be to hold water in the uplands longer, reducing the flow in the river and thus reducing the shear stress imparted on the bluff by the flow. Given the uncertainties of changing precipitation patterns, this would also provide more resiliency in the face of climate change.

Table 6.1: The total number of bluffs, the number of traced bluffs, and the average retreat rate of bluffs in each aspect group.

	Le Sueur River			Maple River			Cobb River		
	Total # bluffs	# Traced Bluffs	Measured retreat rate	Total # bluffs	# Traced Bluffs	Measured retreat rate	Total # bluffs	# Traced Bluffs	Measured retreat rate
0˚-45˚	33	14	0.18	8	5	0.04	16	11	0.23
45˚-90˚	28	12	0.10	13	7	0.09	6	4	0.22
90˚-135˚	29	9	0.05	19	15	0.03	25	12	0.24
135˚-180˚	36	16	0.09	17	11	0.07	20	8	0.11
180˚-225˚	33	18	0.14	14	10	0.19	20	9	0.04
225˚-270˚	30	9	0.18	18	10	0.21	9	3	0
270˚-315˚	19	10	0.16	23	15	0.20	7	1	0
315˚-360˚	25	15	0.24	9	7	0.09	23	12	0.13

Table 6.2: The total number of bluffs, the number of traced bluffs, and the average retreat rate of bluffs in each vegetation group. (The total number of bluffs may be greater when considering vegetation because some bluffs were divided into vegetated and non-vegetated components.)

		Le Sueur River			Maple River			Cobb River		
		Total # Bluffs	# Traced Bluffs	Measured retreat Rate	Total # Bluffs	# Traced Bluffs	Measured Retreat Rates	Total # Bluffs	# Traced Bluffs	Measured Retreat Rates
Vegetated	Above Gauges	22	5	0.10	24	14	0.12	33	12	0.08
	Between Gauges	96	32	0.09	60	40	0.18	44	22	0.13
	Below Gauges	56	22	0.15	14	6	0.14	15	9	0.22
	Little Cobb							6	2	0.09
Unvegetated	Above Gauges	16	6	0.05	3	3	0.24	1	1	0.25
	Between Gauges	85	60	0.20	42	34	0.20	24	9	0.24
	Below Gauges	34	23	0.17	6	5	0.21	15	8	0.15
	Little Cobb							1	1	0.37

Table 6.3: The total annual fine sediment load from each river for each measuring technique. (An average migration rate was used to find the load from the Cobb River bluffs.)

Up-Scaling technique	Total annual volume of sediment from the Le Sueur (tons/yr)	Total annual volume of sediment from the Maple (tons/yr)	Total annual volume of sediment from the Cobb (tons/yr)
Vegetation	93,100± 40,000	32,100± 10,900	57,000± 23,000
Aspect	84,500± 36,300	31,000± 10,500	42,000± 17,000
TLM	47,500± 15,700	28,550± 9,400	39,500± 13,000

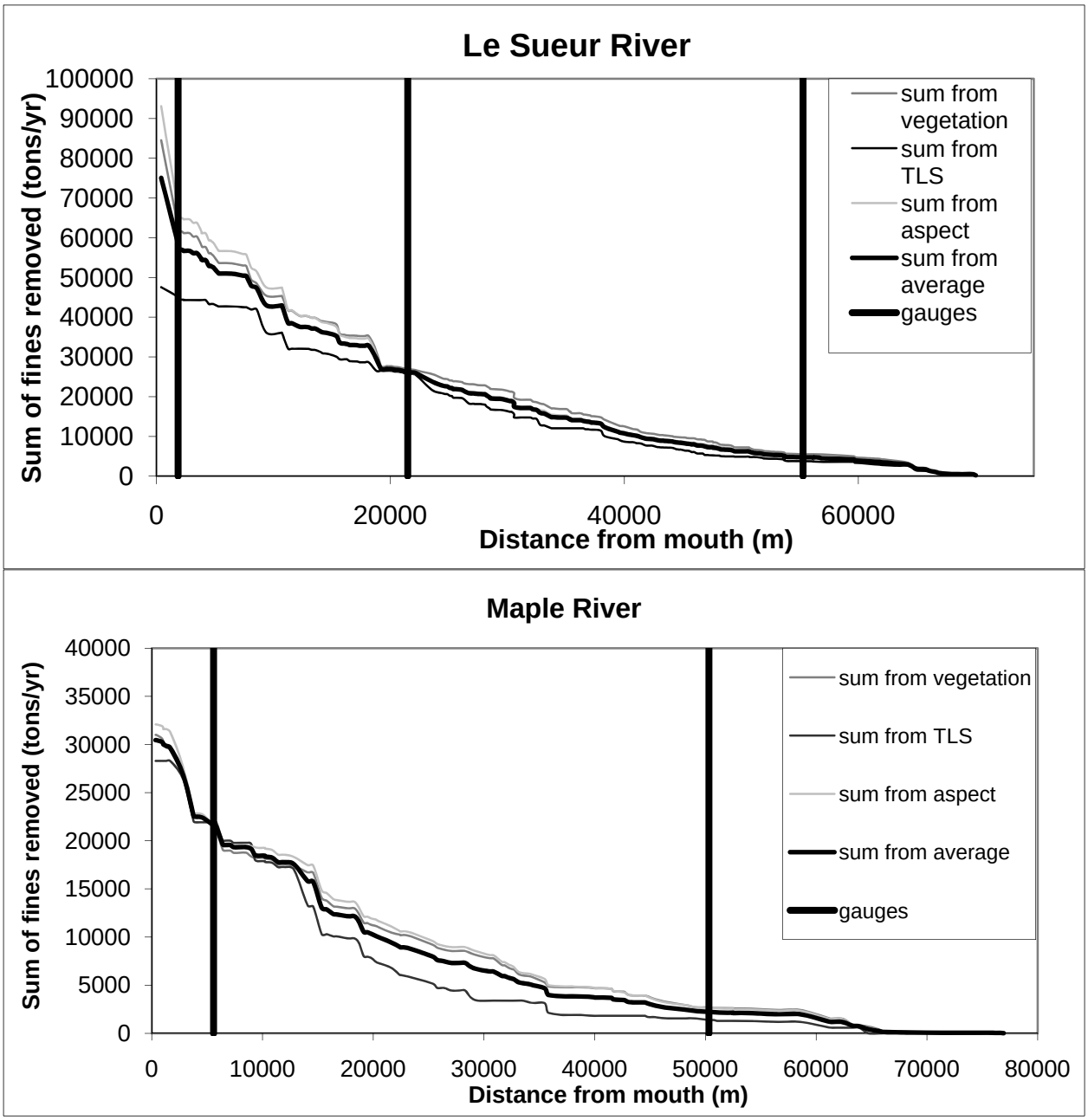

Figure 6.1: These charts show the sum of sediment eroded from bluffs moving downstream. Notice the change in slope downstream of the lower gauge. This increase indicates that a disproportionate amount of sediment is coming from these bluffs.

7. Geomorphology of bank erosion and channel-floodplain dynamics

Background

Landscapes naturally develop fluvial channels and associated floodplains to convey water and sediment. These systems are highly dynamic and can exert strong influence on fine sediment loads carried by rivers. Therefore, understanding how and why river channels change over time is essential for understanding stream turbidity and implementing strategies for turbidity reduction. In this section we briefly introduce mechanisms by which channel geometry changes and discuss the implications for sediment budgeting. Below, we describe the various methods by which we have measured channel change in the Le Sueur watershed and synthesize our results.

Channels and floodplains are both dynamic in time. Sediment loads in some rivers have been shown to be dominated by bank erosion due to a large amount of historic sediment storage in the valley bottom. Typically such rivers have historically aggraded due to accelerated watershed erosion and/or extensive damming of stream channels and more recently incised through those historic alluvial deposits (Trimble, 1999; Walter and Merritts, 2008), creating anomalously large, eroding banks. As we document below, this evolutionary cycle is not evident in the Le Sueur watershed in any significant way. Rather, the primary mechanisms by which bank erosion contributes sediment in the Le Sueur watershed is through channel widening and channel migration.

Over annual to decadal timescales, channel width and depth adjust in response to the range of flows encountered as well as the amount and type (mud, sand, gravel) of sediment supplied (see Eaton and Church, 2011 for an excellent review on the topic). Because discharge is directly proportional to stream power, but inversely proportional to frequency, channel geometry is most strongly influenced by relatively infrequent, high flows that typically occur once every one to three years (Wolman and Miller, 1960; Leopold et al., 1995). Therefore, if the magnitude of that one/three year event changes and or the amount or type of sediment supplied changes, so changes the channel geometry. For the purposes of developing a fine-sediment budget (silt and clay) we are primarily concerned with the net exchange of the fine-sediment between the channel and floodplains as the channel widens or narrows.

Another important feedback mechanism influencing channel geometry is sediment exchange between the channel and floodplain. Floodplains are temporary sediment storage reservoirs that are readily accessible to the channel. If high flows increase in magnitude and/or frequency, the frequency of floodplain inundation increases, resulting in more floodplain deposition, which causes a deeper channel, thereby providing a negative feedback on floodplain inundation. As a river channel laterally migrates, material from the outside bend is typically eroded and other material is deposited on the inside bend, forming a point bar (Figure 7.1). Typically, this process results in a net local influx of sediment to the channel because a) point bars tend to be built to a lower elevation than the cut bank and b) along a reach, the inside bend is shorter in length owing to the curvature of the bend (Lauer and Parker, 2008a). In a so-called graded river reach this net local influx is balanced by overbank floodplain deposition on decadal timescales.

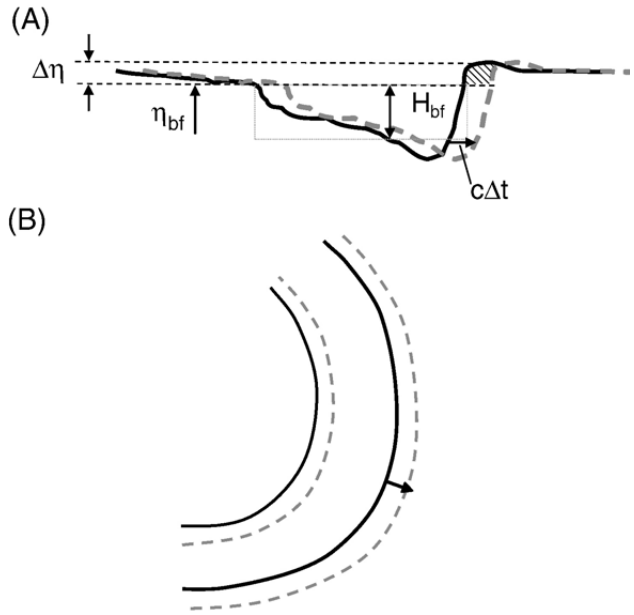

Figure 7.1. Schematic taken from Lauer and Parker (2008a), illustrating the two factors that promote a net contribution of sediment in a meander bend. A) Channel cross section showing point bars built to a lower elevation than cut banks (with the difference in elevation identified as Δη). B) Plan view showing the eroding bank is longer than the depositing bank, an effect that is enhanced as the bend migrates and curvature increases.

In developing a sediment budget at the reach scale, we assume that sinuosity is relatively constant over time and therefore any local net contributions of sediment that result from the difference in length of the eroding and depositing banks (mechanism b above) are negated by other locations of net removal where sinuosity is decreasing or meander cutoffs are being filled. The calculations presented below represent sediment contributions as a result of the migration rate and the difference in eroding and depositing banks (mechanism a above), where the net local sediment contribution is shown in the hatched box on the right bank in Figure 7.1 A. The net local sediment contribution to the channel (in Mg y^{-1}) via this mechanism can be computed as:

$$E = l \times \Delta\eta \times c \times \Delta t \times \rho \times f_{w,b} \qquad (7.1)$$

where l is the length in the up/downstream direction in meters, $\Delta\eta$ is the difference in the bank heights in meters, c is the lateral migration rate in meters per year, Δt is the duration of time considered (typically 1 year), ρ is the bulk density in Mg m^{-3} y^{-1}, and $f_{w,b}$ is the fraction of the sediment contribution that is washload (w) or bedload (b). Note that while ρ and $f_{w,b}$ must be constrained by field measurements, l, $\Delta\eta$, and c can be measured from lidar topography data and historic air photos.

Because hydrology dictates channel size, it is assumed that the average channel width and depth do not change as a result of channel migration. However, in systems for which an increase in magnitude and/or frequency of high flows can be demonstrated, channel widening may cause a net influx of sediment to the channel. The net contribution of sediment to the channel can simply be computed as:

$$E = l \times \Delta b_c \times h_c \times \Delta t \times \rho \times f_{w,b} \qquad (7.2)$$

where Δb_c is the widening rate in meters per year and h_c is the average channel depth in meters.

For the purposes of this document we refer to the area flooded for a given hydrologic condition as the *inundated width* or *inundated area* and we refer to the low-relief landform that is shaped by the river as a result of migration and deposition as the *geomorphic floodplain*.

Quantifying bank erosion from meander migration

The process of estimating the net local contribution of sediment from streambanks that results from channel migration requires several steps that can be accomplished using basic spreadsheet software (e.g. MS Excel) and the Planform Statistics Tool for ArcGIS that was developed by Wes Lauer and Gary Parker and is available for free download from the NCED Stream Restoration Toolbox (http://www.nced.umn.edu/Stream_Restoration_Toolbox.html). This method has been used in peer-reviewed literature including Lauer and Parker, (2008b), Aalto et al., (2008), and Parker et al., (2011). The process we applied is as follows:

Step 1: In ArcGIS, hand-digitize the right and left banks from aerial photos taken in 1938 and 2005.

Step 2: Use the Planform Statistics tool in ArcGIS to interpolate a centerline for each set of banks.

Step 3: Use the Planform Statistics tool in ArcGIS to segment the centerlines, creating a computational node every 10 meters. Measure the direction and distance of lateral migration of the river between each comparable 1938 and 2005 node.

Step 4. Buffer the 2005 channel banks with polygons and extract the elevation of the banks that correspond to each computational node on the segmented centerline.

Step 5. Export the segment lengths, migration data, and bank elevation data to a spreadsheet. Manually remove the segments where the river has been artificially moved and/or ditched, because the migration rates computed for this reach do not represent actual migration of the river. Manually remove the locations where bluffs are adjacent to the river. Bluff failure occurs by very different processes and therefore must be accounted for using other methods, which are described in Chapter 6 above.

Step 6. Calculate net sediment contributions for segments where the river is migrating in the direction of a higher bank using Equation 7.1 above.

Figure 7.2 shows the primary shapefiles generated for the calculation of net bank inputs as a result of differences in bank heights during lateral migration. Figure 7.3 A and C show the raw migration data obtained from the Planform Statistics Tool for the Le Sueur River and Maple River, respectively, over the 67 year study period. A positive migration distance indicates migration toward river right and a negative migration distance indicates migration toward river left. Figure 7.3 B and D show the migration rates (in absolute values) after the data have been filtered using a moving 2.5-km smoothing window.

.

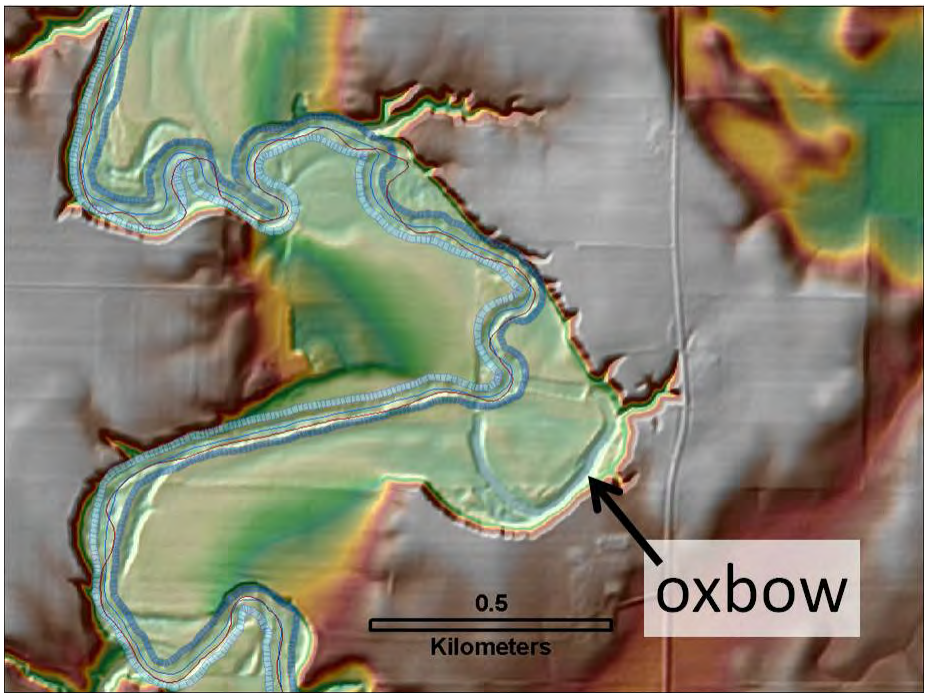

Figure 7.2. Depicts a false-color Digital Elevation Model (DEM) overlain by the GIS files generated in calculation of meander migration rates and net sediment contributions from banks including river centerlines from 1938 (red line) and 2005 (blue line) as well as polygons used to extract bank elevations from the 2005 lidar DEM for the right (dark blue polygons) and left (light blue polygons) banks. Also note an oxbow lake that has been cut off and is currently filling with sediment during high flow events.

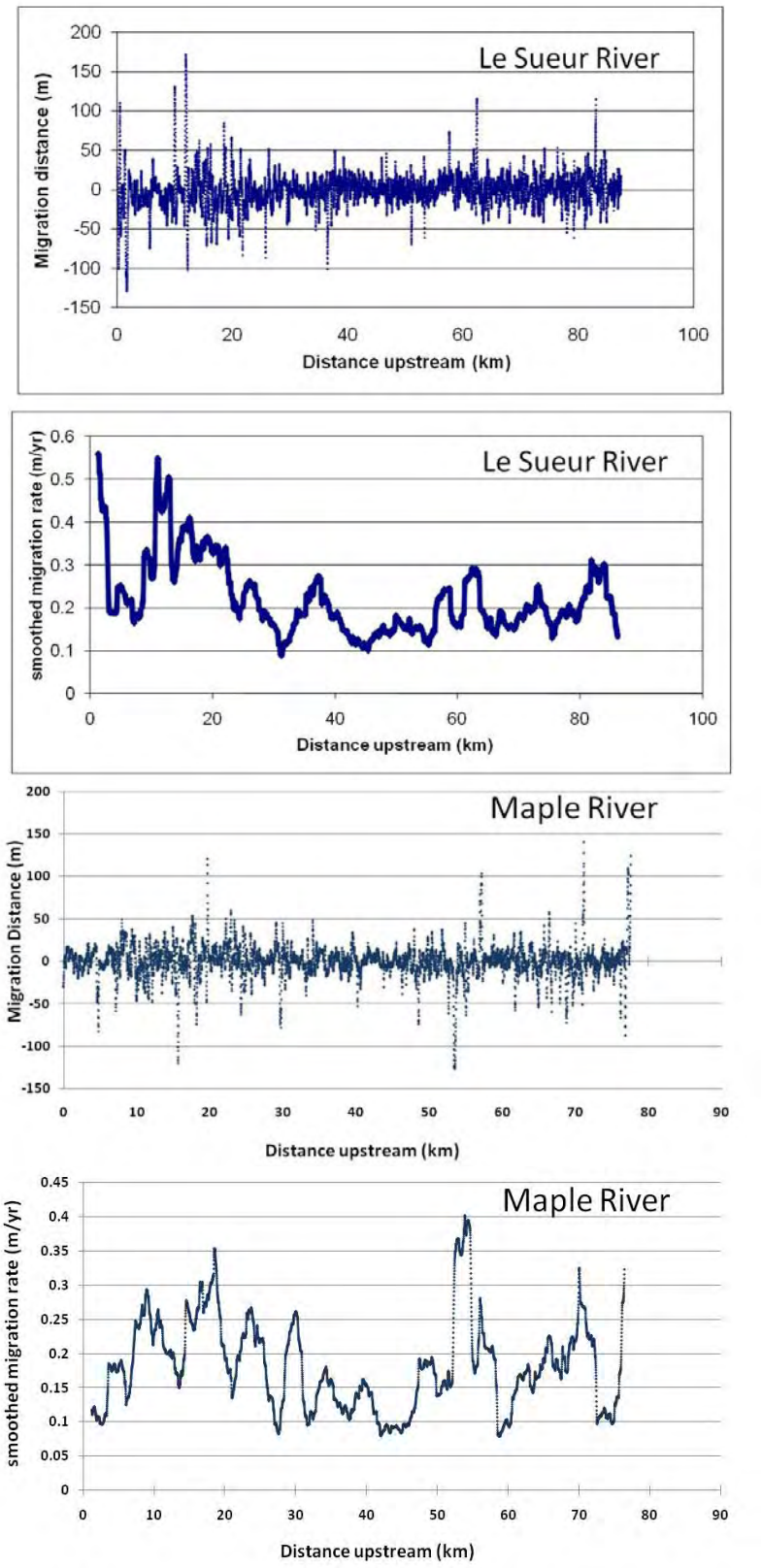

Figure 7.3. Lateral migration distances for the Le Sueur and Maple rivers (A and C), respectively, between 1938 and 2005. Annual average migration rates for the Le Sueur and Maple rivers (B and D), respectively, after the absolute values of the raw data have been filtered using a moving 2.5 km averaging window.

Because of the unique incisional history of the Le Sueur River, we organized net sediment contributions from banks by their spatial location with respect to the knick zone. Table 7.1 shows preliminary results of the net sediment contributions from banks for the Maple and Le Sueur Rivers within Blue Earth County. The calculations have been performed separately for the river above the upper gauging station, between the upper and lower gauging stations, and below the lower gauging station for comparison with sediment loads measured at the gauges. Column 1 indicates the reach being considered, column 2 indicates the net volume of sediment contributed from banks as a function of the migration rate and difference in bank heights. Column 3 uses a bulk density of 1.3 Mg per m^3 to covert the net volume to a mass and column 4 assumes the fraction of washload to be 50% of the eroded material (from the average of >150 bank samples). Note that these numbers do not represent the net source of sediment from the combined channel-floodplain system because floodplain deposition has not yet been taken into account, as is discussed below.

Table 7.1. Net sediment contributions from banks as a result of lateral migration in the Maple and Le Sueur Rivers.

	Net volume of sediment eroded (m^3/yr)	Net mass of sediment eroded (Mg/yr)	Net mass of washload input to channel (Mg/yr)	Unit net streambank washload to channel (Mg/m/yr)
Entire Maple River within Blue Earth County	6400	8380	4140	0.0533
Maple River above upper gauge, but within BEC	1700	2150	1080	0.0289
Maple River between upper and lower gauges	4500	5860	2930	0.0843
Below Lower Maple Gauge	200	2760	130	0.0242
Entire Le Sueur River within Blue Earth County	5300	6930	3470	0.0488
Le Sueur River above upper (St. Clair) gauge, within BEC	980	1260	630	0.0397
Le Sueur River between St. Clair and Highway 8 gauges	2560	3330	1660	0.0418
Le Sueur River below Highway 8 gauge	1800	2340	1170	0.0769

We use the unit net streambank erosion rates measured within the knick zone and above the knickpoint to extrapolate bank erosion rates to the portion of the stream network that is actively migrating. The stream lengths over which this calculation are made and rates applied are shown in Table 7.2 A, B, and C for the Le Sueur, Maple, and Cobb Rivers, respectively.

Table 7.2A. Input data used to compute net, local streambank erosion as a function of channel migration on the Le Sueur River

Le Sueur River	**Length (m)**		
Strahler order	Above Upper Gage	Between gages	Below Lower Gage
6	9619	40524	15179
5	77484		3857
4	54972	13493	
3	82453	22782	
2	211317	56101	9730
1	201304	53559	4591
Orders 6, 5, and 4 - total length (m)			
Above upper gage	Between gages	Below lower gage	Total
75847	54018	19036	148900
Length in bluffs (m; %)			
3550	16540	10300	meters
0.05	0.31	0.54	%
Length for migration source calculation (m)			
72297	37478	8736	
Rate for migration source calculation (Mg/m channel length)			
Above knickpoint	Within knickzone		
0.040	0.059		
Migration source (Mg/y)			
Above knickpoint	Within knickzone		Below lower gages
2870	2742		518

Table 7.2B. Input data used to compute net, local streambank erosion as a function of channel migration on the Maple River.

Maple River	**length (m)**		
Strahler order	Above Upper Gage	Between gages	Below Lower Gage
6			
5	36329	36105	9319
4	77383		
3	86579		
2	162707	14680	2436
1	133018	10607	1740
Orders 6, 5, and 4 - total length (m)			
Above upper gage	Between gages	Below lower gage	Total
75020	36105	9319	120444
Length in bluffs (m; %)			
4190	14570	3770	meters
0.06	0.40	0.40	%
Length for migration source calculation (m)			
70830	21535	5549	
Rate for migration source calculation (Mg/m channel length)			
Above knickpoint	Within knickzone		
0.029	0.084		
Migration source (Mg/y)			
Above knickpoint	Within knickzone		Below lower gages
2045	2283		468

Table 7.2C. Input data used to compute net, local streambank erosion as a function of channel migration on the Cobb River.

Cobb River	**length (m)**		
Strahler order	Above Upper Gage	Between gages	Below Lower Gage
5	24218	32665	9554
4	38542	52114	
3	37990	53803	
2	79385	96861	3538
1	70380	81081	4466
Orders 6, 5, and 4 - total length (m)			
Above upper gage	Between gages	Below lower gage	Total
43489	84779	9554	137821
Length in bluffs (m; %)			
7960	10520	3560	meters
0.18	0.12	0.37	%
Length for migration source calculation (m)			
35529	74259	5994	
Rate for migration source calculation (Mg/m channel length)			
Above knickpoint	Within knickzone		
0.029	0.084		
Migration source (Mg/y)			
Above knickpoint	Within knickzone		Below lower gages
1026	6765		505

Quantifying bank erosion from channel widening

Channel width change may represent a significant source of sediment in the Le Sueur watershed. In general, width can be measured using either ground-based approaches or by aerial photograph analysis. When historic cross-sections have been surveyed, the ground-based approach allows for the reconstruction of detailed sediment budgets (Trimble, 1997; Trimble, 2009) and has the advantage of identifying geometric change across the entire cross section, not just near the top of bank. However, ground-based methods are not feasible where carefully monumented historic cross-sections are unavailable (as in the Le Sueur basin) and would not provide representative coverage without an extremely large number of sites. Where ground-based surveys are not available, aerial photograph analysis has been used to document geomorphic changes in channel bankfull width and associated sediment fluxes. For example, Buckingham et al. (2007) developed a sediment budget for a reach of the Las Vegas Wash, Nevada, using historic photographs from three periods, 1975, 1989, and 1999. Sediment

production was based on estimates for channel volume at each of the three time periods. Galster et al. (2008) used aerial photography to analyze changes in width for two streams in the Lehigh Valley, Pennsylvania. Based on two photographic periods, 1946/1947 and 1999, they concluded that width change is discernable for streams ranging from 6 to 15 m wide given a sufficiently large sample size. Other studies have used sequential aerial imagery to estimate alluvial sediment loads on larger rivers such as the Fraser River, British Columbia (e.g. Martin and Ham, 2005).

For the present study, channel width changes were assessed using aerial photograph analysis for the time period between 1937 and 2009. Historic photographs, obtained from the Minnesota Department of Natural Resources and the John R. Borchert map library at the University of Minnesota, were aligned (georeferenced) to year 2009 National Agricultural Imagery Program (NAIP) aerial photographs using a minimum of ten ground control points and a second-order polynomial transformation (see Hughes et. al, 2006, although note that any photograph alignment error between historic and modern images would be unlikely to influence scale-related parameters such as width or channel planform area). Once aligned and correctly scaled, channel banks, defined as the transition from a vegetated to non-vegetated surface, were delineated on the background images. We did not use the water level on the day of the photograph to define the geomorphic width because this parameter varies with flow conditions. Rather, we use the vegetation line to define the channel under the assumption that the vegetation line is controlled by some integral of previous flow events and is much less likely to be influenced by short-term fluctuations in discharge.

Highly variable photographic quality as well as light and dark regions associated with shadows prevented the bank delineation from being automated. Instead, banks were identified by hand in a GIS along each study reach. In general, the bank position was relatively obvious on the outside of meander bends, particularly where lighting conditions were good. However, some judgment was required when delineating banks located on freshly deposited point bars or where shadows or overhanging trees obscured cut banks. Where shadows and/or overhanging vegetation were an issue, the operator attempted to find points where water or unvegetated bar sediment could be conclusively identified and then interpolated the bank line across intervening obstructions. Because shadows were most likely to be an issue on the oldest photographs, this process may have resulted in a small overestimate of width early in the record, thereby causing our overall width change estimates to be conservative.

Banks were defined through this process on 14 separate river reaches each approximately 10 meander bends in length. The average width for each reach was computed by dividing the total planform area between banks by the reach's centerline length. The process utilized a total of a total of 36 pre-2000 photographs distributed across the Le Sueur watershed and in adjacent basins (Table 7.3). In all but one case, the oldest photograph in the dataset extends back to the late 1930s. Because the relative importance of error in identifying bank position increases as overall channel width decreases, we focused primarily on the largest tributaries of the Minnesota River and did not perform the analysis on channels less than about 10 m in width. Several reaches of the Minnesota River itself were also included in the analysis, both because the photographic record was more complete within the Minnesota Valley and because the Minnesota River's relatively large size helps minimize the importance of classification error associated with the determination of bank position.

Table 7.3: Reaches considered in width change analysis.

Reach Name	Midpoint Coordinate	Typical Length (km)	Typical Width (2000s average) (m)	Photograph Years
Minnesota R. @ Jordan	93°37'29"W, 44°42'49"N	7.02	107.3	1937, 1940, 1951, 1963, 1964, 1991, 2003, 2004, 2005, 2006, 2008, 2009
Minnesota R. @ Fort Snelling	93°27'46"W, 44°48'23"N	11.40	90.8	1937, 1940, 1951, 1960, 1962, 1967, 1971, 1991, 2003, 2004, 2005, 2006, 2008, 2009
Minnesota R. @ Judson	94°7'34"W, 44°10'56"N	8.31	88.5	1938, 1949, 1950, 1958, 1964, 1971, 1991, 2003, 2004, 2005, 2006, 2008, 2009
Little Cobb R. Downstream	93°59'17"W, 44°01'57"N	1.69	20.3	1939, 1949, 1991, 2003, 2004, 2005, 2006, 2008, 2009
Little Cobb R. Upstream	93°59'24"W, 44°01'22"N	2.62	17.7	1939, 1949, 1991, 2003, 2005, 2006, 2008, 2009
Watonwan R: Downstream	94°14'23"W, 44°01'03"N	1.89	36.7	1938, 1949, 1964, 1991, 2003, 2004, 2005, 2006, 2008, 2009
Watonwan R: Middle	94°32'05"W, 44°03'04"N	1.54	15.2	1939, 1991, 2003, 2006, 2009
Watonwan R: Upstream	94°35'34"W, 44°04'02"N	1.38	11.5	1939, 1991, 2003, 2009
Cottonwood R.	94°32'33"W, 44°17'11"N	7.05	38.0	1938, 1955, 1991, 2003, 2004, 2005, 2006
Le Sueur R.	94°01'51"W, 44°06'26"N	9.42	47.5	1939, 1949, 1950, 1958, 1964, 1971, 1991, 2003, 2004, 2005, 2006, 2008
Blue Earth R. Upstream	94°05'52"W, 44°01'59"N	5.84	49.0	1939, 1949, 1973, 1991, 2003, 2004, 2005, 2006, 2008, 2009
Blue Earth R. Downstream	94°06'08"W, 44°07'17"N	14.01	58.2	1939, 1949, 1973, (1980), 1991, 2003, 2005, 2006, 2008, 2009
Maple R.	94°01'04"W, 44°04'21"N	4.62	24.8	1938, 1949, 1964, 1971, 2003, 2004, 2005, 2006, 2008, 2009
Chippewa	95°47'43"W, 45°05'57"N	5.75	34.2	1938, 1956, 1991, 2003, 2006, 2008, 2009, 2010

Figure 7.4 shows a small portion of a typical reach of the Lower Minnesota River near Jordan. Banks digitized on the 1940 portion of the image are overlain on the 2009 image of the same reach, illustrating a noticeable increase in width at this location. The image is also characterized by what appears to be an increase in floodplain vegetation and a decrease in active farmland immediately adjacent to the river.

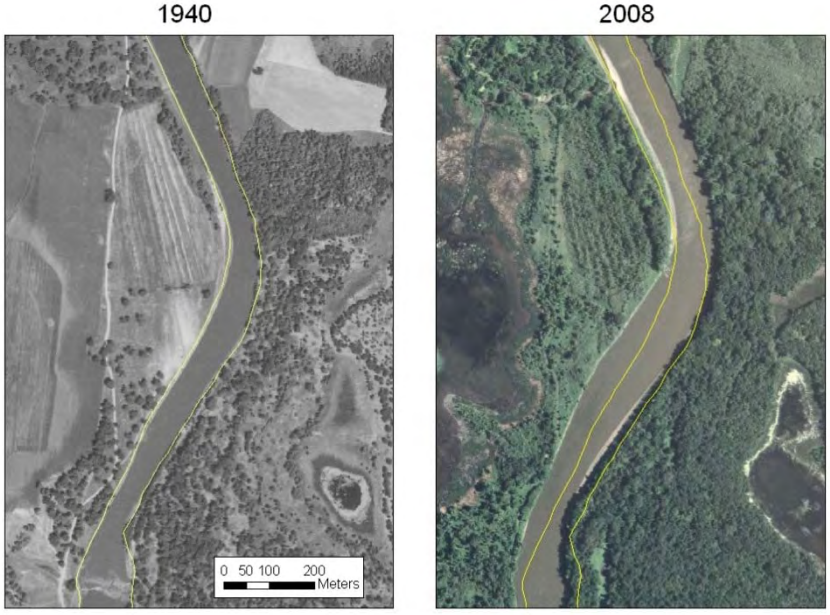

Figure 7.4. Width change on the Minnesota River near Jordan.

Figure 7.5 presents width relative to the mean value estimate for all photographs taken after the year 2000 for each reach in the analysis. We observe overall increases in bankfull channel width for each of the reaches in the dataset. However, our confidence in the rate of increase is stronger for the larger rivers, where the relative error in visually determining bank position is lowest.

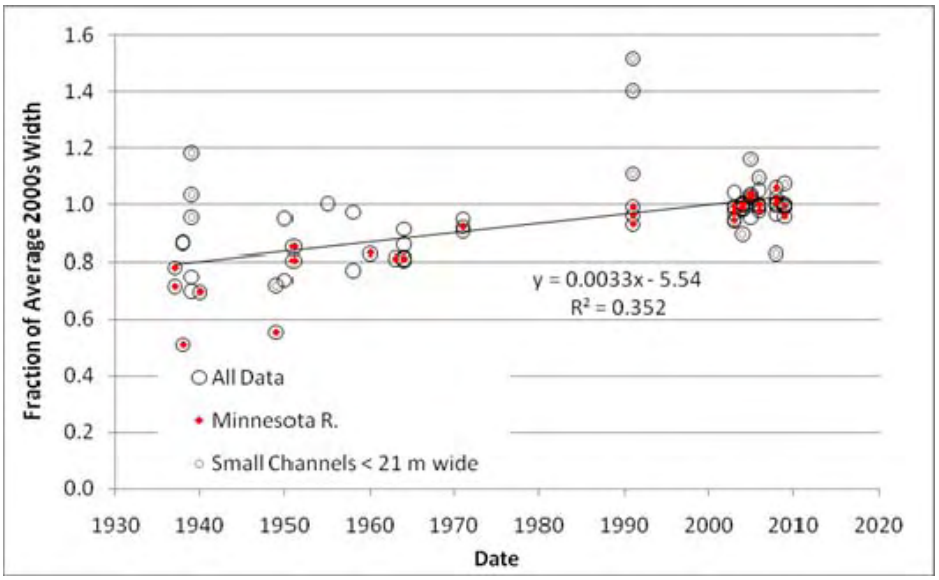

Figure 7.5. Trends in normalized width over time.

Reach-by-reach average rates of increase in width, derived by computing the slope of a simple regression line placed through the raw width data or through the width relative to the 2000s average for a given reach are summarized in Table 7.4. While many of these slopes are not individually statistically significant, the overall trends are strongest for the largest (and thus least error prone) reaches—particularly for the Minnesota River. For the smallest channels (less than 25 m in width), the trend is relatively flat.

Table 7.4. Summary of Width Analysis Results

Reach Name	Rate of Increase (m/yr)	Annual Rate of Increase relative to average 2000s width
Minnesota R. @ Jordan	0.43	0.40%
Minnesota R. @ Fort Snelling	0.33	0.36%
Minnesota R. @ Judson	0.65	0.74%
Little Cobb R. Downstream	-0.07	-0.36%
Little Cobb R. Upstream	0.02	0.11%
Watonwan R: Downstream	0.15	0.41%
Watonwan R: Middle	-0.03	-0.18%
Watonwan R: Upstream	0.0004	0.001%
Cottonwood R.	0.05	0.14%
Le Sueur R.	0.18	0.38%
Downstream Blue Earth R.	0.05	0.08%
Upstream Blue Earth R.	0.23	0.48%
Maple R.	0.05	0.21%
Chippewa	0.06	0.17%
Minnesota R. only	n/a	0.49%
All reaches excluding Minnesota R.	n/a	0.18%
Reaches > 25 m wide only	n/a	0.39%
Tributaries > 25 m wide only	n/a	0.30%
Tributaries < 25 m wide only	n/a	0.00%
All Data	n/a	0.29%

The overall trend of bankfull width increase over time for all large channels in the dataset implies that channels in the Minnesota River watershed are either changing geometrically (and thus probably exporting sediment), or that the vegetation line is moving up the bank, presumably in response to an increase in discharge. We tested the possibility that changes observed on the aerial photographs could be due to shifts in vegetation by developing local at-a-station relationships for hydraulic geometry relationships for water surface width using the available imagery at the two sites on the Lower Minnesota River with the longest flow records, Jordan and Fort Snelling. At these locations, we determined average water surface width (water surface area / reach length) for each historic image and related the width of the water surface to the mean daily discharge on the date of the photography. For dates that did not have associated discharge data, we estimated discharge using a relationship developed between each respective gauge and the Mankato gauge (USGS 05325000).

Results of the at-a-station hydraulic geometry analysis are presented in Figure 7.6. For both Jordan and Fort Snelling, the relationship between discharge and width appears to have changed over time, with recent relationship tending toward a wider channel for a given in-bank

discharge. This implies that the entire cross-section of the channel is changing over time, rather than just the vegetation line, at least for the lower Minnesota River. The simplest interpretation is that the channel is widening through a process whereby bank material eroded by the river is not completely replaced in nearby point bar sediment. It is thus likely that any silt/clay size sediment eroded through the bank widening process can be considered a net source of sediment in the overall sediment budget.

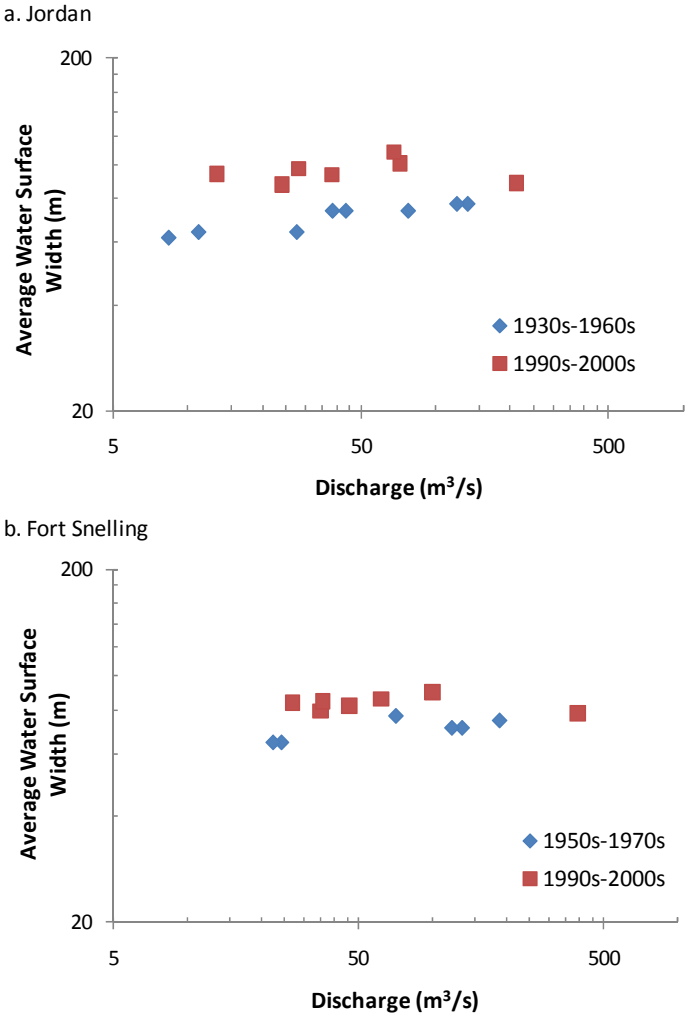

Figure 7.6. At-a-station hydraulic geometry for reach-average water surface width as observed in the air photo record along the lower Minnesota River for a) Jordan and b) Fort Snelling. In both cases, the water surface width for a given below-bankfull discharge has increased over time.

Channel incision as a sediment source

The knick zone of the Le Sueur, Cobb, and Maple Rivers have been actively incising since the base level fall 13,400 years ago. The incision rate has slowed over time as the channel gradient in the knick zone has decreased. However, two lines of evidence suggest that the knick zone continues to incise in the present day. First, the difference in eroding and depositing bank heights is elevated within the knick zone (approximately 40 cm greater on average than above the knickpoint). This implies that the channel has lowered by that amount over the timescale by which it sweeps across the valley bottom. Second, the Le Sueur has left behind an excellent

record of strath terraces (old floodplains) that preserve the incision record (discussed in section 2). The most recent terraces that we have dated suggest that the river is currently incising at a rate of 1.2 m per thousand years. As the river incises, it erodes the glacial sediments that underlie the channel bed and therefore must be included in the sediment budget.

The vertical incision rate, channel length, and channel width can be used to estimate the flux of sediment contributed solely from the incision process.

$$E = l \times b_c \times i \times \Delta t \times \rho \times f_{w,b} \qquad (7.3)$$

where b_c is the channel width in meters and i is the incision rate in meters per year. Using an average bulk density for till of 1.8 Mg/m^3, an average channel width of 25 m, an average incision rate of 0.0012 m/yr, and 65% silt and clay, Table 7.5 shows the total stream lengths and total average washload contributed to the channel within the knick zone.

Table 7.5. Sediment loads from channel incision in the knick zone

	Incising stream length (m)	Washload mass generated from incision (Mg/yr)
Maple River	45,423	1,600
Le Sueur River	73,053	2,600
Cobb River	47,295	1,700
Entire knick zone	165,772	5,800

Floodplains as a sediment sink

Once sediment is introduced into the channel, some portion of it will typically be deposited in floodplains. We have accounted for floodplain deposition by the process of lateral accretion implicitly in our meander migration calculation above, following Lauer and Parker, (2008a). In this section we discuss our approach to computing decadal-scale overbank deposition rates above the knickpoint and within the knick zone.

Short-term (decadal scale) overbank deposition rates are notoriously difficult to quantify because the depositional events are infrequent and the amount of deposition is extremely spatially heterogeneous and depends strongly on the concentration of sediment in the water, which can vary more than two orders of magnitude over a few short hours. A number of field observations indicate that sediment storage is not a dominant component of the sediment budget in the Le Sueur watershed. First, the channel network sits on a relatively thin mantle of alluvial sediment, negating the possibility that significant aggradation is occurring. In-place glacial till is exposed in the channel throughout the knick zone and has even been observed in a few locations above the knickpoint on the Le Sueur River. Second, very few locations were observed to have received floodplain sediment deposition during the four year course of our study. One commonly used method to constrain overbank deposition rates is measurement of the burial depth of vegetation (e.g., depth of sediment overlying root crowns, buried leaf litter layers, etc.). In the Le Sueur we have found very few locations where significant deposition is observed. Above the knickpoint large woody debris jams locally and temporarily dam the river (with a frequency of occurrence of once every few km), causing small and highly variable deposition sites. In these limited locations we observed buried root crowns, however, a comprehensive survey was not deemed necessary, given the limited occurrence. Overbank floodplain deposition above the

knickpoint is highly variable, occurring primarily behind large woody debris jams and during infrequent high flow events. Even during the flood of record in September 2010 very little deposition was observed throughout most of the knick zone, except for the lowest 10-15 km, near the mouth. Following the September 2010 event we mapped floodplain deposition within a few hundred meters of the road crossings along the Maple and Le Sueur Rivers. These numbers cannot necessarily be used to quantify annual deposition because this was such an anomalous event and our observations are limited to road crossings, which may influence the hydraulics of the river and therefore sediment transport, however, the pattern of deposition indicates very little storage is occurring within the middle section of the knick zone.

Despite the fact that field evidence suggests that overbank deposition is not a dominant component of the sediment budget, it should not be neglected entirely. In an attempt to constrain average annual overbank deposition rates we make two key assumptions. Above the knickpoint the longitudinal profiles of the Le Sueur, Maple, and Cobb appear to be reasonably well graded, with a concavity of approximately 0.5. In the absence of field evidence suggesting otherwise, we assume long-term mass balance with the computed net, local streambank inputs from channel migration, estimated to be ~6000 Mg per year above the knickpoint. Within the knick zone we know that the channel is vertically incising and therefore long-term mass balance equilibrium cannot be assumed. Instead we computed floodplain deposition as the difference between predicted loading (based on our measured source erosion rates under a balanced budget condition, which sum to 45,000 Mg/yr) and measured loads at the lower gauges on the three main branches and the gauge at the watershed mouth (which infer additional loading of only 27,000 Mg/yr between the gauges). The difference between these numbers (18,000 Mg/yr) provides an estimate of net floodplain storage. It is conceivable that some portion of this difference could also be accounted for by MPCA error in gauge loads and/or our predicted loads.

Section III: Morphodynamic Modeling

8. Sediment routing model

Introduction

Developing accurate sediment budgets using isotopic sediment fingerprints requires a sediment routing model that allows for variation in time and space of the volume of sediment and isotopes stored in the floodplain. While many water quality models allow for net deposition and/or net erosion onto or from a river bed (AnnAGNPS, HSPF, WEPP), they generally do not account for floodplain storage. Furthermore, these models do not account for the decay of radioisotopes while sediment is stored in off-channel reservoirs, nor do they account for in-floodplain production of these tracers. Both of these processes could have important implications for short-lived isotopic tracers that pass through large floodplains. The model framework presented here includes mechanisms for tracing sediment based on fingerprints derived from cosmogenic or radiogenic nuclides in either the sand or mud fractions.

Because the model has been developed from scratch, it is important to ensure that it provides reliable results that are numerically accurate. Much of our modeling effort has thus involved a) basic model development, including the addition of theoretical improvements relative to the model presented in the 2009 annual report, b) the development of methods for varying sediment, water, and tracer inputs over time, with the ultimate goal of allowing users to test a range of potential hypotheses regarding basin history, and c) developing and implementing model tests to ensure that the model provides reasonable results. This report focuses primarily on presentation of the basic theory behind the current version of the model and describes simplified model runs that illustrate how the rivers in the Le Sueur basin may have responded to simplified changes in water and sediment loads as the basin was historically developed for agriculture.

The numerical runs presented in this section demonstrate that the basic numerical implementation is providing reasonable results in the context of the Le Sueur River basin. These runs have been performed to illustrate how the routing model can be applied to investigate the effects that changes in the input of water and sediment to the modeled reaches may have in terms of sediment load. They do not focus on a detailed accounting of every change that might have occurred within the basin over the past centuries. They instead present all the modeling steps needed for a reliable site-specific application of the model at engineering time scales.

The first phase of a site-specific application of the model, which we refer to as “spin-up”, is done to set the initial conditions for short-term applications. In the applications presented below, we focus on applying the spin-up process to build the pre-settlement river system. Simplified changes in sediment loads and river flows in the post-settlement era are then simulated in order to reproduce relatively realistic present-day conditions in terms of sediment loads and channel geometry. Finally, the effects of two different restoration scenarios in terms of sediment loads in the river are investigated. In the first scenario we assume that all the sediment sources do not change in the next 140 years (i.e. until 2150). In the second, we discuss potential effects of a hypothetical future reduction of the sediment contributed from eroding bluffs.

Modeling Overview

Five primary sources of sediment have been recognized in the Le Sueur River basin: lower order tributaries, incision of ravines, erosion of bluffs, erosion of uplands and exchange of sediment between the river and the floodplain. The model accounts for the first four sources by allowing the user to arbitrarily specify the rate at which the given source provides sediment and tracer material. Rates may be constant or may vary over time. Once sediment and/or tracer enters the river, it is mixed with whatever is being conveyed downstream according to mass conservation equations that differ only minimally from those used in standard contaminant routing models. The model differs from traditional models in the way it handles the fifth term — that associated with sediment storage and exchange with the floodplain. Here, rather than simply allowing the user to specify a floodplain-related sediment source associated with streambank erosion, the model specifically allows the volume of sediment stored in the floodplain to grow or shrink over time as the system evolves. If the system is overloaded with sediment, the sediment can be stored temporarily in the floodplain until channel migration eventually causes it to be resupplied to the channel, after which it is transported further downstream. Morphological feedbacks are included to ensure that the floodplain evolves toward a steady state for both sediment storage capacity and isotopic tracer concentration. The steady state depends on water and sediment loads, so that when these loads are perturbed, the floodplain may take many years to re-achieve sediment flux balance. In the intervening time, the floodplain may represent either a net source of sediment or a net sink, depending on the nature of the perturbation. The model is intended to be used to test the response of the channel/floodplain system to changes that occur over timescales of decades to centuries. It is not appropriate for use over sub-annual time scales.

The three main rivers in the Le Sueur River basin are characterized by a knickpoint that is slowly migrating upstream. These knickpoints formed approximately 13,400 yrbp when the Minnesota River valley was excavated. Below the knickpoints, channels are slowly incising into consolidated glacial tills. Above the knickpoints there has not been much incision since the last glaciation. It is not entirely clear how strongly knickpoint dynamics affect sediment fingerprints in the present-day system. In a slowly incising system, the timescale for the variation of bed elevation due to the migration of the knickpoint is probably much longer than the timescale necessary to completely rework the floodplain, implying that the migration of the knickpoint can be neglected in modeling the geomorphic evolution of the modern floodplain. However, knickpoint migration and the associated slow incision of the downstream reach represent a source of uniquely fingerprinted sediment to the lower part of the floodplain in the lower reach. Furthermore, the slow incision of the reach below the knickpoint may affect the steady state that the floodplain evolves toward, leading to cut banks that are significantly higher than they might otherwise be. We account for the migration of the knickpoints by dividing each river in the Le Sueur River basin (we present results for the Le Sueur and Maple Rivers here) into two segments: a reach above and a reach below the knick zone. The two reaches are linked by a moving boundary, the knickpoint, where the bed elevation is a continuous function but the slope (i.e. derivative of bed elevation) experiences a discontinuity.

Four different radioisotopes are routed through the systems. Two are associated with the sand fraction, i.e. in-situ produced ^{10}Be and ^{26}Al, and two are associated with the mud fraction, i.e. meteoric ^{10}Be and ^{210}Pb. (Note, however, that the model is not limited exclusively to radioisotopic tracers—it is straightforward to include conservative geochemical tracers as well). The ratio between the concentrations of in-situ produced ^{26}Al and ^{10}Be in sand is a measure of the accumulation of cold (i.e. from the erosion of bluffs and ravines) or hot (i.e. from the

uplands) sediment. The concentration profiles of the radioisotopes associated with the mud represent a different measure of the source of sediment. In the case of mud, sediment eroded from the uplands and/or floodplain has a much higher tracer concentration than the sediment eroded from bluffs or ravines.

The application of models of river morphodynamics to engineering problems is generally done in two phases. It is first assumed that the unperturbed river is at steady state, i.e. in a state in which all the variables are constant in time, and the model is initialized using a "spin-up" process until it achieves a reasonable initial (i.e. not-perturbed) steady state (e.g. Lauer and Parker, 2008 b and c, Viparelli et al., 2010). This initial condition is then perturbed by adjusting forcing parameters, such as water and sediment supplies, over engineering time scales.

Because the present report is focused both on validating model results and on illustrating how the model can be used to simulate the response to realistic changes in forcing parameters, the spin-up process is divided into two parts. The model is first run to reach steady state for a simplified case in which the lateral sources of sediment (i.e. tributaries, uplands, bluffs and ravines), incision rate, and consequently the migration rate of the knickpoint, are neglected. During the initial spin-up period, water discharge is not allowed to increase downstream. The only parameters that vary in the streamwise direction are the channel slope (i.e. above and below the knickpoint) and the floodplain width. The primary purpose of this initial spin-up period is to allow long-lived tracers such as ^{10}Be to accumulate to realistic levels in the floodplain, a process that can take hundreds or thousands of years. Furthermore, the simple boundary conditions for this initial spin-up period allow the steady state that is achieved after spin-up to be compared with analytical tracer profile solutions presented by Lauer and Willenbring (2010), thereby validating the numerical implementation of the model. This first, simplified steady state is then used as the initial condition for a second 1000-year spin-up run that that incorporates a more realistic representation of streamwise variability of water discharge, lateral sources of sediment and the incision in the reach below the knickpoint. The model results at the end of this second phase are assumed to be representative of pre-settlement river conditions.

The model is then run for 160 years under conditions that increasingly diverge from the baseline of the second spin-up period (post-settlement runs). The run crudely represents gradual changes since the 1850s of several key parameters and boundary conditions. For our modeling purposes, we assume that parameters increased linearly for 150 yrs from pre-settlement values to present-day values, and then remain constant for 10 years (i.e. from 2000 to 2010). Finally, the model is run for other 140 years (i.e. from 2010 to 2150) under two different conditions to illustrate how the model can be used to predict the effects that different restoration strategies might have on a river system (restoration runs). In the first scenario, it is assumed that the present inputs of sediment and water discharge to the river are kept constant in time. In the second case, we simulate the effects of a hypothetical bluff protection project along the main channels in 2010 that instantaneously halves the input of sediment from the bluffs. The two scenarios are compared in terms of mean annual sand and mud loads.

It is important to point out that the assumptions made in our post spin-up scenarios are not representative of all known changes in the Le Sueur River basin and represent a rather significant oversimplification. Their goal is to demonstrate of the kind of changes the model can simulate over engineering time scales. Because of these simplifications, the modeling approach presented in this report should be thought of as illustrative of the steps required for a site-specific model application/validation rather than a detailed simulation or prediction. Additional simulations are recommended once more is known regarding the variability of water and

sediment loads over the post-settlement era. It may also be worth revisiting the model if future field-based observations of floodplain deposition allow for more confidence in the specification of some of the empirical parameters controlling channel/floodplain sediment exchange.

The numerical model: assumptions, hypothesis and approximations

The sediment routing model describes the co-evolution of a river with its floodplain considering sources and sinks of sediment and the variation in the downstream direction of water discharge, sediment transport rates and cross sectional geometry. The model is based on the work of Parker et al. (1996) and Lauer and Parker (2008 a and b).

The main assumption is that at steady state, the tendency for sediment to accrete on the floodplain due to overbank deposition is balanced by the tendency for the river to remove floodplain sediment through lateral migration. This condition is necessary if the floodplain volume is to remain unchanged on average over time while still allowing for both erosion and deposition of floodplain material. Clearly, real floodplains are usually not at such a steady state at any given time, and we do not make the assumption that the floodplains in the Le Sueur basin are presently in equilibrium. However, the evolution toward steady state provides a mechanism for simulating changes in floodplain sediment storage and channel hydraulic capacity over time, thereby allowing the model to simulate how changes in hydrology or sediment supply would affect channel/floodplain sediment exchange and ultimately the export of sediment and tracer from the system.

Other assumptions are:

a) The river is assumed to constantly rework the floodplain over geomorphic time, and the river and its floodplain can be divided into well-mixed layers;
b) The river is not immediately able to build its inner (accreting) bank to the same height as the outer (eroding) bank, resulting in a net removal of sediment. The difference in elevation between the banks is denoted as $\Delta\eta$;
c) The equations for the flow are simplified using the quasi-steady approximation (de Vries, 1965) because the problem of interest is the morphodynamic evolution of the river channel and its floodplain, which should occur over timescales of decades to centuries.
d) The range of flows can be represented by a flow duration curve representative for the watershed; for each portion of the flow duration curve, the hydraulics can be represented using uniform flow;
e) Since the model is intended to characterize channels at reach scale, the lateral migration speed of the channel, c, is represented using a single reach-average value, with no node-to-node variability;
f) Sediment participating in wash load (mud) is assumed to be so fine that its concentration in the water column can be considered uniform; this sediment is not assumed geomorphically unimportant, however, and is tracked by the mass conservations equations of the model.
g) Bed material transport is dominated by sand; gravel transport is assumed to be small compared to sand transport and thus is neglected.

Channel geometry

The floodplain is divided in three well-mixed layers: substrate, active layer, and floodplain, as represented in Figure 8.1, where B_c denotes the width of the channel, B_f represents the width of the floodplain, $\Delta\eta$ is the difference in elevation between the inner (accreting) and the outer (eroding) bank, H_{pb} is the height of the point bar, L_a and L_f are the thicknesses of the active layer and of the floodplain above the channel bed respectively. The total thickness of the floodplain is equal to $L_a + L_f$, and L_f is equal to $H_{pb} + \Delta\eta$. The elevation of the channel bed above the datum is denoted as η_b.

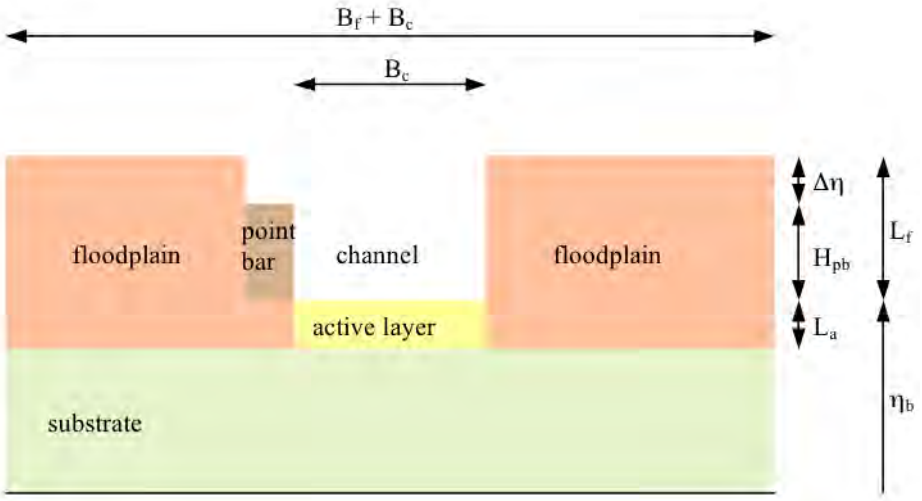

Figure 8.1: Division of the cross section in well-mixed layer and definition of the main parameters for channel geometry.

Sediment exchange between the river and the floodplain

The region immediately below the channel bed that is frequently reworked as bedforms migrate through is called the active layer (see Figure 8.1) and is assumed to be composed entirely of sand. The active layer thickness is assumed constant in time because it depends on bedform dynamics which in turn depend on the grain size of the channel bed sediment (assumed constant) and average characteristics of the flow.

There are several mechanisms by which the model allows sediment to enter the floodplain. These include point bar deposition, overbank deposition, and movement of material from the substrate into the floodplain as the channel incises. The exchange of sediment between channel and floodplain is not necessarily an even one. It instead depends on both overbank deposition history and the rate at which the channel is incising into the valley. Because of the potential elevation difference between the height of the point bar and the floodplain (i.e. $\Delta\eta$), channel movement can result in a transfer of more sediment from floodplain to channel at eroding cut banks than is returned from channel to floodplain in the form of a new point bar.

Since $\Delta\eta$ depends on point par height, H_{pb} plays an important role in moderating channel/floodplain exchange. The height of the point bar is assumed to depend primarily on the average characteristics of the flow and is thus assumed constant in time during the spin-up period and to vary as the flow rate increases in the post-agriculture runs discussed below.

Overbank deposition on the floodplain is computed independently from the lateral supply of sediment from floodplain to channel. Consequently, the net transfer of sediment between these two regions can be positive or negative, depending on a) the relative bank height difference $\Delta\eta$, and b) the frequency of flooding and the concentration of suspended sediment in floodwater. Because the model explicitly solves for floodplain thickness L_f and difference in elevation between the banks $\Delta\eta$ in each time step, the floodplain grows in height and floods less often if the net transfer of sediment is toward the floodplain. This reduces the overbank deposition rate. On the other hand, if the net transfer of sediment is from floodplain to channel, the floodplain becomes lower on average, which increases overbank deposition rates. This stabilizing feedback allows the system to evolve toward a condition where the net loss of sediment at eroding bends is balanced by overbank deposition.

The overbank deposition of suspended sediment per unit channel length, D_f, is computed with the formulation due to Parker et al. (1996). Under the assumption that the sediment in suspension in the water column is not too fine and that the flow on the floodplain is not too slow

$$D_{fk} = Fl_k \cdot C_k \frac{Q_f}{B_f} \tag{8.1}$$

where k is a subscript that denotes the size range, i.e. k = s for the sand / bed material and k = m for the mud / wash load, C_k is the volumetric concentration of sediment in suspension in the channel above the floodplain, Q_f is the flow discharge on the floodplain and Fl_k is a user specified parameter called floodplain number (see Viparelli et al., submitted, for further details on the implementation).

The two-reach model for the Le Sueur River basin

To apply the model in the Le Sueur River basin, additional assumptions are necessary because of the process of incision driven by the migration of the knickpoint. While the model framework allows the channel bed elevation to evolve as a function of the supply of bed material sediment, we have elected not to implement this feature here because in preliminary runs, it did not provide realistic results (probably because the profile is controlled in many locations by coarse channel lags). Instead, the river is presently modeled as a below capacity system, meaning that the transport rate of sand is not computed with a standard equation relating sediment load to either bed shear stress or stream power (e.g. Engelund and Hansen, 1967; Brownlie, 1981; Wright and Parker, 2004) but instead is assumed to be a simple sum of all accumulated sediment sources minus all accumulated sediment sinks. In other words, the channel is modeled as supply-limited rather than capacity-limited for both sand and mud (Viparelli et al., submitted and Viparelli et al., in preparation a). One of the drawbacks of modeling the system as below capacity is that the model cannot be used to simulate either bed aggradation or degradation caused by an excessive perturbation of bed material sediment supply. For instance, the model as implemented cannot be used to determine whether a large reduction in sand and/or gravel supply caused by a program designed to stabilize eroding bluffs would lead to incision of the downstream channel. Likewise, it would not be possible to determine whether a change in hydrology in the basin leading to a reduction in peak discharge, in the absence of a reduction of bed material supply, would lead to channel bed aggradation. We explore the potential for using the at-capacity features of the model in (Viparelli et al., submitted).

Realistic incision rates (and thus realistic rates of supply of radio-isotopes by incision of the valley floor into the underlying glacial till) are ensured by holding channel bed elevation constant above the knickpoint and by specifying an incision rate below the knickpoint. The incision in the reach below the knickpoint is modeled as a rigid rotation of the longitudinal profile around its downstream end, where the channel bed elevation is assumed fixed. A schematic representation of the model for knickpoint migration is represented in Figure 8.2, where η_{knick} denotes the channel bed elevation of the knickpoint, x_{knick} is the streamwise position of the knickpoint, σ is the incision rate at the upstream end of the knick zone, s_{knick} denotes the migration rate of the knickpoint, t is the temporal coordinate and Δt is a time interval.

In this formulation, the knickpoint is defined as a point where the channel bed elevation is a continuous function but the slope (derivative of bed elevation) experiences a discontinuity. Thus, imposing the continuity for the time rate of change of bed elevation of the knickpoint (Viparelli et al., in preparation b), the upstream migration rate of the knick is a function of the incision rate and of the difference between the bed slope above, S_{above}, and below, S_{below}, knickpoint,

$$s_{knick} = -\frac{\sigma}{S_{below} - S_{above}} \tag{8.2}$$

where σ is assumed to be a positive number.

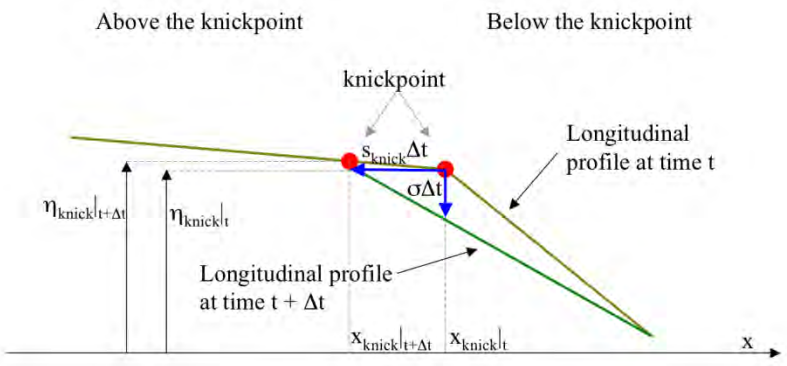

Figure 8.2: Conceptual scheme to model the migration of the knickpoint. x denotes the downvalley distance from the upstream end of the modeled river reach.

Calculation of mean annual values

In the model, the flow is specified in terms of a flow duration curve discretized into $N_{discharge}$ bins. To compute the load of sand and mud and the concentration of tracers in the water column, the equations of conservation of mass are solved in each bin of the flow duration curve. Mean annual values of sediment transport rates and overbank deposition rates are computed as

$$X_k = \sum_{j=1}^{N_{discharge}} X_{kj} p_{wj} \tag{8.3}$$

where p_{wj} represents the fraction of time that the flow is in a specified discharge bin of the flow duration curve and X_{kj} denotes the value of variable X_k computed for the j-th bin of the flow duration curve. (Throughout this report, the subscript "j" refers to values computed in each bin of the flow duration curve. Symbols with no subscript "j" represent annual values averaged over the flow duration curve according to equation 8.3). Sources and sinks of sediment and of cosmogenic nuclides are assumed to vary with the flow discharge and are thus computed for each bin of the flow duration curve, as discussed below. The morphodynamic mass conservation equations for the channel/floodplain system, however, are implemented as functions of the mean annual values.

Procedure for channel widening/ narrowing

Time variations in channel width are modeled as source or sink terms in the equations of conservation of sediment. The time rate of change of channel width is assumed to be proportional to the divergence of bed material load per unit channel width, q_b, as

$$\frac{\partial B_c}{\partial t} = \alpha_{Bc} \frac{\partial q_b}{\partial x} \tag{8.4}$$

where α_{Bc} needs to be calibrated from field data. Consequently, at steady state, the bed material load per unit channel width is constant in the streamwise direction. Since many load relations compute the bed material load per unit width as a function of the Shields number (e.g. Garcia, 2008), this result is not too far from the closure of a constant formative Shields number (e.g. Parker et al., 2007 and Wilkerson and Parker, 2010), in the case of an at-capacity system.

Flow of computation

The flow duration curve is expressed in terms of $N_{discharge}$ values of water discharge per unit drainage area, u_j, and the fraction of time p_{wj} each discharge bin occurs. To compute the water discharge in each node, u_j is multiplied for the area of the drainage basin. Appendix A discusses the development of flow duration curves for the model. For each bin of the flow duration curve, the load of sand and mud and the overbank deposition rates are computed with the equations of conservation of channel bed material and wash load in the water column and with equation 8.1. Mean annual values are then estimated with equation 8.3.

The new position of the knickpoint, its elevation above the datum, and the new longitudinal profile of the lower reach are computed with equation 8.2 and the formulation described above. Finally, conservation of mass is imposed to compute the thickness and the fractions of sediment of the floodplain, the difference in elevation between the banks, and the concentrations of radioisotopes in the load and in the floodplain and the loop starts again (see Viparelli et al., submitted for further details on the derivation of the governing equation and their numerical implementation).

Boundary conditions and model parameters

The sediment routing model requires the specification of an initial condition and a set of boundary conditions. The boundary conditions are fixed bed elevation at the downstream end of the lower reach, specified sediment feed rate at the upstream end of the upper reach, a flow duration curve, and the input of sediment and cosmogenic nuclides from uplands, tributaries, bluffs and ravines at each computational node.

Parameters

The parameters of the model can be divided in five groups: 1) those necessary to compute water and sediment loads at model boundaries; 2) those necessary for hydraulic computations; 3) reach-specific parameters necessary for floodplain sediment exchange computations; 4) global constants and 5) computational parameters.
Some of these parameters vary in the downstream direction. Such variability can potentially be expressed in either downvalley (x) or downchannel coordinates (x_c), as shown in Figure 8.3.

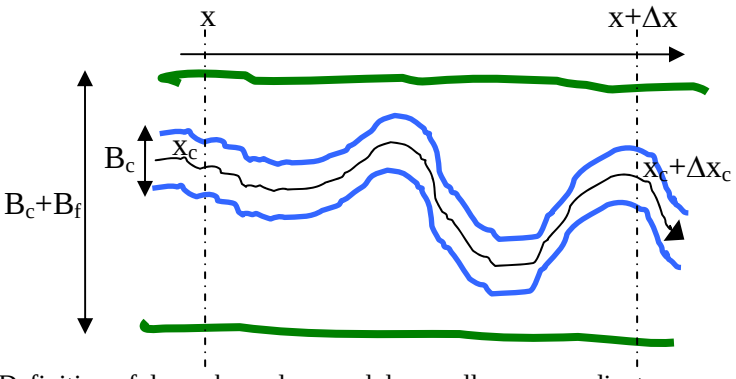

Figure 8.3: Definition of downchannel, x_c, and downvalley, x, coordinate.

For simplicity, and because we are interested primarily in valley-average output, we assume that sinuosity is constant within each channel reach, so that a given down-channel distance Δx_c can be found by multiplying the corresponding downvalley distance Δx by the average sinuosity Ω.

$$\Delta x_c = \Omega \Delta x \qquad (8.5)$$

For all downvalley or downchannel coordinates, zero is set at the upstream end of the modeling domain.

Parameters to compute water and sediment loads

The flow duration curve at each model node is computed by multiplying the base flow discharge per unit of drainage area, u_j, (Appendix A) by the total area of the drainage basin above the model node. This parameter can be varied through time by multiplying the initial parameter by an arbitrarily specified flow duration adjustment factor. In our runs, flow adjustment factors are held constant during model spin-up. Sediment loads supplied external to the model (i.e. feed rate of sediment from the basin upstream of the modeled reach, sediment input rates from uplands directly connected to the river, tributaries, ravines and bluffs) are computed by decomposing the total drainage area at a given node into the area of uplands

directly connected to the river, the area of tributaries, and the area of ravines, and then multiplying the area of each source times a denudation rate estimated from the data. The mean annual input of sediment from the bluffs reported in Figure 8.4 is specified at each computational node. These can be varied independently over time by multiplying time-varying user-specified adjustment factors for each type of lateral supply. Again, these factors are held constant during model spin-up.

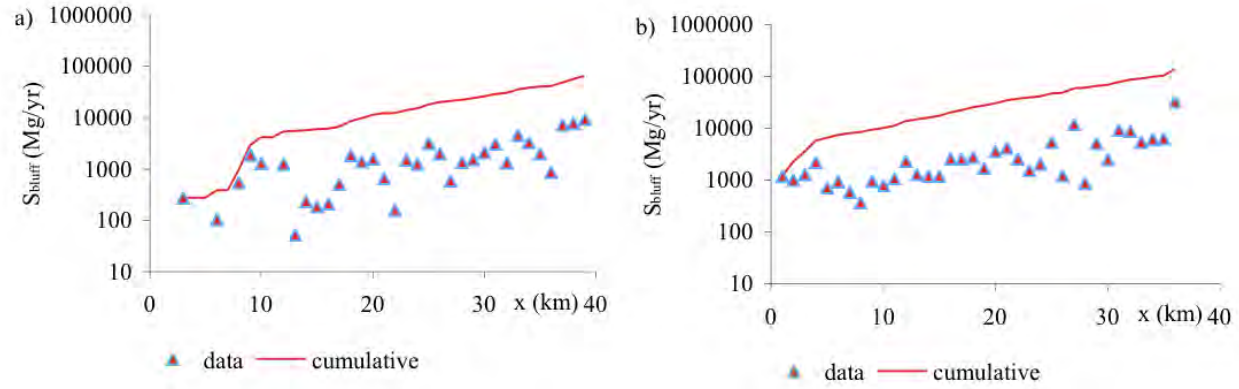

Figure 8.4: Input of sediment (sand and mud) from the bluffs a) Maple River, and b) Le Sueur River. x denotes the downvalley distance from the upstream end of each modeled river reach.

Figure 8.5 illustrates the variability in the downvalley direction of the area of uplands (i.e. agricultural fields), tributaries (also mostly agricultural fields but may include some bluffs and ravines), ravines for the Maple River (a) and the Le Sueur River (b). The red lines represent the synthetic relations to describe the downvalley variability of the directly-connected uplands in the drainage basin.

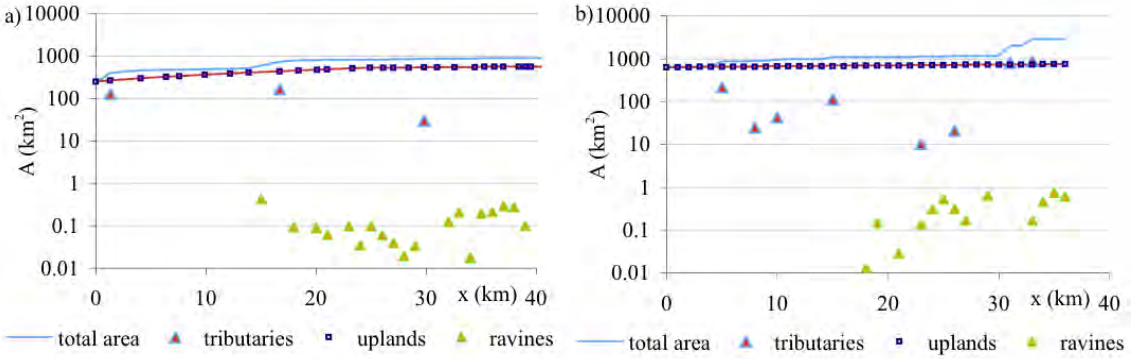

Figure 8.5: Total area of the drainage basin, of the uplands directly connected to the river, of the tributaries and of the ravines for a) the Maple River and b) the Le Sueur River. The red lines represent the synthetic relation to describe the increase of the area of the directly connected uplands in the drainage basin used in the calculation. In these figures, x denotes the downvalley distance from the upstream end of each modeled river reach.

In the Maple River basin, the area of uplands directly connected to the river below the knickpoint increases at a considerably smaller rate than above the knickpoint, thus two linear relations have been fit to the data. A single synthetic linear relation is sufficient on the Le Sueur. The input of sediment at each node is computed by multiplying the change in the appropriate

contributing area between two consecutive nodes by the appropriate denudation rates. The expressions of the synthetic relations along with the denudation rates are reported in Table 8.1.

Table 8.1: Parameters to compute water and sediment loads supplied external to the model. The concentrations of radioisotopes on the first rows are for the isotopes associated with the sand fraction (i.e. in-situ produced ^{10}Be and ^{26}Al). Concentrations on the second row are for tracers associated with the mud fraction (i.e. meteoric ^{10}Be and ^{210}Pb). The subscript "m" denotes meteoric ^{10}Be, ^{10}Be with no subscript refers to in-situ produced ^{10}Be.

Parameter	Maple River	Le Sueur River	Description
A_u (km^2)	11 x + 252 (above) 2.5 x + 463 (below)	3.16 x + 626.4	area of uplands in the drainage basin
D_{entrib} (Mg/km^2/yr)	17.9	60.5	denudation rate for the tributaries
D_{enrav} (Mg/km^2/yr)	2220	2220	denudation rate for the ravines
D_{enup} (Mg/km^2/yr)	10	10	denudation rate for the uplands
F_{strib}	0.1	0.1	fraction of sand in the sediment contributed from tributaries
F_{sB}	0.35	0.35	fraction of sand in the sediment contributed from bluffs
F_{srav}	0.35	0.35	fraction of sand in the sediment contributed from ravines
F_{sup}	0.1	0.1	fraction of sand in the sediment contributed from the uplands
T_{trib} (atoms/gr)	$5.3\cdot10^4$ (^{10}Be), $3.1\cdot10^5$ (^{26}Al), $2.2\cdot10^8$ (^{10}Be)$_m$, $4.3\cdot10^3$ (^{210}Pb)	$3.07\cdot10^4$ (^{10}Be), $1.8\cdot10^5$ (^{26}Al), $1.25\cdot10^8$ (^{10}Be)$_m$, $2.5\cdot10^3$ (^{210}Pb)	concentration of radioisotopes in the sediment contributed from the tributaries
T_{bluff} (atoms/gr)	$2.5\cdot10^4$ (^{10}Be), $7.5\cdot10^5$ (^{26}Al), $8.1\cdot10^6$ (^{10}Be)$_m$, $1\cdot10^2$ (^{210}Pb)	$2.5\cdot10^4$ (^{10}Be), $7.5\cdot10^5$ (^{26}Al), $8.1\cdot10^6$ (^{10}Be)$_m$, $1\cdot10^2$ (^{210}Pb)	concentration of radioisotopes in the sediment contributed from the bluffs
T_{rav} (atoms/gr)	$3\cdot10^4$ (^{10}Be), $9\cdot10^5$ (^{26}Al), $1.98\cdot10^8$ (^{10}Be)$_m$, $1\cdot10^2$ (^{210}Pb)	$3\cdot10^4$ (^{10}Be), $9\cdot10^5$ (^{26}Al), $1.98\cdot10^8$ (^{10}Be)$_m$, $1\cdot10^2$ (^{210}Pb)	concentration of radioisotopes in the sediment contributed from the ravines
T_{up} (atoms/gr)	$6\cdot10^4$ (^{10}Be), $3.6\cdot10^5$ (^{26}Al), $2.48\cdot10^8$ (^{10}Be)$_m$, $5\cdot10^3$ (^{210}Pb)	$6\cdot10^4$ (^{10}Be), $3.6\cdot10^5$ (^{26}Al), $2.48\cdot10^8$ (^{10}Be)$_m$, $5\cdot10^3$ (^{210}Pb)	concentration of radioisotopes in the sediment contributed from the uplands

In Table 8.1 the synthetic relation to compute the area of uplands in the drainage basin, A_u, is reported along with the present denudation rates (D_{entrib}, D_{enrav}, D_{enup}), the fractions of sand (F_{strib}, F_{sB}, F_{srav}, F_{sup}) and concentrations of radioisotopes (T_{trib}, T_{bluff}, T_{rav}, T_{up}) assumed for tributaries, bluffs, ravines, and directly connected uplands, respectively. Together, these terms provide the annual average loading of sediment and radioisotopes at each node in the reach. The denudation rate for the tributaries is computed using the sediment yield at the upstream end of the modeled reaches. The fraction of sand in the sediment contributed from small tributaries is set equal to 0.1, while for the Maple and the Cobb River it is assumed equal to 0.2 to account for the presence of bluffs and ravines in the basins. The concentration of radioisotopes in the sediment contributed from the tributaries is assumed approximately equal to the. 85% and 50% of the concentration in the sediment eroded from the uplands on the Maple and on the Le Sueur

respectively, based on meteoric ^{10}Be measurements at the gauges. Finally, the concentration of radionuclides in the sediment contributed at the upstream end of the modeled reach from the non-modeled portion of the basin is set equal to the concentration in the sediment contributed form lower order tributaries.

The input of mud at the upstream end of the modeled domains is computed as a function of the flow discharge, Q_{water}, at the upstream node of the modeled reach. The rating curves for the mud have been computed from the data of the upper gauges on the Maple River and on the Le Sueur River. The rating curves, shown in Figure 8.6, are based on the 2006-2007 data for the Maple River, and on the 2006-2007 and 2010 data for the Le Sueur River. These curves have been scaled to match the 2000-2010 sediment budget by factors of 2.22 and 2.87 on the Maple River and on the Le Sueur River, respectively.

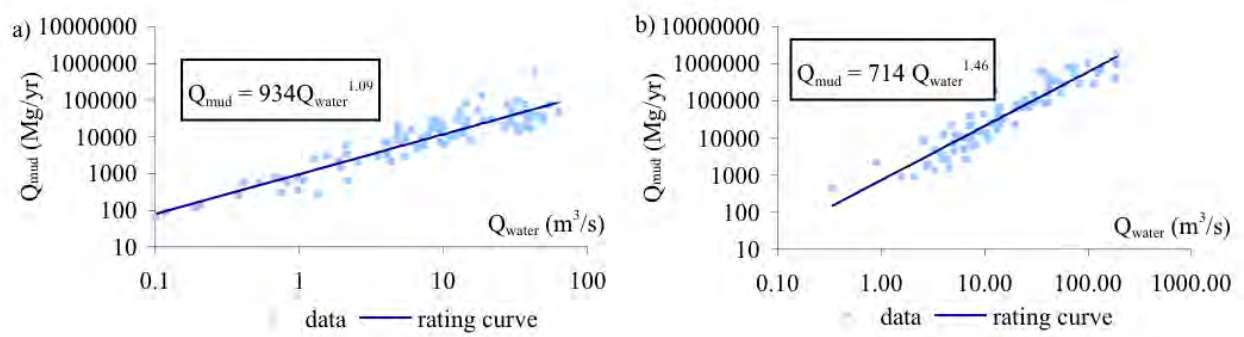

Figure 8.6: Rating curve for the mud a) at the upper gauge on the Maple River, and b) at the upper gauge on the Le Sueur River.

For the numerical runs discussed below, a feed rate of mud, Q_{mfeedj}, is computed for each discharge bin of the upper 75% of the flow duration curve and then a mean annual value, Q_{mfeed}, is estimated with equation 8.3. The mean annual input rate of mud at the upstream end of the modeled reaches are 5048 Mg/yr for the Maple River, and 34107 Mg/yr for the Le Sueur River.

The mean annual input rate of sand at the upstream end of the modeled reaches is computed assuming that the fraction of mud is equal to 0.9. The estimated mean annual sand feed rate is thus equal to 451 Mg/yr on the Maple River and 3790 Mg/yr on the Le Sueur River. The total sediment input rate is 4513 Mg/yr for the Maple River and 37896 Mg/yr for the Le Sueur. The sediment yield for the basins upstream of the modeled reaches is 17.8 Mg/km^2/yr on the Maple River and 60.5 Mg/km^2/yr on the Le Sueur River. These values for the upstream basins are also used to characterize the sediment loading from the several tributaries that enter the study reaches.

The sand load and the sediment loads supplied external to the model are given in terms of mean annual values that have to be partitioned over the flow duration curve. The partition is done assuming that the loads scale with the flow discharge with the same relation as the mud. For example, the sand feed rate in each discharge bin is defined as

$$Q_{sfeedj} = Q_{sfeed} \cdot S_{wj} = Q_{sfeed} \frac{Q_{mfeedj}}{Q_{mfeed}} \tag{8.6}$$

All the lateral input rates of sediment are partitioned over the flow duration curve using equation 8.6. On the other hand, the exchange of sediment between the channel and the floodplain through channel migration and changes in channel width, as well as the exchange of sediment between the active layer/floodplain and the substrate through channel bed aggradation/degradation are assumed to be evenly distributed over the portion of the flow duration curve discretized by the model (i.e. they occur at a constant rate for all relatively large flows—the upper 25% of discharges are used here).

Parameters for hydraulic computations

The parameters necessary for the hydraulic computations are the width of the channel and of the floodplain, B_c and B_f, the channel sinuosity, Ω, and the friction factors for the channel and for the floodplain, C_{fc} and C_{ff}. While channel width is allowed to vary over the model run, an initial value is required. The other parameters are simply specified for the entire run. The observed downvalley variability in channel width and the synthetic relations used as the initial condition are shown in Figures 8.7 a) and b) for the Maple River and the Le Sueur River respectively.

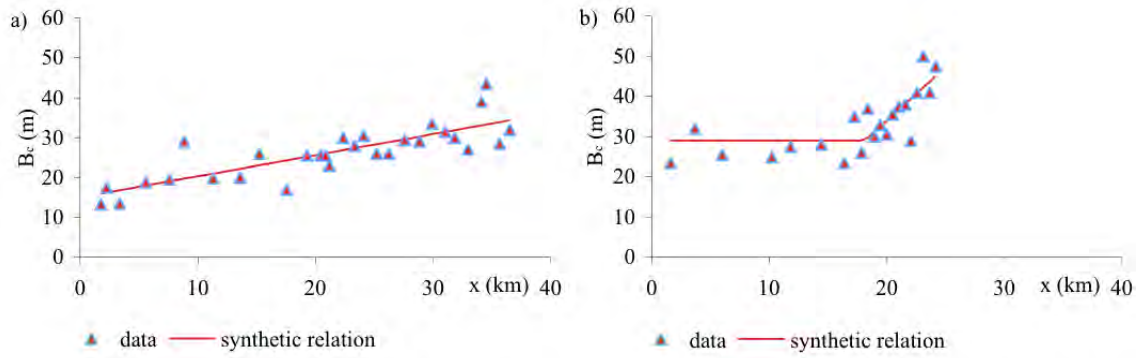

Figure 8.7: downvalley variation of the channel width a) on the Maple River and b) on the Le Sueur River. x denotes the downvalley distance from the upstream end of each modeled river reach.

The hydraulic parameters are summarized in Table 8.2. Note that while the channel width increases in the downvalley direction, the floodplain becomes narrower downstream, probably as a result of incision processes. The friction coefficients for the channel and the floodplain, C_{fc} and C_{ff} are used to compute the water depth for the composite cross section represented in Figure 8.8 with equations 8.7a and 8.7b. Their value corresponds to a non-dimensional Chezy coefficient of 10 (e.g. Parker, 2004).

Table 8.2: Parameters for hydraulic computations

Parameter	Maple River	Le Sueur River	Description
B_c (m)	0.53 x +14.9 (above and below)	29 (above) 2.64 x + 18.9 (below)	channel width
B_f (m)	-3.3 x +197.1 (above and below)	120 (above) - 4.1 x + 197.6 (below)	floodplain width
Ω	2 (above) 2.2 (below)	1.89 (above) 2 (below)	channel sinuosity
C_{fc}	0.01	0.01	friction coefficient for the channel

C_{ff}	0.01	0.01	friction coefficient for the floodplain

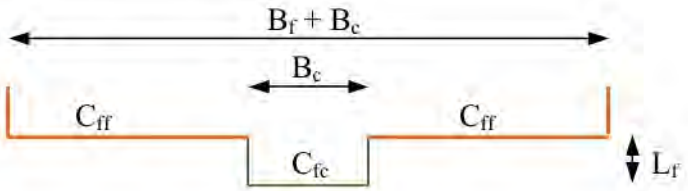

Figure 8.8: schematic representation of the cross section used for the hydraulic calculations.

The flow is assumed steady and uniform (assumption d above), thus in a Chezy-type formulation the water depth in the channel and on the floodplain are equal to

$$H_c = \left(\frac{C_{fc} Q_c^2}{B_c^2 g S_c} \right)^{1/3} \qquad H_f = \left(\frac{C_{ff} Q_f^2}{B_f^2 g S_f} \right)^{1/3} \qquad (8.7a \text{ and } 8.7b)$$

where H_f represents the water depths on the floodplain, Q_c and Q_f denote the water discharge in the channel and on the floodplain and S_f is the valley slope, related to the channel slope, S_c, through channel sinuosity, defined in equation 8.5 as

$$S_f = \Omega \cdot S_c \qquad (8.8)$$

The problem is characterized by two equations, i.e. 8.7a and 8.7b, and four unknowns, H_c, H_f, Q_c and Q_f. The two additional equations to close the problem express the continuity of water discharge and water depth (i.e. same water elevation in the channel and on the floodplain)

$$Q_{water} = Q_c + Q_f \qquad H_f = H_c - L_f \qquad (8.9a \text{ and } 8.9b)$$

Reach-specific parameters necessary for floodplain sediment exchange computations

The parameters needed for floodplain sediment exchange computations are the channel migration rates, c, the thickness of the active layer, L_a, and the height of the point bar, H_{pb}. The channel migration rate, c, has been estimated by comparing aerial photos of the Maple River in the Blue Earth County taken in 1937, 2000 and 2002, as reported in Belmont et al. (submitted).

The active layer represents the zone of sediment within the channel bed that is frequently reworked. Its thickness (and that of the corresponding basal floodplain sediment reservoir) is assumed to scale with the height of the bedforms, which themselves probably scale with channel depth. For the Maple River and the Le Sueur River, it has been assumed that the active layer thickness is approximately equal to one fifth to one tenth of the reach-averaged channel depth.

The height of the point bar on the Maple River has been estimated as the difference in elevation between the surveyed average channel depth and the difference in elevation between the banks, $\Delta\eta$, estimated from lidar images, i.e. 0.64 m above the knickpoint and 1.14 m below

(Belmont et al., submitted). The analysis revealed that on the Maple River the height of the point bar is relatively constant in the downvalley direction with an average value of 1.23 m, as shown in Figure 8.9.

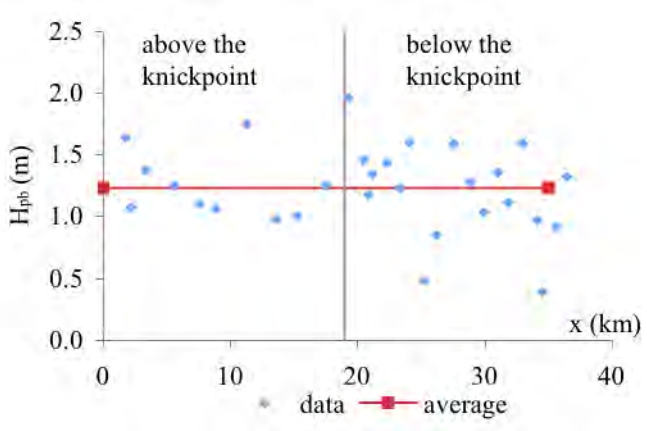

Figure 8.9: Downvalley variation of the height of the point bar on the Maple River. x denotes the downvalley distance from upstream end of each modeled river reach.

Estimates of the difference of elevation between the banks, $\Delta\eta$, are not available for the Le Sueur River, thus the height of the point bar has been estimated from the surveyed cross sections assuming the same $\Delta\eta$ of the Maple River. The average value of the estimated height of the point bar, approximately 1.5 m, has been assumed constant in space for the entire modeled reach.

Table 8.3: Reach-specific parameters for floodplain exchange computations

Parameter	Maple River	Le Sueur River	Description
L_a (m)	0.3 (above) 0.4 (below)	0.3 (above) 0.4 (below)	thickness of the active layer
c (m/yr)	0.185 (above and below)	0.172 (above) 0.276 (below)	channel migration rate
H_{pb} (m)	1.23 (above and below)	1.5 (above and below)	height of the point bar

Other global constants

Other global parameters required to compute the exchange of sediment between the channel and the floodplain are the floodplain numbers for the sand and the mud, Fl_k, in equation 8.1 (these represent a sort of sediment trap efficiency for the floodplain), and the fractions of sand and mud deposited in the lower part of the floodplain, i.e. in point bars for the simplified cross section considered in the model, F_{pbk}.

Finally, the incision rate in the knick zone, σ, has to be specified to model the exchange of sediment between the substrate and the active layer/ floodplain in the lower reach and to compute the evolution in time of the longitudinal profile. The values of these constants, assumed equal for the Maple River and the Le Sueur River, are presented in Table 8.4.

Table 8.4: Values of the global constants

Parameter	Value	Description and notes
Fl_s	0.025	Floodplain number for the sand (Lauer and Parker 2008 c)
Fl_m	0.025	Floodplain number for the mud
F_{pbs}	0.8	Fraction of sand in the load deposited in point bars
F_{pbm}	0.2	Fraction of mud in the load deposited in point bars
σ (mm/yr)	1.2	Incision rate in the knick zone
λ_p	0.4	Overall porosity of the system

Computational parameters

Computational parameters include the downvalley length of the modeled reaches (24 km above the knickpoint and 15 km below for the Maple and 19 km above the knickpoint and 17 km below on the Le Sueur), the spatial step length in downvalley coordinate, Δx, equal to 1 km, and the numbers of iterations in a year, m, set equal to 50. The temporal step length Δt for the output is equal to one year.

Initial conditions

Initial conditions for the model are given in terms of a longitudinal profile and a thickness of the floodplain. Initial values for the fractions of sand and mud and of the concentration of cosmogenic nuclides in each layer are also necessary. Longitudinal profiles of the Maple River and of the Le Sueur River are represented in Figure 8.10 with the location of the gauges and the average downchannel slopes above and below the knickpoint.

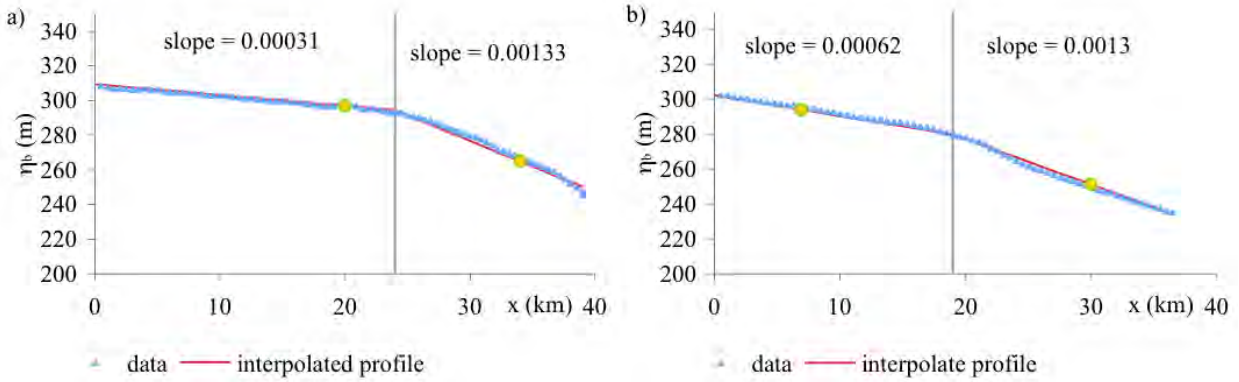

Figure 8.10: Initial longitudinal profiles. The yellow dots represent the location of the gauges mentioned in this section. x denotes the downvalley distance from the upstream end of each modeled river reach.

Initial values of floodplain thickness, fractions of sand and mud in the sediment reservoirs and concentration of radioisotopes are not reported because they have only been used to initialize the model for the steady state runs. Noting that the steady state solution is independent from the initial conditions, the only variable that is affected by the initial conditions is the time that the model needs to converge to steady state. The steady state solution achieved at the end of the first spin-up period represents the initial condition for the second spin-up run, and the results of the second spin-up run are the initial condition for the post-settlement run.

In Table 8.5, fractions of sand and bed material and concentration of radioisotopes in the substrate, assumed equal for the Maple River and for the Le Sueur River, are reported. These

parameters affect the results of the pre-settlement and post-settlement runs, in which the incision rate is not neglected and substrate material is entrained in the active layer and in the floodplain for channel bed degradation.

Table 8.5: Fractions of sand and concentrations of radioisotopes in the substrate.

Fraction sand	0.35
t_{sub} ^{10}Be (atoms/gr)	$2.5x10^4$
t_{sub} ^{26}Al (atoms/gr)	$2.5x10^4$
t_{sub} ^{10}Be (meteoric) (atoms/gr)	$1.0x10^6$
t_{sub} ^{210}Pb (atoms/gr)	$1.0x10^2$

Boundary conditions

The downstream boundary condition for the routing model is expressed as a fixed bed elevation at the downstream end of the lower reach where the stiff substrate is exposed even at moderate and low flows. The upstream boundary condition is given in terms of the duration curve for unit discharge (i.e. discharge per unit area—discharge is found by multiplying the unit discharge in each bin by drainage area) and sediment feed rate, as described previously. In Table 8.6 the discretization of the flow duration curve used in the model runs is presented (see appendix A for derivation of the flow duration curve). To reduce the computation requirements for the runs and to stabilize the model, unit flow discharges with a probability of exceedence smaller than 75% were not considered. In effect, this means that all bank erosion and floodplain deposition occurs at a constant rate over the 25% of the time resolved by the calculation, and that the system is geomorphically static the rest of the time. Note that this approximation may cause short-term inaccuracies in modeling 1) channel migration, and 2) mud transport. Specifically, it is assumed that bank erosion/deposition does not occur at the low or moderate flow not resolved in the numerical calculations, or, alternatively, that that any bank erosion that were to occur during low flow periods would result in short-term storage of the eroded material on the channel bed. This material would not be entrained in the flow (or potentially deposited on the floodplain) until the next reasonably large flow event.

Table 8.6: Flow duration curve

Probability of exceedence	p_{wj}	u_j (mm/day)
0.2	0.2	0.042
0.4	0.2	0.12
0.5	0.1	0.2
0.6	0.1	0.3
0.7	0.1	0.5
0.75	0.05	0.62
0.8	0.05	0.8
0.85	0.05	1
0.9	0.05	1.7
0.925	0.025	2
0.95	0.025	2.3
0.975	0.025	4
0.99	0.015	7
0.995	0.005	8
0.9975	0.0025	10

Numerical results

The application of the routing model to the Maple and Le Sueur Rivers is done in four consecutive steps. The routing model is first run for a very simplified pre-agriculture scenario in which the incision in the knick zone and the downstream variability of water discharge, of all the lateral sources of sediment (i.e. uplands, bluffs, ravines and tributaries) and of channel width is neglected. The solution from the first run is then used as input in a second spin-up run that lasts another 1000 years and includes the pre-agriculture lateral loads and the incision in the reach below the knickpoint. The numerical result at the end of this second phase is assumed to be representative of the pre-settlement Maple River and Le Sueur River. The channel width in the pre-settlement runs is assumed constant in time.

The model is then run for 160 years (post-settlement runs) to investigate the effects of the post-settlement change in land use in terms of channel geometry (i.e. channel depth and width), fractions of sand and mud in the floodplain, concentration of radioisotopes in the floodplain and mean annual sediment load at the gauges. This simulation assumes that all the sources increased linearly from the pre-settlement to the present values, i.e. in the first 150 years of simulation. This assumption does not capture all historic changes in the Le Sueur River watershed, both because the historic changes are not at present fully understood and because changes are still being made to the landscape today. However, it illustrates how the model can be used to reproduce changes in hydrology and sediment inputs as additional data become available for constraining these parameters. Finally the model is run for additional 10 years (restoration runs) to predict the effects that two different restoration scenarios may have on the river in terms of sediment loads. In the first scenario, it is assumed that the inputs of water and sediment to the modeled reaches do not change from the present (i.e. 2000-2010) values. In the second, the input of sediment from the bluffs is set equal to a half of the 2000-2010 value, i.e. a very simplified representation of a diffuse bluff protection project along the main rivers.

Numerical results of the first three phases are compared against the available field data and the analytical solution for the steady state concentration of radionuclides in the load and in the floodplain.

Pre-settlement flow duration curve and sediment sources used in model spin-up

The flow duration curve and the sediment sources for the pre-settlement spin-up runs have been determined by multiplying the present flow duration curve and loads by the adjustment factors reported in Table 8.7.

The majority of the adjustment factors presented in Table 8.7 have been determined from the budgets for the mud in the Maple River basin described in other sections of the present report. The adjustment factor for the flow duration curve has been determined based on a simple comparison of the mean April-November discharge for the first and last 10 years of record for the Mankato gauge on the Minnesota River (USGS 05325000), which was installed in 1903. While discharge changes at this location may not be identical to discharge changes in the Le Sueur basin itself, it is difficult to find other data on flow in the watershed that goes back so close to the pre-settlement era. On average, the first 10 years in the record are characterized by 57% of the mean discharge during the last 10 years in the record.

We arbitrarily assume that this may be too large a change for the smaller Le Sueur basin and select a factor of 0.6, characteristic of the upper 10% of the flow duration curve at the Mankato gauge. The pre-settlement mud load computed with the reduced flow duration curve and the rating curves represented in Figure 8.6 at the upstream end of the modeled reach is equal to 25% of the present value, in agreement with the ratio between pre and post-settlement mud loads at the mouth of the Maple River. Assuming that the fraction of mud in the pre and post-agriculture sediment input rates does not change considerably, the same adjustment factor has been used to scale the input of sand to the modeled reaches. The adjustment factors for the input of sediment from bluffs, ravines and uplands have also been determined from the comparison of pre and post-settlement budgets, as reported in section 2 and 5 of this report and in Gran et al. (2009) and Belmont et al. (submitted).

Table 8.7: Adjustment factors for the pre-settlement spin-up runs

Source	Maple River	Le Sueur River
flow duration curve	0.6	0.6
channel width	0.75	0.75
mud feed rate	0.25	0.25
sand feed rate	0.25	0.25
input of sediment from the bluffs	0.3	0.3
input of sediment from the ravines	0.6	0.6
input of sediment from the uplands	0	0
input of sediment from the tributaries	0.25	0.25
channel migration rate	0.5	0.5
height of the point bar	0.65	0.65
concentration of ^{10}Be in sand from tributaries	1	1
concentration of ^{26}Al in sand from tributaries	1	1
concentration of ^{10}Be (meteoric) in mud from tributaries	1	1
concentration of ^{210}Pb in mud from tributaries	1	1

The adjustment factors for the migration rate c and point bar height H_{pb} have been specified so that these parameters are also smaller during the pre-agriculture era. However, further research is needed to bracket a reasonable range for these parameters. The adjustment factor for the channel width has been specified to be generally consistent with the aerial photograph analysis reported in section 7 of this report, with observed rates projected back 150 years.

Initial spin-up

Boundary conditions for the initial spin up runs used to characterize steady-state are 1) constant input of water and sediment at the upstream end of the modeled reach adjusted with the values of Table 8.7, 2) constant - in space and time - channel width (equal to the value at the upstream end of the modeled reach) adjusted with the factor of Table 8.7, i.e. 12 m for the Maple River and 19.5m on the Le Sueur River, and 3) incision rate and lateral sources of sediment and water equal to zero. The input parameters that are allowed to vary in the streamwise direction are the floodplain thickness (relation of Table 8.2) and the channel slope (Figure 8.10).

While the spin-up runs are intended only to provide a stable starting point for the simulation of the post-settlement evolution of the basin, it is important to determine whether the model is capable of predicting reasonable results. For this we assess the geomorphic results of the spin-up runs and also compare the output of the initial spin-up run with analytical solutions for tracer concentration characteristic for the same boundary conditions.

The output of the routing model is given in terms of longitudinal profiles of floodplain thickness above the channel bed, L_f, difference in elevation between the banks, $\Delta\eta$, mean annual sand, Q_{sand}, and mud, Q_{mud}, load, fraction of sand in the floodplain, F_{fsand}, and concentration of radioisotopes in the floodplain, T_f, and in the load, t_{load}. In Figure 8.11 the longitudinal profiles of B_f (constant in time), L_f, Q_{mud}, Q_{sand} and F_{fs} at steady state after the initial spin-up period are reported for the Maple River. It is evident that in the reach above the knickpoint (first 24 km of the modeled reach) there is a noticeable variability in the downvalley direction of all the parameters except the mean annual sand load. Below the knickpoint, all the parameters attain a nearly constant value.

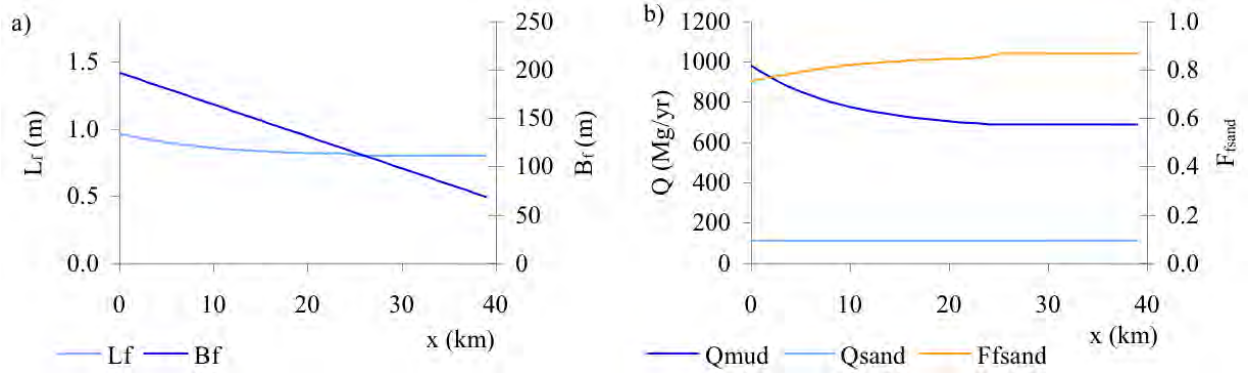

Figure 8.11: longitudinal profiles at steady state for the Maple River. a) downvalley variation of floodplain width and thickness of the floodplain above the channel; b) downvalley variation of mean annual sand and mud load and of the fraction of sand in the floodplain. x denotes the downvalley distance from the upstream end of each modeled reach.

The strong downvalley variability of the model parameters at steady state in the reach above the knickpoint is a consequence of modeling a low slope sand bed river as a below-capacity river, which cannot adjust the bed slope and thus tends to reach a constant transport capacity for the sand by modifying the shape of the cross section.

The comparison between the numerical and the analytical solution of Lauer and Willenbring (2010) for the concentration of radioisotopes in the load, t_{load}, and in the floodplain, T_f, is presented in Figure 8.12 for in-situ produced ^{10}Be (a) and ^{26}Al (b) in sand, and for the meteoric ^{10}Be (c) and the ^{210}Pb (d) in mud. In the reach below the knickpoint, the numerical results match the analytical solution reasonably well. In the reach above the knickpoint, where the downvalley variability of all the parameters represented in Figure 8.11 is not negligible, the model results cannot reproduce the analytical solution. The analytical solution has been derived under the assumption of constant floodplain width, floodplain thickness, sediment load and fraction of sand in the floodplain, thus it cannot reproduce the numerical reach above the knickpoint. In order to assess the validity of the numerical solutions for tracer concentration above the knickpoint, three different analytical solutions have been plotted in Figure 8.12 for different combinations of the parameters represented in Figure 8.11 to bracket a reasonable range of values for the concentrations of radioisotopes. Specifically, the continuous orange and yellow

lines in Figure 8.12 are analytical solutions obtained with reach averaged values, while the dashed lines have been calculated with values at the upstream end and at the knick zone. For all the tracers, the numerical solution at steady state after the initial spin-up run is in the expected zone, as bounded by the dashed lines.

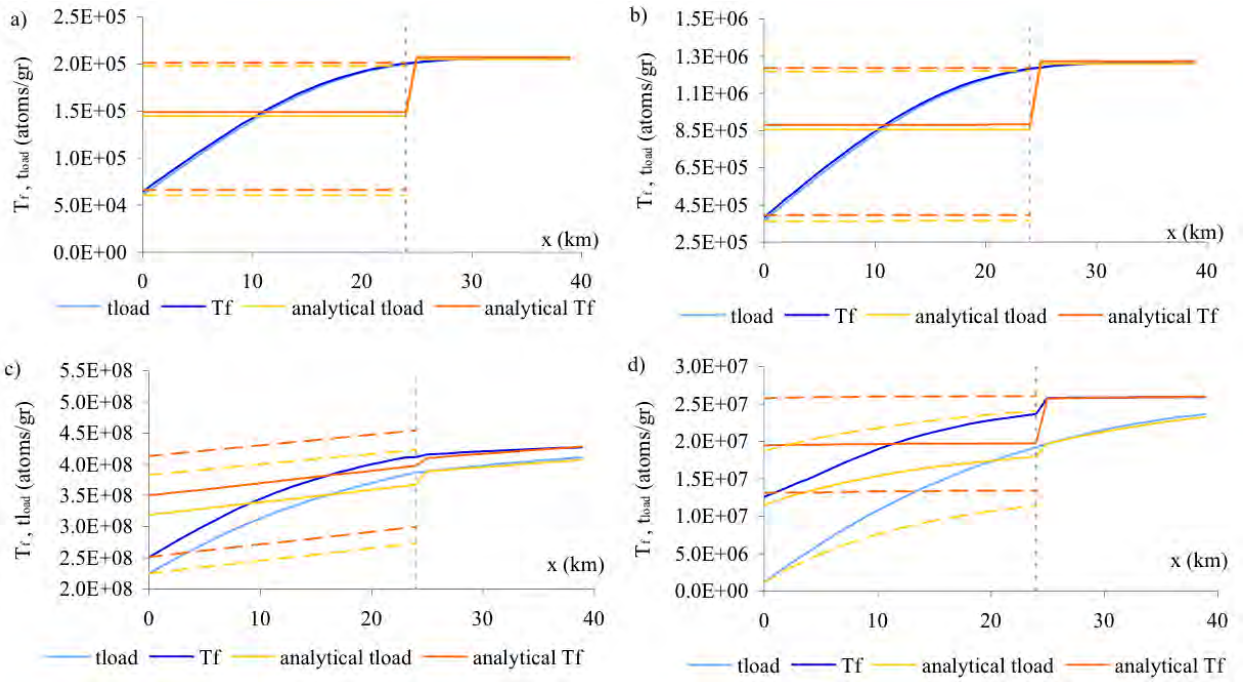

Figure 8.12: comparison between the numerical and the analytical longitudinal profiles of concentration of tracers at steady state for the Maple River. a) in-situ produced ^{10}Be; b) in-situ produced ^{26}Al; c) meteoric ^{10}Be; d) ^{210}Pb. The continuous yellow and orange lines are the analytical solutions for reach averaged values; the dashed lines are the analytical solutions with the values at the upstream end of the reach and in the knick zone; and the vertical dotted line identifies the position of the knick zone. x denotes the downvalley distance from the upstream end of each modeled reach.

Analogous plots for the Le Sueur River are reported in Figures 8.13 and 8.14. As for the Maple, the steady state achieved after initial spin-up for the Le Sueur River appears reasonable but does not perfectly match the analytical solution because of the downvalley variability of floodplain thickness and width, fractions of sand in the floodplain and mean annual mud load.

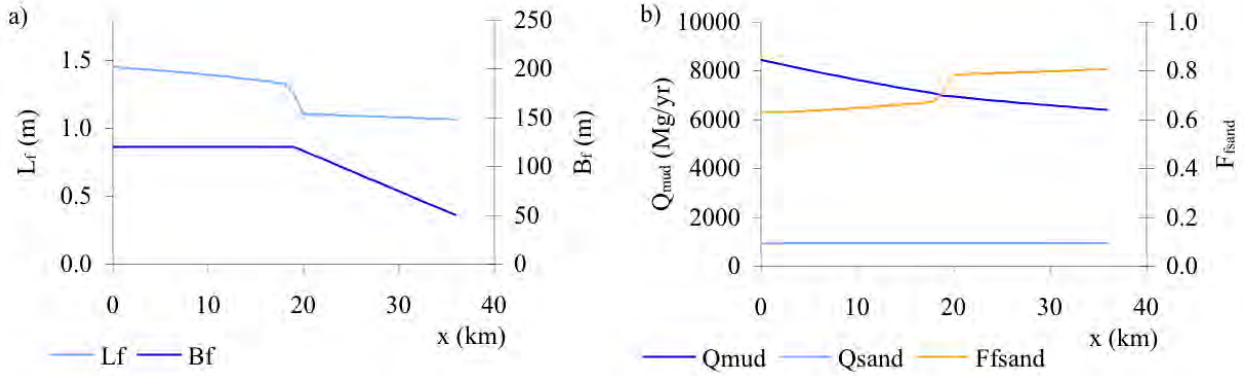

Figure 8.13: longitudinal profiles at steady state for the Le Sueur River. a) downvalley variation of floodplain width and thickness of the floodplain above the channel; b) downvalley variation of mean annual sand and mud load

and of the fraction of sand in the floodplain. x denotes the downvalley distance from the upstream end of each modeled reach.

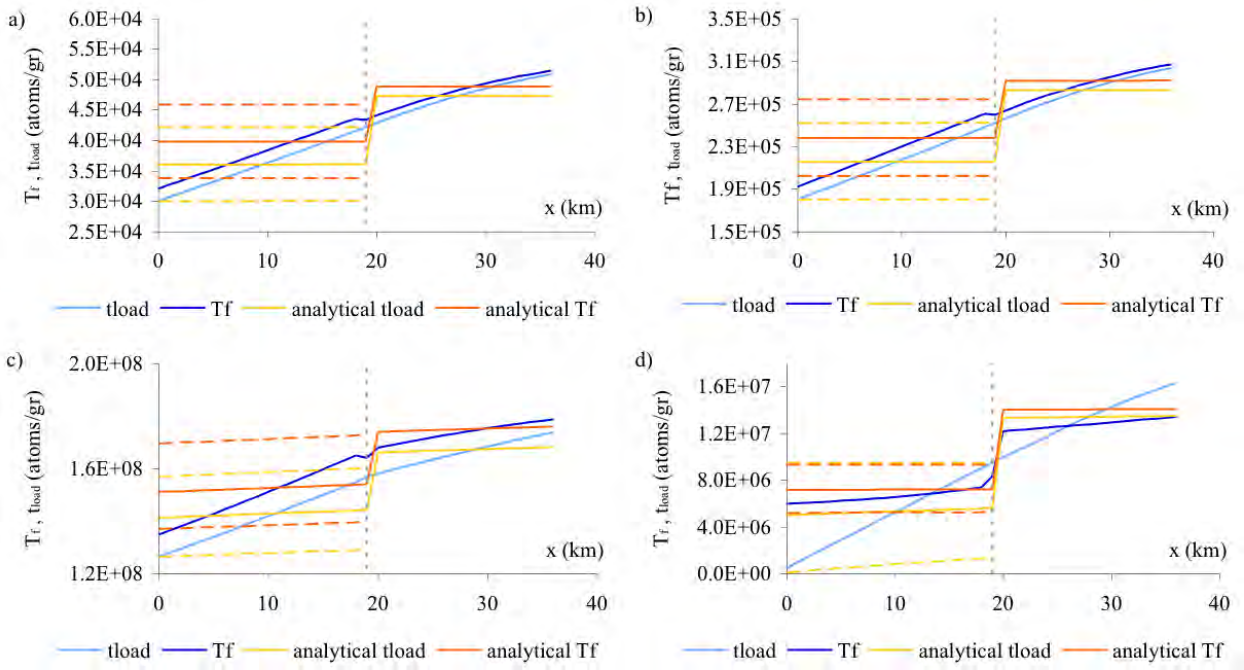

Figure 8.14: comparison between the numerical and the analytical longitudinal profiles of concentration of tracers at steady state for the Le Sueur River. a) in-situ produced ^{10}Be; b) in-situ produced ^{26}Al; c) meteoric ^{10}Be; d) ^{210}Pb. The continuous yellow and orange lines are the analytical solutions for reach averaged values; the dashed lines are the analytical solutions with the values at the upstream end of the reach and in the knick zone; and the vertical dotted line identifies the position of the knick zone. x denotes the downvalley distance from upstream end of each modeled reach.

Final spin-up

The steady state solution resulting from the initial spin-up described above is used as the starting point for an additional 1000-year spin-up period that accounts for 1) downvalley variability of channel width and water discharge, 2) the incision in the reach below the knickpoint, and 3) all the lateral sources of sediment to reproduce pre-settlement conditions for the Maple River and the Le Sueur River that are more realistic that those used during the initial spin-up. The parameters governing the input of sediment in the river and the exchange of sediment between the rivers and their floodplains have been scaled with the adjustment factors reported in Table 8.7.

The comparison between post spin-up floodplain thickness and that estimated by Gran et al., (2009) for pre-settlement conditions for the Le Sueur River is reported in Figure 8.15. The model reasonably reproduces the thickness of the floodplain below the knickpoint, but it overestimates it above the knickpoint. This inconsistency is probably caused by the rather strong assumption that point bar height and channel migration rate do not vary down-channel within the upper Le Sueur River. The channel thus probably builds point bars that are too deep at several locations in the reach. In any case, the predicted mean annual mud load at the mouth of the Le Sueur River, 64,835 Mg/yr is close to the average Holocene (i.e. pre-settlement) mud load of 55,000 Mg/yr estimated in chapter 2.

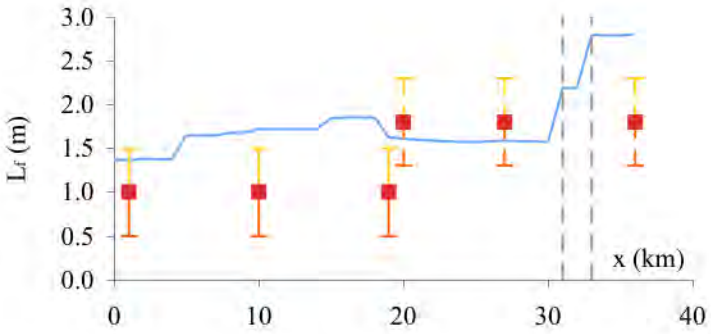

Figure 8.15: comparison between the numerical (line) and the estimated pre-settlement floodplain thickness (points) on the Le Sueur River. The error bars represent 50 cm above and below the pre-settlement floodplain thickness. The two dashed vertical lines represent the confluences with the Cobb and the Maple rivers. x denotes the downvalley distance from the upstream end of the modeled reach.

Post-settlement runs

We assume (although we recognize that this is an oversimplification) that agriculture begins in 1850 and that water and sediment loads, as well as channel migration rate and height of the point bar, on the Le Sueur and Maple Rivers have been linearly increasing for 150 years from the pre-settlement value used in model spin-up to present-day values. After the 150-year increase, the parameters are held constant for a decade with modern (2000-2010) input variables. This is not what has happened in the Le Sueur River, as conditions continue to change, but it does allow us to test the model at engineering time scales.

The concentration of radionuclides in the sediment sources at the boundaries of the modeled reaches (i.e. upstream feed rate, bluffs, ravines, uplands and tributaries) is assumed not to change in time during these runs, i.e. it is assumed to be equal to the concentration used in the spin-up model runs. Thus the variation on the supply of tracers to the modeled reach only depends on the linear increase of the sediment sources. We acknowledge that the assumption of constant concentration of tracers in the sources of sediment does not account for the changes in sediment loads on the tributaries and in the upstream and non-modeled portion of the basin. For example, if the input of hot sediment from the uplands increases, the concentration of radionuclides in the sediment contributed from the tributaries and fed at the upstream end of the modeled river reaches should also increase in time. This effect is neglected in the post-settlement runs because the pre-settlement concentration of radionuclides in the sediment contributed from the tributaries is not yet a well-constrained parameter.

The temporal variation of channel geometry, i.e. width and depth, has not been imposed but it has been simulated internally by the model with the aid of equation 8.4, with $\alpha_{Bc} = 15$ on the Maple River and 35 on the Le Sueur River. Note, however, that the starting width is not taken from the final spin-up run. Instead, the initial condition for channel width (i.e. in 1850) is obtained by multiplying the best-fit line for the present channel width (Table 8.2) by the adjustment factor (Table 8.7), i.e. 0.75. The initial condition for channel depth is the channel depth after model spin-up. The comparison between predicted and measured channel geometries is presented in Figure 8.16, where the lines represent the numerical results and the dots the field data.

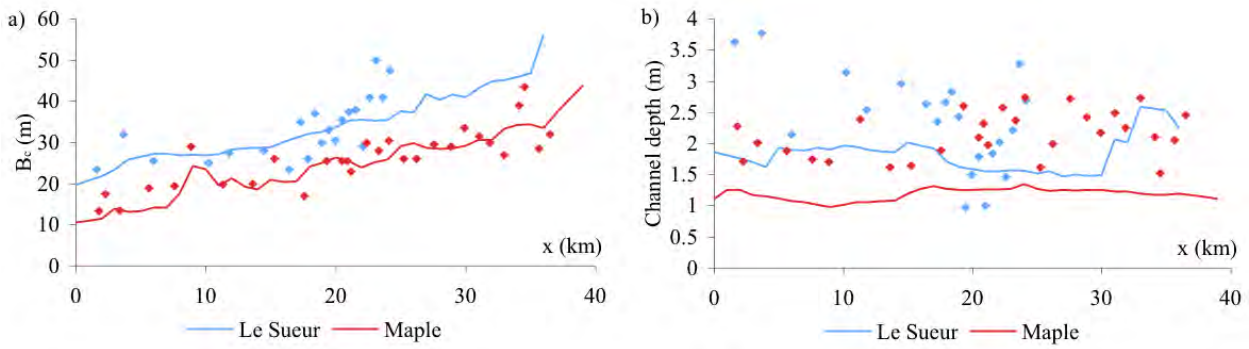

Figure 8.16: comparison between the predicted and measured geometry of the cross section on the Maple River and on the Le Sueur River in terms of a) channel width, and b) channel depth. The lines represent the numerical results and the dots are the field data. x denotes the downvalley distance from the upstream end of each modeled reach.

The good agreement between observed and computed channel widths shows that the model can capture the sand balance on both rivers. On the other hand, the relatively poor agreement between channel depths shown in Figure 8.16b clearly shows that the height of the point bars is not a well-constrained parameter, particularly on the Maple. Notwithstanding this limitation, the predicted input of sediment from channel migration is on the order of 118 Mg/river km/yr on the Le Sueur River, value that is very close to Gran et al.'s 2009 estimate of 130 Mg/river km/yr. This implies that the overall storage dynamics for floodplain sediment are being handled reasonably well, providing confidence in tracer dynamics simulated by the model.

The ratio between pre-settlement and the simulated modern (i.e. model year 2010) mud load at the gauges on the Maple River, on the Le Sueur River and at the mouth of the Le Sueur varies from 2.94 at the lower gauge on the Maple River and 3.71 at the upper gauge of the Le Sueur River (with values of 3.55 and 3.31 respectively at the mouth of the Le Sueur River and at the upper gauge on the Maple). Although these numbers underestimate the 4-5 fold increase in the mud load presented in this report from valley excavation, they are similar to the increase in mud load seen when all sources are taken into consideration.

The response of the system to the post-settlement loading in terms of floodplain thickness above the channel bed and fraction of sand is represented in Figure 8.17 for the Maple River (a and c) at the upper and lower gauge and for the Le Sueur River (b and d) at the upper gauge, middle gauge and at the mouth.

The model shows a very small but noticeable change in the volume of sediment stored in the floodplain on the Maple River. On the Le Sueur River the volume of sediment stored in the floodplain slightly increases at the upper gauge and remains almost constant at the lower gauge. At the mouth of the Le Sueur River the volume of sediment stored in the floodplain slightly decreases at the very beginning of the simulation and then remains constant. Noting that the rivers are modeled as capacity-limited and thus cannot change the bed slope, this behavior should be interpreted as an attempt of the system to adjust to the changes in sand load during the post-settlement era. On the Maple River, where the simulated present-day sand load is up to 5.7 (values increase in the streamwise direction from 1.3 to 5.7) times larger than the pre-settlement value, the cross-section tends to become deeper and wider to increase the transport capacity. On the Le Sueur, where the ratio between pre-settlement and present sand loads decreases in the streamwise direction from 3.9 to 2.9, the cross section becomes wider to adjust the transport capacity. The fraction of sand in the floodplain, F_{sand}, slightly decreases in time on the Maple

River and at the upper gauge on the Le Sueur River because as the cross section becomes deeper, the overbank deposition of suspended sand decreases in time. On the lower Le Sueur River (i.e. lower gauge and mouth), where the depth of the channel sections are nearly constant in time, the fraction of sand stored in the floodplain also remains nearly constant in the post-settlement era.

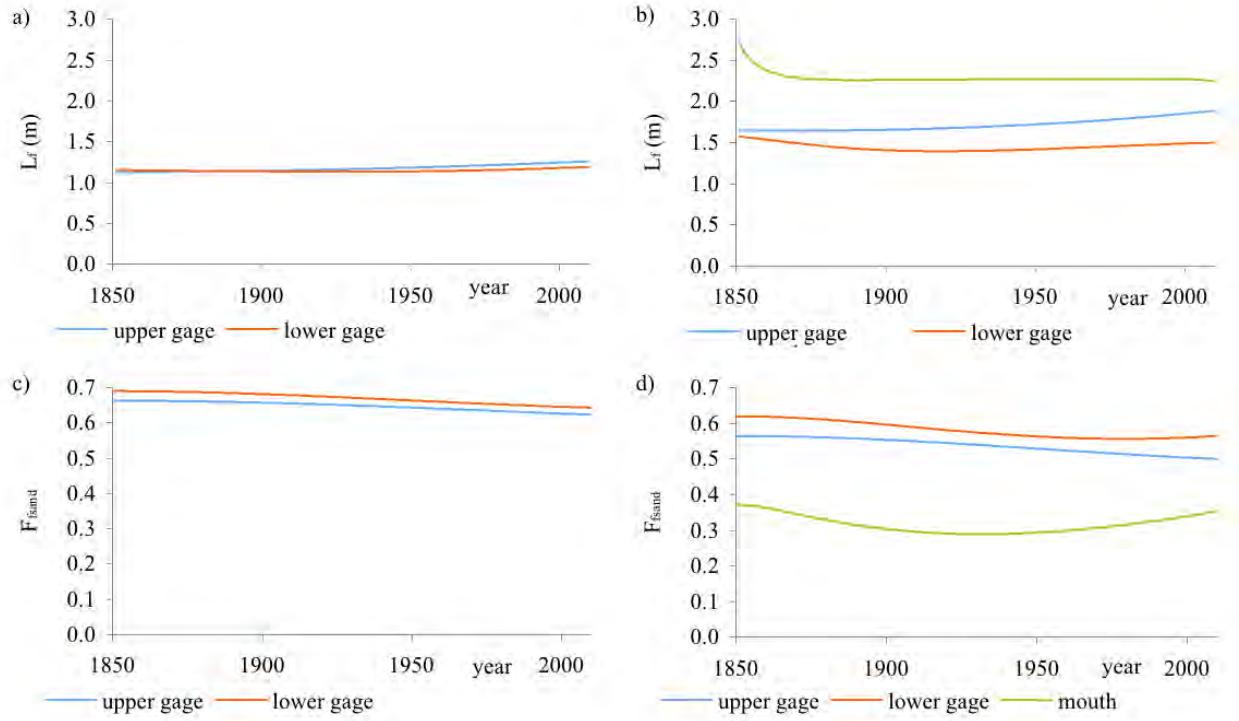

Figure 8.17: temporal evolution of the floodplain thickness L_f (a and b) and of the fraction of sand in the floodplain F_{sand} at the gauges on the Maple River (a and c), and at the gauges and at the mouth of the Le Sueur River (b and d).

To investigate the effects of channel widening on the numerical solution, post-settlement runs have been repeated assuming a constant channel width in time, i.e. equal to 75% of the present value. The numerical results showed a higher storage of sediment in the floodplain for both the Maple River and the Le Sueur River with a consequent increase in the depth of the cross sections to maintain the same transport capacity for the sand and of the mud fractions.

The small change in storage in the floodplain is reflected in the temporal evolution of the radioisotope concentration represented in Figures 8.18 and 8.19. In Figure 8.18 the change of the ratio between concentrations in the floodplain material of in-situ produced ^{26}Al and ^{10}Be is reported at the gauges and at the mouth of the Le Sueur River. The only profile that shows a significant change in time is that for the upper gauge on the Le Sueur River, where the denudation rate for the tributaries is much higher than on the Maple River (60.5 Mg/km^2/yr versus 17.8 Mg/km^2/yr) and most of the new sediment is contributed from agricultural fields, with a high ratio between the concentrations of in-situ produced ^{26}Al and ^{10}Be. None of the other profiles show a significant change, even if the absolute value of the concentrations decreases in the downvalley direction as “cold” sediment is contributed to the rivers from bluffs and ravines. This is because both tracers are diluted by “cold” sediment at approximately the same rate.

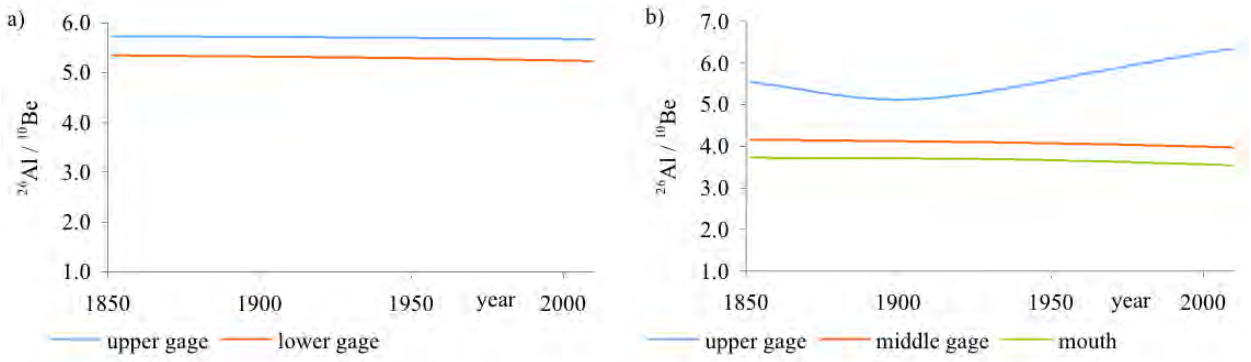

Figure 8.18: evolution of the ratio between the concentrations of in-situ produced 26Al and 10Be a) at the gauges on the Maple River, and b) at the gauges and at the mouth of the Le Sueur River.

The temporal evolution of the concentration in the floodplain of tracers, T_f, associated with mud, i.e. meteoric ^{10}Be and ^{210}Pb, is represented in Figure 8.19 for the gauges on the Maple River (a and c), and for the gauges and at the mouth of the Le Sueur River (b and d). In the same figure, the concentrations of radionuclides in the sources of sediment at the boundaries of the modeled reach are represented with colored diamonds: orange for the bluffs, green for the tributaries and the upstream input of sediment, blue for the ravines, and red for the uplands (the values are in Table 1 and are also reported on the figure).

The concentrations of meteoric ^{10}Be predicted with the routing model at the lower gauge on the Maple River is lower than that assumed for the tributaries, but still higher than that assumed for bluffs. On the other hand, the concentration of ^{210}Pb predicted with the routing model at the gauges on the Maple River is orders of magnitude higher than that assumed for the lateral sources of sediment, because of the meteoric fallout of ^{210}Pb on the floodplain that is accounted for the in calculations. The slightly lower concentration of ^{210}Pb at the lower gauge is due to the input of cold sediment from bluffs and ravines below the knickpoint.

In Figures 8.19 (b and d) the time rate of change of the concentration of meteoric ^{10}Be and ^{210}Pb in the floodplain at the mouth of the Le Sueur River have been computed assuming that the concentration of tracers in the sediment contributed from the Maple River and the Cobb River is equal to the concentration of tracers in the sediment contributed from the lower order tributaries.

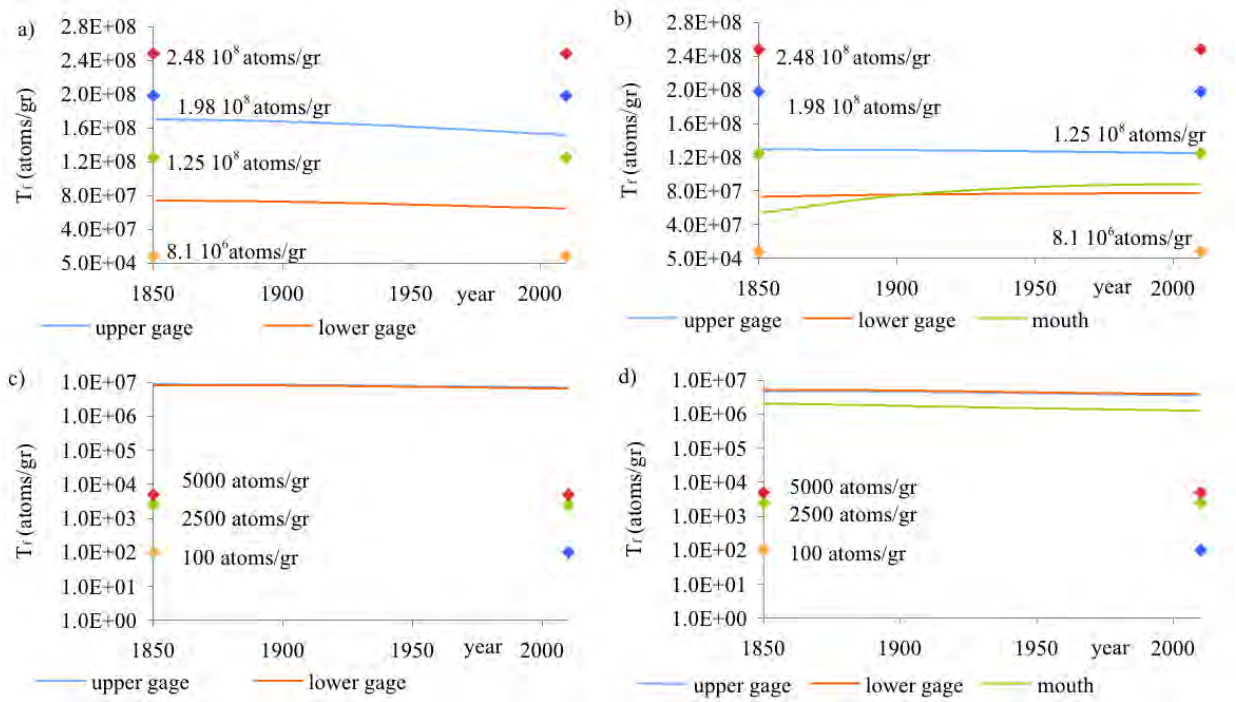

Figure 8.19: temporal evolution of concentrations of meteoric ^{10}Be (a and b) and ^{210}Pb (c and d) at the gauges on the Maple River (a and c), and at the gauges and at the mouth of the Le Sueur River (b and d). The diamonds represent the concentrations of tracers in the sediment contributed from the lateral sources, orange = bluffs, green = tributaries, blue = ravines, and red = uplands.

The concentrations of meteoric ^{10}Be at the gauges on the Maple River and on the Le Sueur remain reasonably constant over the post-settlement period of the simulation. In interpreting this unexpected result, given the considerable increase in sediment loading in a very short period, it has to be kept in mind that the concentration of tracers in the sediment contributed from the tributaries and at the upstream end of the modeled reach is assumed constant in time during the numerical runs. This assumption probably leads to an underestimation of the concentration of tracers in these sources especially when the input of sediment from the lateral sources is higher. This notwithstanding, the relatively constant concentration of tracers in the floodplains is consistent with the small change in sediment storage in the floodplain shown in figure 8.17. Noting that the floodplain is modeled as a well-mixed sediment reservoir, the concentration of tracers T_f is averaged in the vertical and in the transverse direction, thus 160 years of simulation may not be sufficient to cause a significant change.

At the mouth of the Le Sueur, on the other hand, the concentration of meteoric ^{10}Be in the floodplain increases in the first 80 years of simulation. This is probably a consequence of the input of sediment from the Maple and Cobb being characterized by a much higher tracer concentration than is present in sediment from bluffs and terraces (or was present pre-settlement in any system).

On both rivers, the concentration of ^{210}Pb in the floodplain does not vary appreciably between gauges, with the upper and lower gauges on each respective system showing similar concentrations for the entire post-settlement simulation. However, at both gauges, the concentration of ^{210}Pb in the floodplain slowly decreases in time due to the input of depleted sediment from bluffs and ravines. The sudden drop of concentration of ^{210}Pb in the floodplain at the mouth of the Le Sueur River, also observed in the final spin-up runs, is due to the presence of

several big bluffs, which are characterized by a very low concentration of ^{210}Pb. The concentration of ^{210}Pb in the floodplain at the mouth of the Le Sueur decreases somewhat in time (green line in Figure 8.19d).

Restoration runs

Two hypothetical restoration scenarios are simulated on the Maple River and on the Le Sueur River for 140 years to investigate 1) how long would it take to the river to adjust to a change in the input of water and sediment, and 2) how the mean annual sediment loads at the gauges might change if the input of sediment from the bluffs is reduced to a half of the present value. The evolution of the channel cross section (i.e. floodplain height and channel width) are not discussed because relevant parameters, such as the height of the point bars, need to be better constrained. It suffice to say here, that while it has been assumed a liner increase of the height in the post-settlement runs, H_{pb} is kept constant and equal to the present value in this last group of numerical tests, which is characterized by a flow duration curve that does not change in time.

In the first restoration scenario it is assumed that the flow duration curve and the input of sediment from the sediment sources at the boundaries of the modeled system remain constant in time and equal to the 2000-2010 values. The temporal evolution of the mean annual sediment loads (Q_{mud} and Q_{sand}) from the 1850 to the 2150 is shown in Figure 8.20 for the gauges on the Maple River (a and c) and on the Le Sueur River and at the mouth of the Le Sueur River (b and d). In Figures 8.20 (a and b) the points represent the mean annual loads of mud estimated for the 2000-2010.

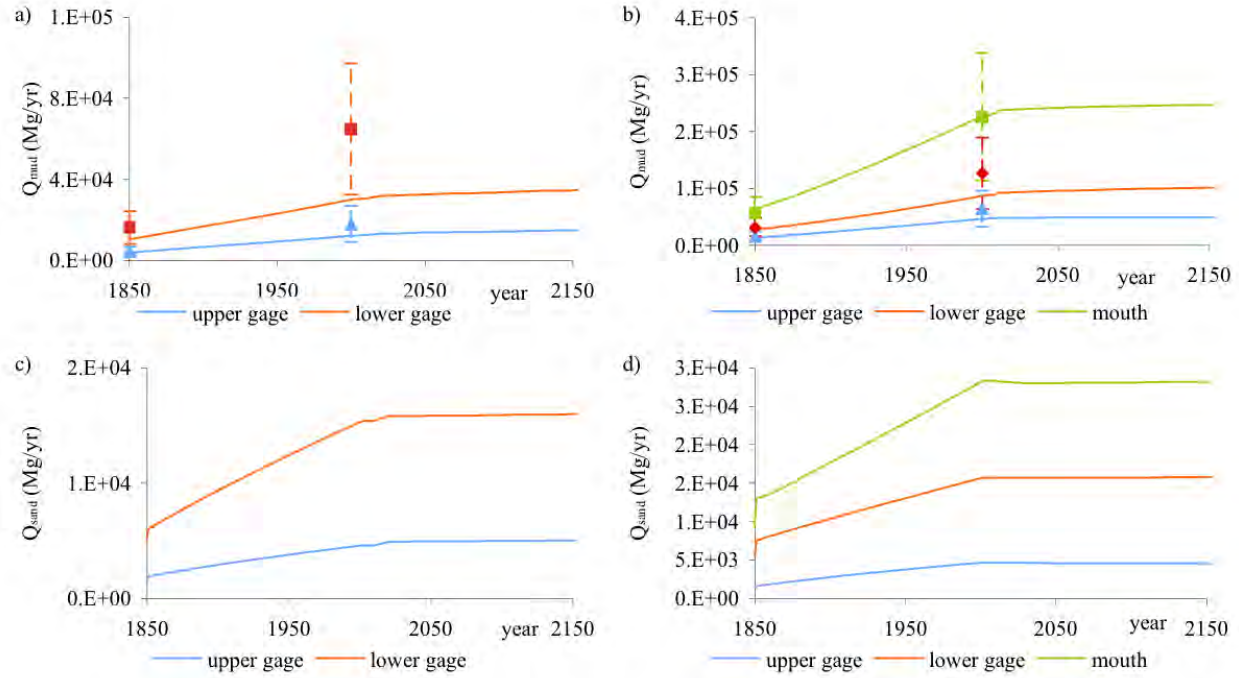

Figure 8.20: evolution of the wash load (a and b) and of the bed material load (c and d) at the gauges on the Maple River (a and c), and at the gauges and at the mouth of the Le Sueur River (b and d). The blue, red and green points (a and c) represent the estimated mean annual load of mud for the decade 2000-2010. For the pre-settlement era it is assumed that the mean annual load of mud was the 25% of the present value. The error bars represent a 50%

difference from the estimated value. Blue symbols refer to the upper gauge, red symbol to the lower gauge and the green symbol to the mouth of the Le Sueur River.

The sand and the mud load at all points in the reach linearly increase during the 1850-2000 period and then become fairly constant during the following 150 years, mirroring sediment supply. This quick response to the change in sediment supply (i.e. from a linear increase to a constant value) is a consequence of modeling the system as capacity limited. In an at-capacity system, other changes are possible as a result of the somewhat independent evolution of the bed (Viparelli et al., submitted, Lauer, in press). To the extent that the bed elevation is not permanently fixed by coarse channel lag in the Le Sueur system, it is possible that the bed material load would have attained a constant value over a longer period in an at-capacity run.

In the second restoration scenario it is assumed that the input of sediment from the bluffs is reduced to a half of its present value instantaneously in 2010. All the other inputs of water and sediment, and geomorphic parameters such as point bar height, are assumed to remain equal to the 2000-2010 values.

In Figure 8.21 the results of the numerical runs for the gauges on the Maple River (a and c) and on the Le Sueur River and at the mouth of the Le Sueur River (b and d) are presented. Instead of showing the absolute predicted values of sediment loads, the results are plotted in terms of ratios between the loads predicted in this second case (Q_{mud2} and Q_{sand2}) and the loads shown in Figure 8.20 (Q_{mud1} and Q_{sand1}) for the 2010 - 2150 period. The results thus represent the sensitivity of different portions of the system to a program of bluff stabilization, compared to a program that does not stabilize bluffs but at least prevents them from eroding at a rate higher than is presently observed.

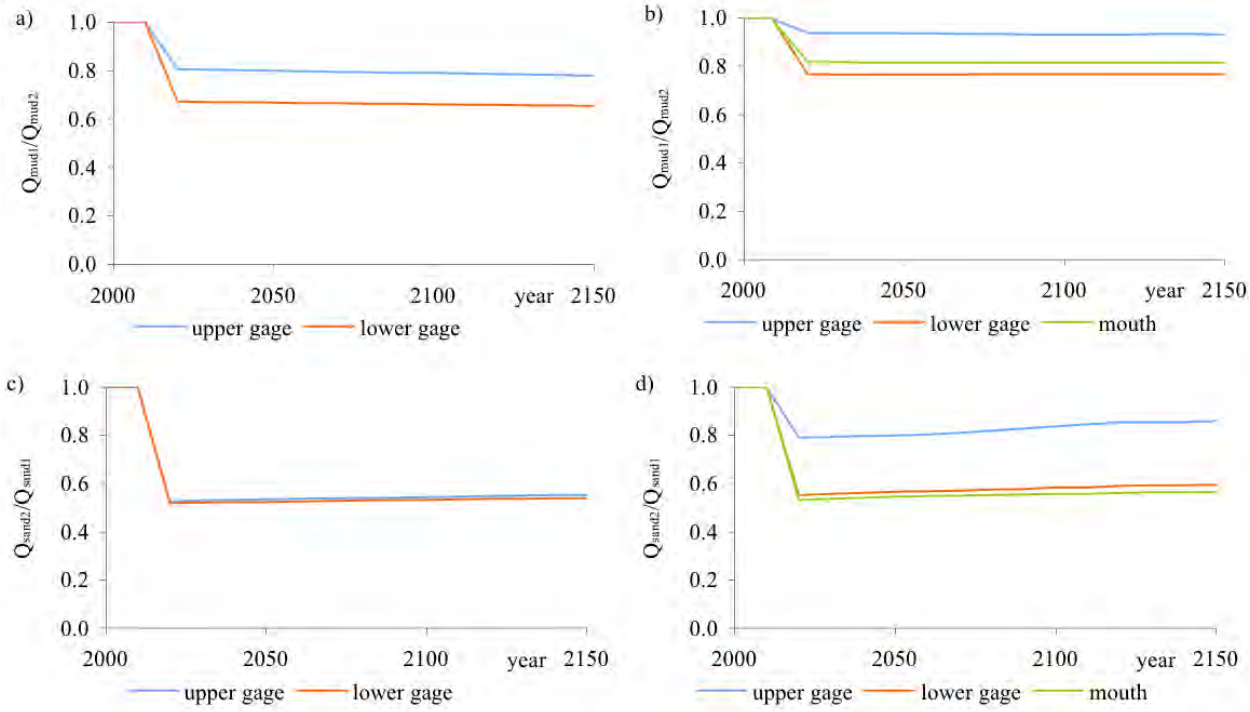

Figure 8.21: evolution of the ratio between mean annual loads of mud (a and b) and sand (c and d) at the gauges on the Maple River (a and c), and at the gauges and at the mouth of the Le Sueur River (b and d).

Major changes in sediment load occur in the first 20 years of simulation on both rivers, with a more significant reduction in the sand load than the mud load. The mud load at the upper gauges does not significantly change on the Le Sueur, while it slightly decreases ($Q_{mud2}/Q_{mud1} \approx 0.8$) on the Maple River. At the lower gauges the reduction of the mud load is more significant on both the rivers. A more significant reduction of the sand load is observed at the two gauges on the Maple River and in the lower Le Sueur. At the upper gauge on the Le Sueur the reduction of the sand load is much smaller because of the smaller number of bluffs in the upper portion of the basin.

The results of the restoration runs have to be interpreted considering the limitations of the routing model and, in particular, of the below capacity formulation implemented for the rivers in the Le Sueur River basin. In the below capacity formulation, channel bed elevation can change only for a user specified incision rates in the knick zone, thus the potential deposition and erosion of sediment from the channel bed cannot be captured, as well as the changes in bed material grain size. Moreover, changes in channel width and floodplain thickness are only partially captured in the incising reaches, because a subroutine that accounts for the temporal variation of the geometry of the floodplain for the incision process is not implemented. Finally, changes in hydrology that are continuing and that are most likely responsible for changes in the height of the point bars (and possibly in the migration rates) are not simulated. Future work is needed to link the model parameters related to channel migration with the hydrology.

The quick response of the rivers to the new inputs of water and sediment observed in this last set of model runs is at least partially a consequence of having neglected erosion and deposition of sediment from the channel bed (i.e. of the below capacity formulation). If the exchange of sediment with the channel bed results to be negligible sin the sediment budget for the bed material, these results have important implications from a management perspective. In particular, they show that a reduction in sediment loads in the main rivers can be rapidly obtained reducing the input of sediment from the lateral sources of sediment, i.e. uplands, bluffs and ravines.

Conclusions

The numerical simulations presented in the present section show two main results. First, the sediment routing model predicts reasonable concentrations of radioisotopes in the floodplain and in the load that are in agreement with those predicted with the analytical solution (Lauer and Willenbring, 2010). Second, its site-specific version for the Le Sueur River basin, i.e. the version with the moving knickpoint and the incision in the reach below the knickpoint, can reasonably reproduce sediment loading and channel geometry in the Le Sueur River basin for non-steady state conditions, if the model is properly zeroed. Thus, it can be used at engineering time scales to predict the effects that changes in sediment sources and flow duration curves may have on the main rivers in the basin in terms of channel/floodplain geometry and sediment loading.

The application of the sediment routing model to the Maple River and to the Le Sueur River described in this section focuses on all the steps that are necessary for field scale application but does not attempt to precisely replicate the sediment budget illustrated in the other sections of the present report. For more realistic applications to the rivers in the Le Sueur River basin some of the parameters assumed for the steady state and the pre-settlement runs should be

better constrained, as should the variation in space and time of the flow duration curve and of some sediment sources.

The use of the present version of the sediment routing model for predictive purposes requires 1) better constrained spin-up runs, as discussed in the paragraph below, and 2) the definition of the input parameters (e.g. flow duration curve, input of sediment from the lateral sources, channel migration rates) for the different scenarios that need to be tested. Once the model properly reproduces the present conditions, it can be run with the new input parameters to predict 1) the temporal and spatial variability of the sediment budget and of the geomorphic characteristics of the rivers (e.g. channel width, floodplain thickness), and 2) the time required for the system to adjust to the new water and sediment inputs.

Further research is needed to investigate the effects that different hydrographs may have on the sediment load in the rivers in different seasons. For this type of study, the flow cannot be assumed steady and uniform, and different models to compute the input of sediment from the lateral sources as a function of the characteristics of the flow in the main channel need to be developed. Finally, these models have to be coupled with the sediment routing model to fully describe the evolution of the system.

Recommendations for Future Work

The majority of the input parameters for the post-settlement runs are well constrained from the present sediment budget. However, the application presented in this section considers the simplest possible scenario, which is not entirely representative of the changes in hydrology and sediment loading in the Le Sueur River basin. A more realistic representation of the post-settlement conditions would probably considered 1) the increase of the input of sediment from fields starting just before 1850, reaching a maximum in the 1930s-1950s and then slowly declining, 2) a change in the flow duration curve that causes flow to increase not linearly over the entire post-settlement period, and 3) a gradual increase of the input of sediment from bluffs and ravines. This and other scenarios in which we investigate the effects of varying rates of sediment contribution from bluffs and fields will be discussed in Viparelli et al. in preparation (b).

While the numerical model is capable of simulating a range of what-if scenarios, we have not attempted this here for several reasons. One of the most important is the lack of any defensible pre-settlement flow duration curve. This is probably the most important parameter requiring constraint and should be the focus of future MPCA work. The pre-settlement flow duration curve for the simulations described above has been derived using simple rescaling the upper tail of the present flow duration curve (i.e. probability of exceedence higher than 75%). A better understanding of the effect of drain tiles, land use, and climate change on the hydrology of the region will probably lead to a more realistic representation of the pre-settlement hydrology. Moreover, parameters related to channel migration and bank erosion, i.e. the height of point bars, migration rates, and widening rates, from the hydrologic regime also probably depend on hydrology. Additional discharge information could thus be particularly helpful 1) for building a more realistic geometry of the pre-settlement river channel, 2) for simulating channel change over the past 200 years, and 3) for providing realistic estimates of response time to changes in sediment input and flow discharge.

Even if pre-settlement hydrology were well understood, several of the other parameters in the model would benefit from additional field data collection efforts. The most important of

these are associated with sediment deposition, both in point bars and overbank. In the runs we have performed thus far, the timescale of evolution of the model is sensitive to the height and sand/mud ratios of new point bar deposits. Unfortunately, we are not aware of any datasets that allow us to make reasonable assumptions on how these parameters may have varied historically, or how they may vary in the future as water and sediment supply change. Furthermore, the overbank deposition function (equation 8.1) depends on the parameter Fl that should be specified based on calibration to known overbank deposition rates.

Perhaps the best way to constrain these parameters would be a more extensive floodplain coring and dating campaign than was feasible for the present study. Such a field campaign would require extensive dating using either radiocarbon or optically simulated luminescence (OSL) methods, with the goal of identifying whether point bar geometry, grain size distributions, and overbank deposition rates have changed significantly since the pre-agriculture period. Because the Le Sueur basin may not be representative of all tributaries to the Minnesota River, there would be value in extending such a study beyond the Le Sueur basin. At a minimum, it would be helpful to perform model runs along the Lower Minnesota River, where the existing MPCA sediment sampling program at least provides some opportunity to compute overbank deposition rates, thereby providing a mechanism for calibrating the model's deposition-related parameters. However, even (or perhaps particularly) along the lower Minnesota, it would be helpful to collect enough overbank and point-bar samples so that the relative magnitude of mud storage either overbank or within point-bar deposits could be determined.

Finally, as presently written, the model incorporates a large number of input and output parameters. Because it is convenient to organize these parameters in a spreadsheet, the program has been written as a Visual Basic for Applications macro in Microsoft Excel. However, there are some limitations to this approach. First, code execution is slower than would likely be the case were the code compiled into an executable program. This becomes an issue for long spin-up runs that can take over a day of computer time to execute. Second, using MSExcel as the user interface also limits the ability to run the program with a better resolved continuous hydrograph such as could in principle be generated by an advanced continuous simulation hydrologic model. While the code can easily be modified to run using real hydrographs, the timestep required for this would be much shorter than presently used and would almost certainly require that the code be compiled and executed on a supercomputer rather than as a macro in MSExcel. Entering a high resolution continuous hydrograph could also be difficult using the existing MSExcel interface, although this problem could be overcome with minimal code development work.

Works Cited:

Aalto, R, Lauer, JW, Dietrich, WE, 2008, Spatial and temporal dynamics of sediment accumulation and exchange along Strickland River floodplains (Papua New Guinea) over decadal-to-centennial timescales, *Journal of Geophysical Research – Earth Surface.* v. 113: F01S04

Belmont, P, Gran, KB, Schottler, SP, Wilcock, PR, Day, SS, Jennings, C, Lauer, JW, Viparelli, E, Willenbring, JK, Engstrom, DR, Parker, G, 2011, Large shift in sediment source challenges Upper Mississippi River Cleanup, submitted to *Science*.

Blann, KL, Anderson, JL, Sands, GR, Vondracek, B, 2009, Effects of Agricultural Drainage on Aquatic Ecosystems: A Review, *Critical Reviews in Environmental Science and Technology*, v. 39, pp. 909-1001.

Botter, G, Zanardo, S, Porporato, A, Rodriguez-Iturbe, I, Rinaldo, A, 2008, Ecohydrological characterization of flow duration curves and annual minima, *Water Resources Research*, v. 44, no.8:W08418.

Box, GEP, and Cox, DR, 1964, An analysis of transformations, *Journal of the Royal Statistical Society, Series B*, v. 26, no.21, pp. 211-52.

Brownlie WR, 1981, Prediction of flow depth and sediment discharge in open channels, Report No. KH-R-43A, W. M. Keck Laboratory of Hydraulics and Water Resources, California Institute of Technology, Pasadena, California, USA, 232 p.

Buckingham, SE and Whitney, JW, 2007, GIS methodology for quantifying channel change in Las Vegas, Nevada, *Journal of the American Water Resources Association*, v. 43, pp.888-898.

Cancienne, RM, Fox, GA, Simon, A, 2008. Influence of seepage undercutting on the stability of root-reinforced streambanks, *Earth Surface Processes and Landforms*, v. 33, pp.1769-1786.

Castellarin, A, Camorani, G, and Brath, A, 2007, Predicting annual and long-term flow-duration curves in ungauged basins, *Advances in Water Resources*, v. 30, no.4, pp.937-53.

Castellarin, A, Galeati, G, Brandimarte, L, Montanari, A, Brath, A, 2004a, Regional flow-duration curves: Reliability for ungauged basins, *Advances in Water Resources*, v. 27, no.10, pp.953-65.

Castellarin, A, Vogel, RM, Brath, A, 2004b, A stochastic index flow model of flow duration curve, *Water Resources Research*, v.40, no.3: W03104.

Chapman, AS, Foster, IL, Lees, JA, and Hodgkinson, RA, 2005, Sediment delivery from agricultural land to rivers via subsurface drainage, *Hydrological Processes*, v. 19, p. 2875-2897.

Clayton, L and Moran, SR, 1982, Chronology of late-Wisconsinan glaciations in middle North America, *Quaternary Science Reviews*, v.1, p.55-82.

Croker, K.M., Young, AR, Zaidman, MD, Rees, HG, 2003, Flow duration curve estimation in ephemeral catchments in Portugal, *Hydrological Sciences Journal/Journal Des Sciences Hydrologiques*, v.48, no.3, pp.427-39.

Cui Y and Parker, G, 1999, Sediment transport and deposition in the Ok Tedi-Fly river system, Papua New Guinea: The modeling of 1998-1999, Report 7 Environment Department, Ok Tedi Mining Ltd., Tabubil, Papua New Guinea.

Day, SS, Gran, KB, Belmont, P, Wawrzyniec, T, (in review) Change detection on bluffs using terrestrial laser mapping technology, in review for Earth Surface Processes and Landforms.

de Vries, M, 1965, Considerations about non-steady bed-load transport in open channels. *Proceedings*, 11th Congress, International Association for Hydraulic Research, Leningrad: 381-388.

Dingman, SL, 1978, Synthesis of flow-duration curves for unregulated streams in New Hampshire, *Journal of the American Water Resources Association,* v.14, no.6, pp1481-502.

Docker, BB, Hubble, TCT, 2008, Quantifying root-reinforcement of river bank soils by four Australian tree species, Geomorphology, v. 100, pp.401-418.

Eaton, B. C. and Church, M. (2011), A rational sediment transport scaling relation based on dimensionless stream power. *Earth Surface Processes and Landforms*, 36: n/a. doi: 10.1002/esp.2120.

Engelund F and Hansen, E, 1967, *A Monograph on Sediment Transport in Alluvial Streams,* Technisk Vorlag, Copenhagen, Denmark.

Engstrom, DR, Almendinger, JE, Wolin, JA, 2008, Historical changes in sediment and phosphorus loading to the upper Mississippi River: mass-balance reconstructions from the sediments of Lake Pepin. *Journal of Paleolimnology*.

Fennessey, N, 1990, Regional flow-duration curves for ungauged sites in Massachusetts, *Journal of Water Resources Planning and Management,* v. 116, pp. 530.

Fennessey, N, Vogel, RM, 1990, Regional flow-duration curves for Massachusetts, *Journal of Water Resources Planning and Management,* v. 116, n. 4, pp. 530-549.

Fernandez-Luque, R, and van Beek, R, 1976, Erosion and transport of bed-load sediment, *Journal of Hydraulic Research*, v. 14 n.2, p. 127-144.

Finnegan, NJ, Gran, K, Johnson, A, Belmont, P, Wilcock, P, Dietrich, WE, 2010, The importance of downstream bed surface coarsening in predicting the wave of incision in response to a sudden base level drop at the mouth of a river: the Holocene Le Sueur River, Minnesota, USA, Abstract EP52A-01 presented at the 2010 Fall Meeting, AGU, San Francisco, California, 13-17 Dec.

Fox, GA, Chu-Agor, ML, and Wilson, GV, 2007, Erosion of noncohesive sediment by ground water seepage: Lysimeter experiments and stability and modeling, *Soil Science Society of America Journal*, v. 71, p. 1822-1830.

Fox GA, Wilson GV, Simon A, Langendoen, EJ, Akay O, Fuchs JW, 2007, Measuring streambank erosion due to ground water seepage: correlation to bank pore water pressure, precipitation and stream stage. *Earth Surface Processes and Landforms* v.32, pp.1558-1573.

Galster,JC, Pazzaglia, FJ, Germanoski, D, 2008, Measuring the Impact of urbanization on channel widths using historic aerial photographs and modern surveys, *Journal of the American Water Resources Association*, v.44, pp. 948-960.

Garcia MH, ed., 2008. Sedimentation Engineering Processes, Measurements, Modeling and Practice. ASCE Manuals and Reports on Engineering Practice No. 110.

Gran, KB, Belmont, P, Day, SS, Jennings, C, Johnson, A, Perg, L, Wilcock, PR, 2009, Geomorphic evolution of the Le Sueur River, Minnesota, USA, and implications for current sediment loading, *in* James, L.A., Rathburn, S.L., and Whittecar, G.R., eds.,

Management and Restoration of Fluvial Systems with Broad Historical Changes and Human Impacts: Geological Society of America Special Paper 451, p.119-130.
Gulyaev SA, Buckeridge JS, 2004, Terrestrial methods for monitoring cliff erosion in an urban environment, *Journal of Costal Research,* v. 20, pp.871-878.
Guo, Y, and Quader,Y, 2009, Derived flow-duration relationships for surface runoff dominated small urban streams, *Journal of Hydrologic Engineering,* v.14, no.1, pp.42-52.
Hansen, B., Lenhart, C., Mulla, D., Nieber, J., Ulrich, J, and Wing, S., 2010, Ravine, Bluff, Streambank (RBS) erosion study for the Minnesota River basin. Report prepared for the Minnesota Pollution Control Agency, March 8, 2010, 61 p.
Harden CP, Foster W Morris C, 2009, Rates and processes of streambank erosion in tributaries of the Little River, Tennessee, *Physical Geography*, v. 30, pp.1-16.
Howard, A and Kerby, G, 1983, Channel changes in badlands, *Geological Society of America Bulletin*, v. 102, p. 233-242.
Howard, AD, and Knutson, TR, 1984, Sufficient conditions for meandering - a simulation approach, *Water Resources Research*, v. 20, pp.1659-1667.
Hughes, ML, McDowell, PF, Andrew Marcus, WA, 2006, Accuracy assessment of georectified aerial photographs: Implications for measuring lateral channel movement in a GIS, *Geomorphology,* v.74, pp.1-16.
Jennings, CE, 2010, Draft digital reconnaissance surficial geology and geomorphology of the LeSueur River watershed (Blue Earth, Waseca, Fairbault, and Freeborn counties in south-central MN). Open File Report 10-03, Minnesota Geological Survey, map, report and digital files. ftp://mgssun6.mngs.umn.edu/pub4/ofr10_03/.
Jia GW, Zhan LT, Chen YM, Fredlund DG. 2009. Performance of a large-scale slope model subjected to rising and lowering water levels, *Engineering Geology*, v.106, pp.92-103.
Johnson, A, in prep, Timing and Pattern of the valley excavation, Le Sueur River, south central Minnesota, USA. M.S. Thesis, University of Minnesota Duluth.
Kelley DW, Nater EA, 2000, Historical sediment flux from three watersheds in Lake Pepin, Minnesota, USA, *Journal of Environmental Quality,* v. 29, pp.561–568.
Kelley DW, Nater EA, 2000, Source apportionment of lake bed sediments to watersheds in an upper Mississippi basin using a chemical mass balance method, *Catena,* v.41, pp277–292. doi:10.1016/S0341-8162(00)00094-1.
Kudelka, S. for Minnesota River Board, 2010, Minnesota River Basin 2010 Progress Report, 197 p.
Lauer, JW and Parker G, 2008a. Net local removal of floodplain sediment by river meander migration, *Geomorphology,* v.96, pp.123–149.
Lauer, JW and Parker G, 2008b, Modeling framework for sediment deposition, storage, and evacuation in the floodplain of a meandering river: Theory, *Water Resources Research* v. 44, W04425, doi:10.1029/2006WR005528.
Lauer, JW and Parker G, 2008c, Modeling framework for sediment deposition, storage, and evacuation in the floodplain of a meandering river: Application to the Clark Fork river, Montana, *Water Resources Research,* v.44, W08404, doi:10.1029/2006WR005529.
Lauer, JW, Willenbring, J, 2010, Steady-state reach-scale theory for radioactive tracer concentration in a simple channel/floodplain system. *Journal of Geophysical Research*.
LeBoutillier, DW, and Waylen PR, 1993, A stochastic model of flow duration curves. *Water Resources Research* v. 29, no. 10, pp.3535-41.

Leopold, LB, Wolman, MG, Miller, JP, 1995, *Fluvial Processes in Geomorphology*, Dover Publications. New York. 535 pp.

Lim, M, Rosser, NJ, Allison, RJ, Petley DN, 2010, Erosional processes in the hard rock coastal cliffs at Staithes, North Yorkshire, *Geomorphology*, v. 114, pp.12-21.

Lindow, N, Fox, GA, Evans, RO, 2009, Seepage erosion in layered stream bank material, *Earth Surface Processes and Landforms*, v. 34, pp. 1693-1701.

Liu, Q, Xu, G, Liu, X, 2008, Experimental and theoretical study on freeze-thawing damage propagation of saturated rocks, *International Journal of Modern Physics B*, v.22, pp.1853-1858.

Lowell, TV, Fisher, TG, and Comer, GC, 2005, Testing the Lake Agassiz meltwater trigger for the Younger Dryas: *EOS Transactions of the AGU*, v. 86, no. 40, p. 365 – 373.

Magdalene, SC, 2004, From field to stream: Rapid runoff through agricultural tile drainage systems within the Minnesota River Basin, Ph.D. Thesis, University of Minnesota, 157 p.

Marschner, FJ, 1930, Interpretation of Francis J. Marschner's map of the original vegetation of Minnesota: Based on the notes of the Public Land Survey, 1847-1907.

Martin, Y and Ham, D, 2005, Testing bedload transport formulae using morphologic transport estimates and field data: lower Fraser River, British Columbia, *Earth Surface Processes and Landforms*, v.30, pp.1265-1282.

Matsch, CL, 1972, Quaternary Geology of Southwestern Minnesota, *in* Sims, P.K., G.B., Morey, eds., *Geology of Minnesota: A centennial volume*: St. Paul, Minnesota Geological Survey, p. 548-560.

Matsch, CL, 1983, River Warren, the southern outlet of Lake Agassiz, in Teller, J.T. and Clayton, L., eds., *Glacial Lake Agassiz*: Geological Association of Canada Special Paper 26, p. 232 – 244.

Meixell, KJ, Wittkop, C, Rittenour, TM, Makovxky, KA, 2009, Holocene stream capture of the Le Sueur River, Minnesota: Implications for modern sediment loading. Geological Society of America Abstracts with Programs, v. 41, no. 7, pp. 648.

Milan DJ, Heritage GL, Hetherington D, 2007, Application of 3D laser scanner in the assessment of erosion and deposition volumes and channel change in a proglacial river, *Earth Surface Processes and Landforms*, v.32, pp.1657-1674.

Minnesota Department of Natural Resources, 2007, Native Plant Communities and Rare Species of the Minnesota River Valley Counties: Minnesota County Biological Survey, Biological Report 89: St. Paul, Minnesota Department of Natural Resources.

Minnesota Pollution Control Agency, Minnesota Department of Agriculture, Minnesota State University, Mankato Water Resources Center, and Metropolitan Council Environmental Services, 2007, State of the Minnesota River: Summary of surface water quality monitoring 2000-2005. 20 p.

Mohamoud, YM, 2008. Prediction of daily flow duration curves and streamflow for ungauged catchments using regional flow duration curves, *Hydrological Sciences Journal*, v.53, no.4, pp.706-24.

Mulla, DJ, Sekely, AC, 2009, Historical trends affecting accumulation of sediment and phosphorus in Lake Pepin, upper Mississippi River, USA, *Journal of Paleolimnology*, v. 41, pp. 589-602.

Murray, AS and Wintle, AG, 2003, The single aliquot regenerative dose protocol: potential for improvements in reliability, *Radiation Measurments*, v.37, pp.377-381.

Murray, AG, and Wintle, AG, 2000, Luminescence dating of quartz using an improved single-aliquot regenerative-dose protocol, *Radiation Measurements*, v. 32, no. 1, pp. 57-73.
Niadas, IA, 2005, Regional flow duration curve estimation in small ungauged catchments using instantaneous flow measurements and a censored data approach, *Journal of Hydrology*, 314, no.1-4, pp. 48-66.
Novotny, EV, and Stefan, HG, 2007, Stream flow in Minnesota: Indicator of climate change, *Journal of Hydrology*, v. 334, p. 319-333.
Parker, G, Cui, Y, Imran, J, Dietrich, WE, 1996, Flooding in the lower Ok Tedi, Papua New Guinea, due to the disposal of mine tailings and its amelioration. International seminar on recent trends of floods and their preventive measures, 20-21 June, Sapporo, Japan.
Parker, G, 2002, Some ideas on modeling floodplain construction. Report prepared at Tokyo Institute of Technology, July, 11, 14 p, downloadable at http://vtchl.uiuc.edu/people/parkerg/.
Parker, G, 2004, "1D Sediment Transport Morphodynamics with Applications to Rivers and Turbidity Currents". Copyrighted e-book downloadable at http://vtchl.uiuc.edu/people/parkerg/morphodynamics.
Parker, G, Wilcock, PR, Paola, C, Dietrich, WE, Pitlick, J, 2007, Physical basis for quasi-universal relations describing bankfull hydraulic geometry of single-thread gravel bed rivers, *Journal of Geophysical Research*, v. 112, F04005, doi:10.1029/2006JF000549.
Parker, G, Shimizu, Y, Wilkerson, GV, Eke, EC, Abad, JD, Lauer, JW, Paola, C, Dietrich, WE, Voller, VR, 2011, A new framework for modeling the migration of meandering rivers, *Earth Surface Processes and Landforms*, v. 36, pp.70-86.
Resop, JP, Hession, WC, 2010, Terrestrial laser scanning for monitoring streambank retreat: comparison with traditional surveying techniques, *Journal of Hydraulic Engineering*, v. 136, pp. 794-798.
Rosser, NJ, Petley, DN, Lim, M, Dunning, SA, Allison, RJ, 2005, Terrestrial laser scanning for monitoring the process of hard rock costal cliff erosion, *Quarterly Journal of Engineering Geology and Hydrogeology* v. 38, pp. 363-375.
Ruhe. RV and Scholtes, WH, 1959, Important elements in the classification of the Wisconsin Glacial Stage: A Discussion, *The Journal of Geology*, v. 67, no. 5, pp. 585-593.
Russell, MA, Walling, DE, Hodgkinson, RA, 2001, Suspended sediment sources in two small lowland agricultural catchments in the UK, *Journal of Hydrology,* v. 252, pp.1-24.
Schilling, KE, and Helmers, M, 2008, Tile drainage as karst: conduit flow and diffuse flow in a tile-drained watershed, *Journal of Hydrology*, v. 349, pp. 291-301.
Schilling, KE and Libra, RD, 2003, Increased baseflow in Iowa over the second half of the 20th century, *Journal of the American Water Resources Association*, v. 39, no. 4, pp. 851-860.
Schottler, SP and Engstrom DR, 2002, Identification of Sediment Sources in an Agricultural Watershed, Report to the Legislative Commission on Minnesota's Resources, Project W02, ML 1999, Subd 6b, December 30, 2002 St. Paul MN.
Sekely AC, Mulla, DJ, Bauer DW, 2002, Streambank slumping and its contribution to the phosphorus and suspended sediment loads of the Blue Earth River, Minnesota, *Journal of Soil Water Conservation,* v.57, pp. 243–250.
Singh, RD, Mishra, SK, Chowdhary, H, 2001, Regional flow-duration models for large number of ungauged Himalayan catchments for planning microhydro projects, *Journal of Hydrologic Engineering*, v. 6, no.4, pp.310-6.

Smakhtin, VY, Hughes,DA, Creuse-Naudin, E, 1997, Regionalization of daily flow characteristics in part of the eastern cape, South Africa, *Hydrological Sciences Journal*, v. 42, no. 6, pp. 919-36.

Stedinger, JR., Vogel, RM, Foufoula-Georgiou, E, 1993, Frequency analysis of extreme events. In *Handbook of hydrology.*, ed. D. R. Maidment, 18.1-18.66McGraw Hill.

Stone, M, and Krishnappan, BG, 2002, The effect of irrigation on tile sediment transport in a headwater stream, *Water Research*, v. 26, p. 3439-3448.

Tetra Tech. *Minnesota river basin turbidity TMDL and lake Pepin excessive nutrient TMDL: Model calibration and validation report.* Research Triangle Park, N.C.: Prepared for Minnesota Pollution Control Agency by Tetra Tech, Inc., 2008.

Tetra Tech. *Minnesota river basin model, model calibration and validation report.* Research Triangle Park, N.C.: Prepared for Minnesota Pollution Control Agency by Tetra Tech, Inc., 2002.

Thoma, DP, Gupta, SC, Bauer, ME, Kirchoff CE, 2005, Airborne laser scanning for riverbank erosion assessment, *Remote Sensing Environ.*, v.95, pp. 493-501.

Thomas, JT, Iverson, NR, Burkart, MR, 2009. Bank-collapse processes in a valley-bottom gully, western Iowa, *Earth Surface Processes and Landforms*, v. 34, pp. 109-122.

Thorleifson, LH, 1996, Review of Lake Agassiz history, *in* J.T. Teller, L.H. Thorleifson, G. Matile and W.C. Brisbin, 1996, Sedimentology, Geomorphology and History of the Central Lake Agassiz Basin - Field Trip Guidebook B2; Geological Association of Canada/Mineralogical Association of Canada Annual Meeting, Winnipeg, Manitoba, May 27 – 29, 1996.

Trimble, S, 1997, Contribution of stream channel erosion to sediment yield from an urbanizing watershed, *Science*, v. 278, pp. 1442-1444.

Trimble, SW, 1999, Decreased rates of alluvial sediment storage in the Coon Creek Basin, Wisconsin, 1975-93, Science, v. 285, pp.1244-1246.

Trimble, S, 2009, Fluvial processes, morphology and sediment budgets in the Coon Creek Basin, WI, USA, 1975–1993, *Geomorphology*, v. 108, pp. 8-23.

Upham, W, 1890, *Report of exploration of the glacial Lake Agassiz in Manitoba:* Geological Survey of Canada. Annual Report 1888 – 89, part E, 156 p.

Upham, W, 1895, *The Glacial Lake Agassiz*: United States Geological Survey, Monograph 25, 658 p.

Viparelli, E, Gaeuman, D, Wilcock, PR, Parker, G, 2010, A model to predict the evolution of a gravel bed river under an imposed cyclic hydrograph and its application to the Trinity River, *Water Resources Research*, 2010WR009164.

Viparelli, E, Lauer, JW, Belmont, P, Parker, G, A numerical model to Develop Long-term Sediment Budgets Using Isotopic Sediment Fingerprints, submitted to Computer and Geoscience, Special Issue on Modeling for Environmental Change.

Viparelli, E, Lauer, WJ, Parker, G, Modeling the exchange of sediment and cosmogenic nuclides between a sand bed river and its floodplain. Application to the lower Minnesota River in preparation for *Journal of Geophysical Research* (a).

Viparelli, E, Lauer, WJ, Belmont, P, Gran, K, Wilcock, PR, Parker, G, Sediment routing model for the Maple River, Minnesota in preparation for *Journal of Geophysical Research* (b).

Vogel, RM and Fennessey, NM, 1994, Flow-duration curves. I: New interpretation and confidence intervals, *Journal of Water Resources Planning and Management*, v. 120, no. 4, pp. 485- 504.

Water Resources Center, Minnesota State University, Mankato, 2000, Le Sueur River major watershed diagnostic report: Le Sueur River basin implementation framework, MPCA Clean Water Partnership Project #951-1-194-07.

Wallinga, J, 2002, Optically stimulated luminescence dating of fluvial deposits: a review, *Boreas*, v. 31, pp. 303-322.

Walter, RC and Merritts, DJ, 2008. Natural Streams and the legacy of water-powered mills, *Science*, v. 319, pp. 299-304.

Wawrzyniec, TF, McFadded, LD, Ellwein, A, Meyer, G, Scuderi, L, McAuliffe, J, Fawcett, P. 2007. Chronotopographic analysis directly from point-cloud data: A method for detecting small seasonal hillslope change in Black Mesa Escarpment, NE Arizona, *Geosphere*, v. 3, pp. 550-567.

Wilcock, PR, on behalf of the Minnesota River Sediment Colloquium Committee, 2009, Identifying sediment sources in the Minnesota River Basin, MPCA Report wq-b3-43, 16 p.

Wilkerson, GV and Parker, G, 2010, Physical Basis for Quasi-Universal Relations Describing Bankfull Hydraulic Geometry of Sand-Bed Rivers, *Journal of Hydraulic Engineering*, doi:10.1061/(ASCE)HY.1943-7900.0000352.

Wintle, AG and Murray, AS, 2006, A review of optically stimulated luminescence characteristics and their relevance in single-aliquot regeneration, *Radiation Measurments*, v. 41, pp. 369-391.

Wolman, MG and Miller JP, 1960. Magnitude and frequency of forces in geomorphic processes, *Journal of Geology*, v. 68, no. 1, pp. 54-74.

Wright, S and Parker G, 2004, Flow resistance and suspended load in sand-bed rivers: simplified stratification model, *Journal of Hydraulic Engineering*, v. 130, no.8.

Zhang, YK and Schilling, KE, 2006, Increasing streamflow and baseflow in Mississippi River since the 1940's: Effect of land use change, *Journal of Hydrology*, v. 324, pp. 412-422.

Appendix A: Flow Duration Analysis

The numerical modeling framework for routing sediment through the Le Sueur basin represents river discharge using a flow-duration based approach. A flow duration curve (FDC) characterizes the relationship between discharge and a given exceedence probability for that discharge. It is the complement to the cumulative distribution function CDF for all observed flow (that is, the relationship between flow and non-exceedence probability). This section describes the justification for using a regional flow-duration based approach to characterize geomorphically relevant hydrology, the data and methods used for curve development, and the results of a statistical fit to the empirically developed curve. The analysis is based on continuous hydrologic simulation results taken from the Minnesota Pollution Control Agency HSPF model (Tetra Tech 2008). The MPCA model accounts for tile drainage on agricultural land and can be adjusted to represent historic watershed conditions. While we are still awaiting the results of the historic runs, the FDC analysis presented here can be used to quickly develop representative curves for these conditions when the results become available. The analysis can also easily incorporate results of the WEPP study also outlined in this report. In combination with the sediment routing model presented elsewhere in this report, this will provide a mechanism for testing the sensitivity of the channel system to long-term changes in watershed hydrology.

Background

In the context of the present project, the flow duration curve (or the complementary cumulative distribution function, CDF, for discharge) must fulfill certain requirements. First, because a major component of the sediment routing model requires an accurate representation of the deposition of sediment on the floodplain, the FDC needs to characterize a realistic range of floods, not simply the in-bank discharges which dominate the flow record. The accuracy requirements are greatest for the largest flood discharges that transport the most sediment, precluding the use of FDC approaches that are focused on characterizing the risk of minimum in-stream flows. Second, the approach used for developing the FDC should be capable of representing not only modern conditions, where land use in the watershed is primarily agricultural, but also historic pre-agriculture conditions which will be needed for calibrating the sediment routing model. Finally, because sediment is being routed across a relatively long portion of the river, with a correspondingly large range of drainage areas, the flow duration curve needs to vary throughout the channel network.

A range of regional flow duration approaches are described in the literature (Dingman 1978; Fennessey 1990; Singh et al. 2001; Niadas 2005; Mohamoud 2008). Castellarin et al. (2004a) classify them as either statistical, wherein the FDC is represented using parametric probability distribution whose parameters vary regionally, or graphical, wherein no formal probability distribution is used (although ad-hoc analytical relationships between exceedence probability and discharge are sometimes used). In all cases, the analysis usually requires the standardization of raw flow data by dividing by a representative parameter such as mean annual discharge, developing the appropriate regional representative for the standardized FDC, and then generating an appropriate site-specific FDC at an ungauged site as a function of regional descriptive parameters that depend on site geomorphology and/or climate. Drainage area is used as a descriptive parameter in many cases (e.g. Fennessey 1990; Singh et al. 2001; Mohamoud 2008; Castellarin et al. 2004a).

Fennessey and Vogel (1990) exemplify the statistical approach. In their study, a 2-parameter lognormal distribution was used to represent a regional FDC in Massachusetts for flows less than the 50^{th} percentile (i.e. for characterizing the probability of low discharge). The distribution's parameters were assumed to be functions of watershed area and average basin slope. Singh et al. (2001) developed regional flow duration curves for small basins in the Himalaya by fitting a normal distribution to power-transformed (Box and Cox, 1964) daily discharge data standardized by mean annual discharge. The retransformation from the standardized FDC was accomplished by multiplying the standardized discharge by a regional estimate of mean annual flow, which was assumed to be a power function of drainage area. The five parameters (mean, standard deviation, power parameter in the statistical distribution as well as the coefficient and exponent in the mean discharge vs. drainage area relationship) were assumed constant in each of the nine geomorphic regions in the study. Castellarin et al. (2004b; 2007) developed a representation of flow duration distributions that assumed stochastic independence between the mean annual flow series (which in both cases were modeled using a 2-parameter log-logistic model) and shorter term variability within a series of data representing daily discharge divided by the mean annual flow in the year the measurement was recorded. Castellarin at al. (2004b) suggest using a 3-parameter generalized Pareto (GPA) distribution to represent the short term variability, while Castellarin et al. (2007) suggest using a 4-parameter kappa distribution (which includes the GPA as a special case) for this purpose. The method allows estimation of both period-of-record FDC's and annual flow duration curves (c.f. LeBoutillier and Waylen 1993; Vogel and Fennessey 1994). (Annual FDCs represent the probability of occurrence of a given FDC in a given year—in a way representing error bars on a given median FDC. For long term morphodynamic modeling, however, there is little reason to estimate the probability of excessively wet or dry years—all that matters is the long-term average probability of a given discharge).

The graphical approach is exemplified by Smakhtin et al. (1997) who developed regional flow duration curves in eastern South Africa from daily discharge observations standardized by mean annual discharge. The method is empirical in that the standardized regional FDC is computed using "simple averaging," presumably at each quantile of interest. This approach provided good agreement for the upper half (higher flows) of the curve. Croker et al. (2003) developed regional FDC's for potentially ephemeral rivers in Portugal. Mohamoud (2008) used what amounts to a graphical approach to develop estimates for flow per unit area at 15 different arbitrarily selected quantiles. At each quantile, unit discharge was a function of two geomorphic and climate parameters. The parameters used for this purpose varied from quantile to quantile.

Recent literature provides two methods for directly translating rainfall statistics into flow duration curves. Botter et al. (2008) used a statistical approach to relate the shape of a FDC to a set of runoff timing parameters, with a focus on low discharges. The model assumes a Poisson distribution for rainfall and characterizes the rainfall-runoff process using parameters representing soil moisture storage, evapotranspiration, soil transit time, and basin area. The final analytical form for the FDC under their assumptions is a regularized gamma function. The method was tested on a ~50 km² agricultural basin in North Carolina. Guo and Quader (2009) developed a closed-form solution for flow duration curves for small urban catchments (less that ~100 km²), based on the assumption that precipitation patterns can be described through a series of exponential distributions (for volume, duration, and time between events) and a very simple transform between rainfall and runoff. Their results were validated using a continuous

hydrologic simulation model, which they assume to be less simplified and thus more likely representative of real conditions than their derived FDC.

One of the points implicit in the Guo and Quader study is that continuous simulation models are capable of developing useful flow duration data at ungauged sites. They state that "although the resulting FDCs can be accurate and include the effect of many of the catchment characteristics, the computational tasks involved are prohibitive for routine engineering design applications." While the computational effort is certainly large where models do not exist, it is quite beneficial to use these models where they are available. This is the approach taken on the present project, wherein we use an existing continuous simulation model to provide raw input data from which we develop a standardized FDC for the Le Sueur basin. Because parameters in the continuous simulation model can crudely represent pre-agricultural conditions, this approach provides a mechanism for looking at changes in the FDC over time when historic runs become available.

Data

The basic input data for the analysis are simulation results taken from the Minnesota Pollution Control Agency (MPCA) continuous hydrologic simulation model for southeastern Minnesota (Tetra Tech 2002; Tetra Tech 2008). The MPCA simulation was performed using Hydrologic Simulation Program, Fortran (HSPF) on an hourly timestep over the period from January 1, 1986 to December 31, 2006. The simulation is an update to an earlier version of the model (Tetra Tech 2002) that was focused on characterizing Dissolved Oxygen/BOD in the Minnesota River basin. The present model was developed primarily to simulate turbidity, sediment load, and the loads of certain nutrients such as Nitrogen and Phosphorus. Because these water quality parameters depend strongly on sediment transport dynamics, the model addresses many of the hydrologic processes important for routing sediment through the Le Sueur river basin and provides the most complete dataset available for characterizing spatial and temporal hydrologic variability in this region.

The MPCA model was calibrated using a portion of the 21-year dataset (1993-2006) and validated using the remainder of the data (Tetra Tech 2008). For the Le Sueur basin, the error in the calibration portion of the dataset when compared to gauge data for the Le Sueur basin was -6.91% for total volume and -2.85% for the highest 10% of flows. For the validation period, these numbers were -4.74%, and -3.34%, respectively. Since there are minimal differences in model uncertainty for the calibration and validation time periods, the entire 21-year period was used in the present analysis to develop a representative standardized FDC for the Le Sueur basin. While the MPCA model consists of eight detailed sub-basin models spread across the Minnesota River watershed, the FDC analysis presented here is limited to daily average data calculated at ten nodes located within the Le Sueur basin (Figure A.1). The standardized FDC for the Le Sueur Basin is validated using the two USGS gauges in the watershed, the Le Sueur River near Rapidan (USGS 05230500) and the Little Cobb R. near Beauford (USGS 05230270). As discussed below, instantaneous USGS gauge data at these sites indicate that there are minimal differences between FDC's computed from daily and hourly data, respectively. Table A.1 summarizes all data sources used in the analysis.

Table A.1: *Data sources*

Source	Drainage Area	Period of Record
Le Sueur R. near Rapidan (USGS 05230500)	2874 km²	October 1, 1939 – present
Little Cobb R. near Beauford (USGS 05230270)	337 km²	April 1, 1996 – present
HPSF model output at 10 nodes in Le Sueur basin	318 km² to 2771 km²	1986-2006

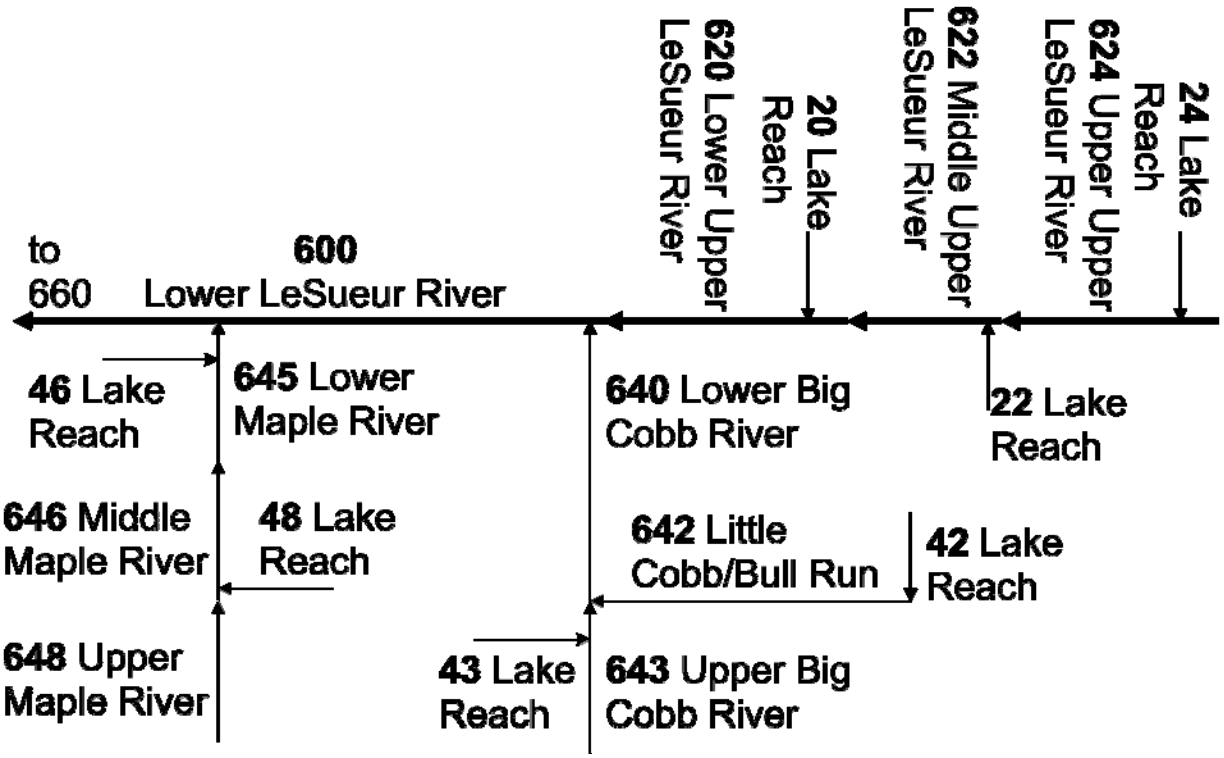

Figure A.1: Schematic of nodes in the HSPF continuous simulation model developed by the MPCA. Simulation results computed at nodes 600, 620, 622, 624, 640, 642, 643, 645, 646, and 648 were used to develop the standardized FDC.

Daily discharge at each gauge or node was divided by drainage area to determine unit discharge. Mean, median, and the 95% non-exceedence unit discharge (representing a typical high discharge) were then estimated at each site for the 1986-2006 period. (Note that representative statistics could not be directly computed at the Little Cobb USGS gauge for the 1986-2006 period because the gauge was not in operation until 1996. Estimates representative of the entire period at the Little Cobb gauge were obtained by multiplying each statistic as computed from the 1996-2006 period of record by the ratio between the same statistic computed at the Le Sueur gauge for the entire 21-year period and for the shorter period.) The results are presented in Figure A.2. None of these statistics varies significantly with drainage area, providing justification for using drainage area (rather than the more commonly used mean discharge) as the standardizing parameter in the flow duration analysis.

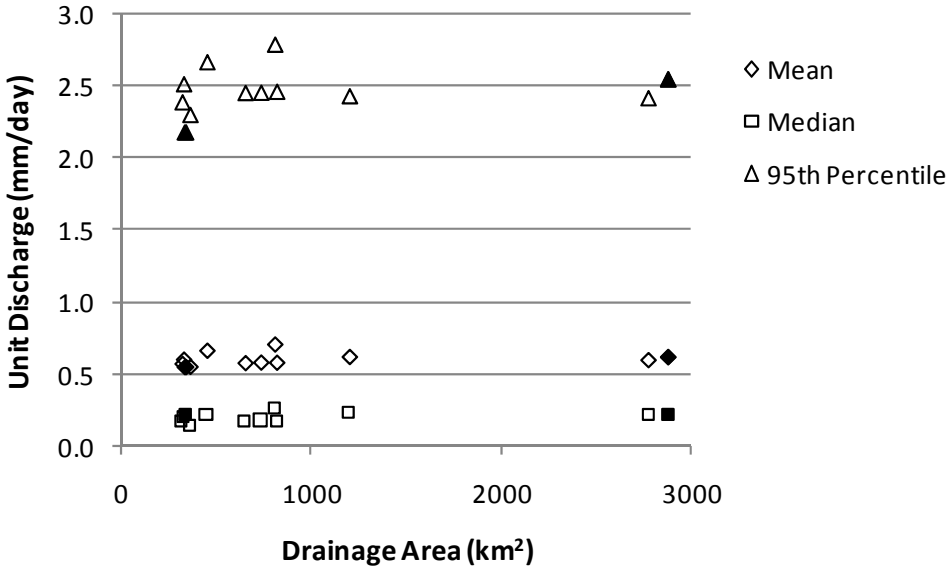

Figure A.2: Relationship between daily unit discharge (i.e. discharge per unit drainage area) and drainage area for USGS gauges (solid shapes) and HSPF output (open shapes). No statistically significant trends are present for the mean, median, or 95th percentile unit discharge. This provides justification for standardizing flow duration curves by unit area rather than by mean annual discharge.

Development of Standardized Unit Flow Duration Curves

The standardized curves were developed using the HSPF output exclusively. The daily unit discharge at each of the ten HSPF nodes were compiled into a single large dataset of length n, sorted from low to high, and assigned an exceedence probability p_i using the Weibull plotting position formula:

$$p_i = 1 - \frac{i}{n+1} \qquad \text{(A.1)}$$

The resulting standardized FDCs for unit discharge are shown in Figure A.3, along with curves computed from each of the HSPF nodes and at the two USGS gauges. The composite standardized FDC computed from the entire dataset (solid black line) falls solidly within the range of the individual HSPF results.

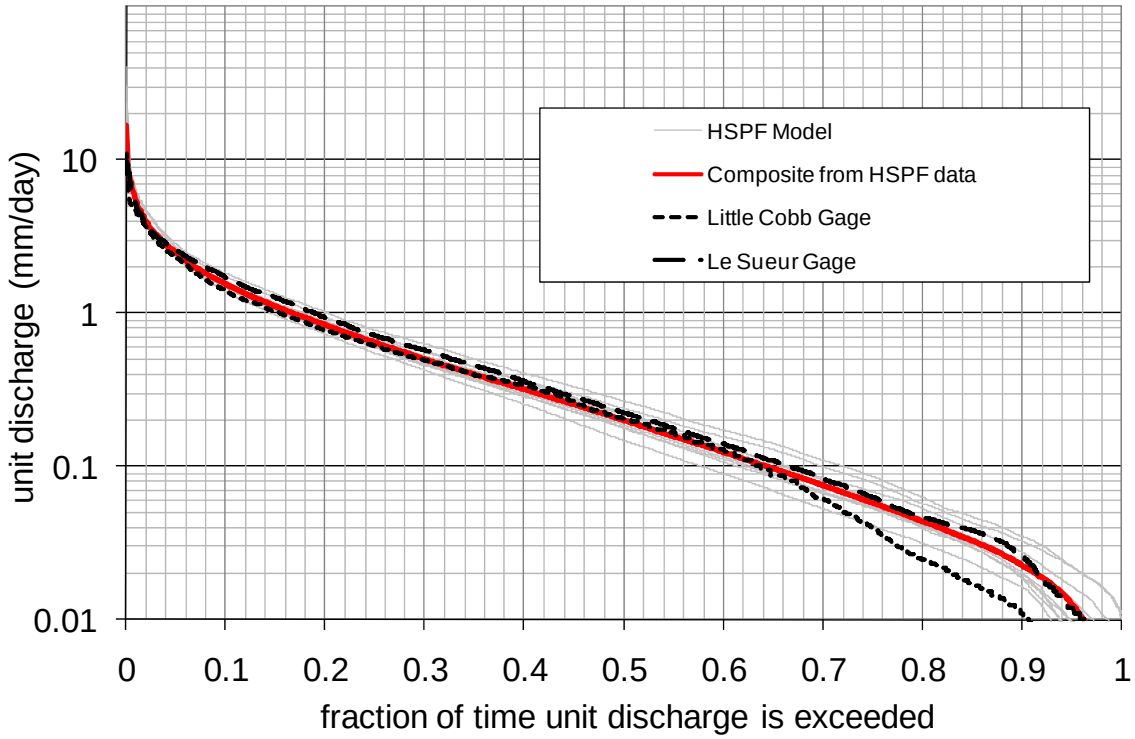

Figure A.3: Standardized flow duration curves for the Le Sueur basin. The thin gray lines represent unit flow duration curves generated from each of the 10 HSPF nodes within the Le Sueur basis. The red line represents a composite average curve generated from the HSPF data. The black dashed lines represent data from USGS gauges. Note that the period of record for the Little Cobb gauge is nearly 10 years shorter than for the rest of the curves, probably explaining its deviation from the rest of the curves at the low end of discharges.

Analytical Description of FDC

While the standardized curve can be used graphically to represent the FDC without any additional analysis, it is sometimes helpful computationally to represent the curves using a parametric probability distribution. It is also useful to use a parametric distribution when projecting near the ends of the input dataset. Both generalized Pareto (GPA) distributions and three parameter log-normal (LN3) distributions were fit to portions of the composite standardized FDC. The CDF for the GPA distribution is given as follows:

$$F(x) = 1 - \left[1 - \kappa \frac{(x-\xi)}{\alpha}\right]^{1/\kappa} \qquad \text{(A.2)}$$

where x is unit discharge and α, κ, and ξ are the parameters of the distribution. The 3-parameter log-normal distribution is best represented as

$$Y = \ln(x - \xi) \qquad \text{(A.3)}$$

where Y is a normally-distributed random variable with mean μ_y and standard deviation σ_y.

A MS Excel spreadsheet with a Visual Basic for Applications macro was developed to quickly compute the composite standardized FDC and find the parameters of the two distributions using the method of L-moments (Stedinger et al. 1993). It was developed primarily to facilitate development of FDC's for new study sites or to incorporate additional historic MPCA data into the present analysis as they become available.

The log-normal distribution fits well for most mid-range discharges (Figure A.4). However, for the upper tail of discharges that are of the most geomorphic significance, the best fit can be obtained by fitting the generalized Pareto distribution to a set of exceedences above a threshold. A non-exceedence threshold F_{min} equal to 0.6 (i.e. the 60th percentile for unit discharge) was arbitrarily used for this purpose. When the distribution is fit to all sample values above the exceedence threshold F_{min}, the CDFs for the GPA and LP3 distributions can be represented as follows:

$$F(x) = F_{\min} + (1 - F_{\min})\left(1 - \left[1 - \kappa\frac{(x-\xi)}{\alpha}\right]^{1/\kappa}\right) \quad \text{(A.4)}$$

$$F(x) = F_{\min} + (1 - F_{\min})(F_{normal}(z)) \quad \text{(A.5)}$$

where F_{normal} is the standard normal CDF evaluated at $z = (\ln(x-\xi)-\mu_y)/\sigma_y$. In equations 4 and 5, the respective CDF is not defined for non-exceedence probabilities below F_{min}. Flow duration curves can then be generated by computing exceedence probability p = 1-F.

The parameters for both the generalized Pareto and log normal distributions are given Table A.2. Figure A.4 shows the fit distributions plotted next to the entire standardized FDC, and Figure A.5 shows the upper 10 percent of the standardized FDC and the Generalized Pareto fit plotted on a log scale. It is clear that the generalized Pareto fit is quite good, particularly for geomorphically important flood flows.

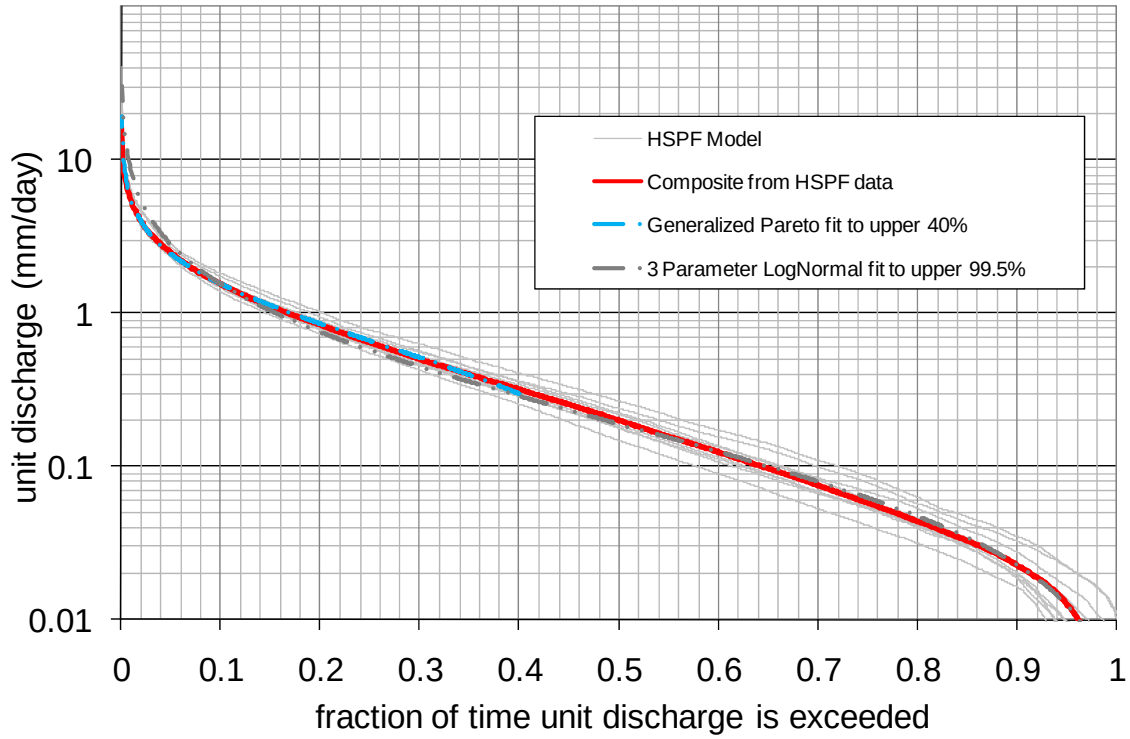

Figure A.4. Statistical distributions fit to composite standardized flow duration curve. A Generalized Pareto distribution was fit to the upper 40% of discharges and provides a good fit in that range. A 3-parameter lognormal distribution does a good job representing the lower ~60% of discharges (which are not particularly relevant geomorphically in any case) but overpredicts significantly for higher discharges. The log-normal curve disregards the lowest 0.5% of unit discharges since including these anomalously low observations dramatically reduces the quality of the fit for the majority of the curve.

Table A.2: Parameters for Fit Distributions

Distribution	Parameters	Notes
Generalized Pareto (GPA)	ξ = 0.296 α = 0.709 κ = -0.330 F_{min} = 0.6	Fit using upper 40% of all unit discharges. Not characteristic for lower 60% of unit discharges.
3-Parameter Log Normal (LN3)	ξ =0.000503 μ_y = -1.655 σ_y =1.639 F_{min} = 0.005	Fit using upper 99.5% of all unit discharges. Recommended for unit discharges exceeded at most 60% of the time.

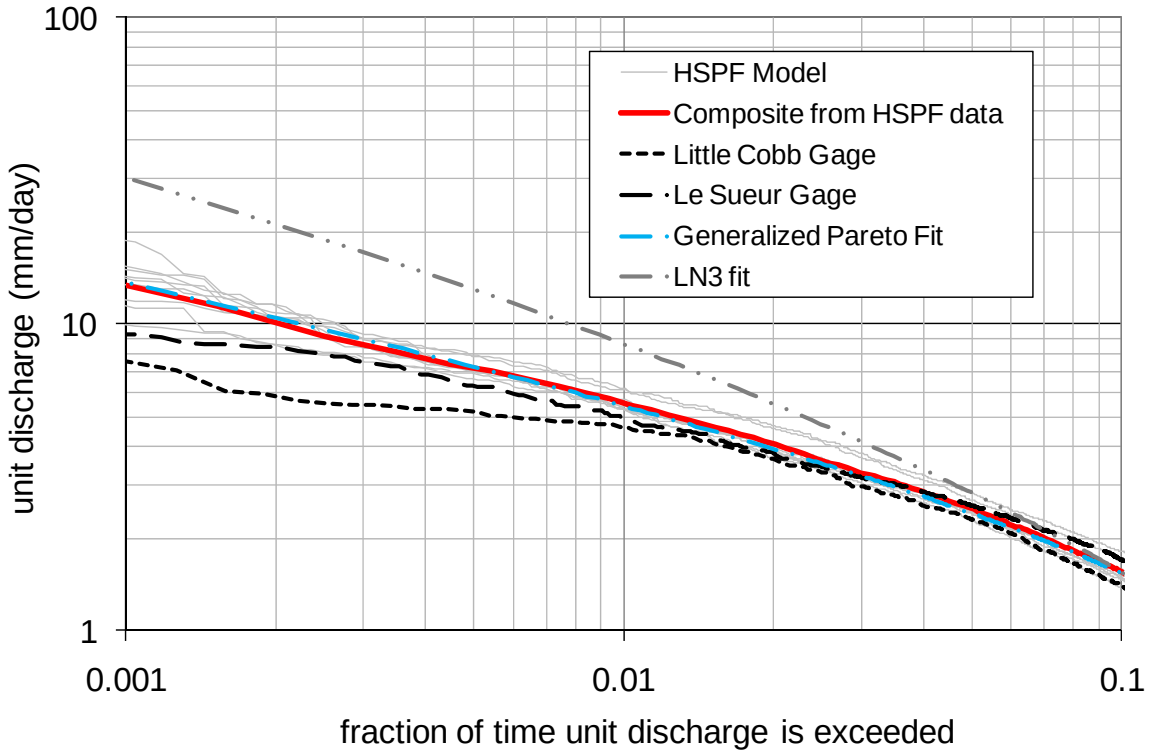

Figure A.5. Upper 10% of standardized flow duration curve with exceedence fraction plotted on a logarithmic scale. The high quality of the Generalized Pareto Distribution fit using the upper 40% of unit discharges is striking. Note that the deviation between the Little Cobb Gauge FDC and the others is probably due to the shorter period of record for the Little Cobb gauge.

Sensitivity to timestep

The analysis presented above uses a daily timestep to develop the standardized FDC's. It is possible that such a large timestep could introduces bias into the results by disregarding large, short-lived flood pulses with durations of hours. To address this issue, instantaneous flow data measured at hourly intervals were downloaded from the USGS data archive (http://ida.water.usgs.gov/ida/) for the Le Sueur near Rapidan gauge (October 2, 1993 to November 29, 2006) and the Little Cobb gauge (April 12, 1996 to August 21, 2008). Standardized FDCs were then developed from a) the raw hourly data and b) the average of the 24 hourly measurements for each calendar day. For consistency, days without 24 non-zero instantaneous flow measurements made on the hour were discarded from the analysis. If the standardized FDC's are sensitive to timestep (i.e. if floods tend to last only a few hours at a time), the curves developed using hourly data should plot significantly below the curves developed using daily averages because the daily averages would be dominated by the few hours of high flow.

The upper 10% of the resulting flow duration curves are plotted in Figure A.6. For the Le Sueur gauge, there is no discernable difference between the daily and hourly curves all the way out to the largest exceedence fraction estimated from the daily dataset (~4 in 10000, estimated using the Weibull plotting position formula). For the Little Cobb gauge, while the two standardized FDC's are nearly identical for the great majority of exceedence probabilities, there

is a small difference (~ 10%) between the daily and hourly FDC's above the discharge that is exceeded 0.3% of the time. This is not entirely unexpected given the relatively small drainage area (336.7 km² for the Little Cobb as opposed to 2875 km² for the Le Sueur gauge). There are significant differences between the curves for the Le Sueur and Little Cobb gauges. These are almost certainly caused by the selection of different time periods for generating the curves at each gauge site, and in particular by the removal from the analysis of days with missing instantaneous flow measurements. Consequently, the curves plotted in Figure A.6 should not be used directly as model input. However, because differences between the hourly and daily FDC are minimal at both sites, and because most of the reaches incorporated into the sediment routing model have much larger drainage areas than the Little Cobb gauge (where small differences are apparent for the highest discharges), use of a daily timestep to develop FDCs is unlikely to bias model results.

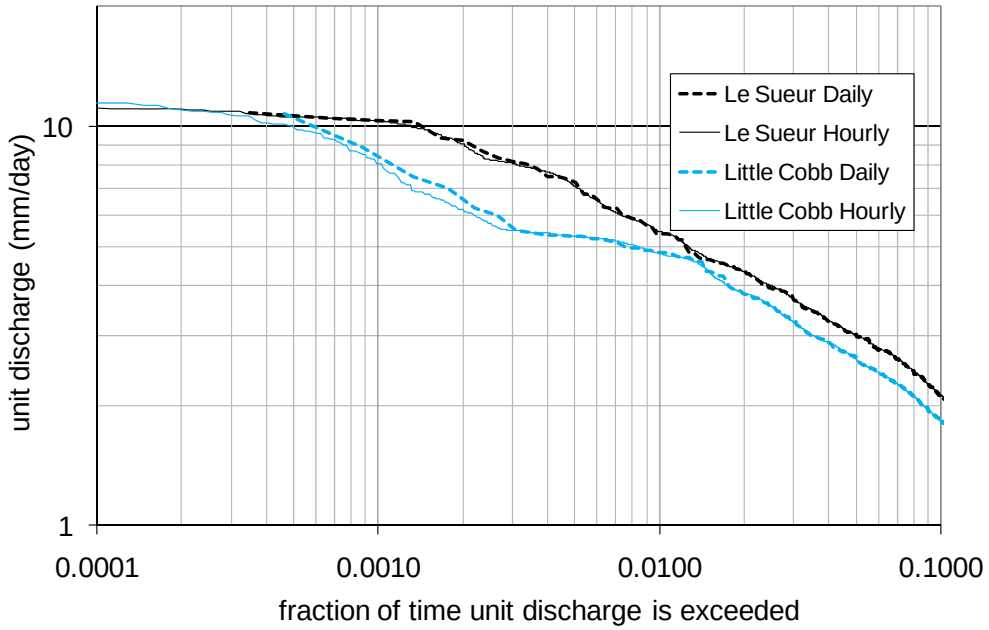

Figure A.6. Flow duration curves at USGS gauge stations developed from instantaneous measurements recorded at hourly timesteps (solid lines) and from the average of the instantaneous hourly measurements for each calendar date (dashed lines). The sensitivity to timestep is minimal, with the daily vs. hourly curves virtually indistinguishable below the 0.003 exceedence probability. Data are from USGS instantaneous data archive for the periods between April 12, 1996 and August 21, 2008 in the case of the Little Cobb and October 2, 1993 and November 29, 2006 in the case of the Le Sueur. Days with incomplete hourly data or zero discharge have been dropped from the analysis.

Spatial Variability and Random Error for Geomorphically Meaningful Flow

The accuracy requirements for the sediment routing model are probably highest for flows that range from just below to just above bankfull. While it is clear that mid-range unit discharges are not highly spatially variable in the basin (see Figure A.6), higher discharges that play a more important geomorphic role are likely more prone to spatial variability. This is primarily because floodplain attenuation of individual hydrographs and an associated downstream decrease in peak unit discharge is expected when discharge exceeds channel capacity. Consequently, it is

important to determine whether the single standardized FDC developed here sufficiently characterizes these geomorphically meaningful flows at all sites in the basin. If downstream changes are significant during high flow, low exceedence probability unit discharges computed from FDC's for the 10 MPCA model nodes should decrease as drainage area increases.

While the bankfull discharge is not precisely known at most locations, field observations indicate that much of the system experienced bankfull or higher flow in June of 2008. Averaging the highest observed June 2008 daily unit discharges for the Little Cobb gauge (3.05 mm/day) and Le Sueur near Rapidan gauge (3.75 mm/day) gives an upper bound for a bankfull unit discharge in the basin of approximately 3.4 mm/day. Equation 4 and the parameters in Table A.2 yield an estimated exceedence probability for this unit discharge of 0.027, indicating that on average, bankfull or higher discharges occur somewhere around 2 to 3 percent of the time within the Le Sueur basin.

We arbitrarily assume that the 97.5^{th} percentile for unit discharge (i.e. that exceeded 2.5% of the time) characterizes this threshold. Presumably, the average for flows above the 97.5^{th} percentile should thus characterize flood flow in the system, and the average for flows between the 95^{th} and 97.5^{th} percentile characterizes a large in-bank flow. Figure A.7 illustrates trends computed for the unit discharge with a 0.975 exceedence probability and for the average of all flows within 2.5% above and below this percentile.

No statistically significant trends are present for the 97.5^{th} percentile unit discharge or for the average of the 2.5% of unit discharges immediately below this level. However, there is a statistically significant ($p = 0.028$) downstream decrease in the upper 2.5% of flows (i.e. for "flood" flow) that represents a decline of approximately 15% across the watershed. The decrease is consistent with floodplain storage causing attenuation of individual hydrographs when flow exceeds bankfull capacity and thus provides corroborative evidence that bankfull exceedence probability is in fact somewhere around 2 to 3 percent. In any case, because the downstream decrease in unit discharge is not significant for most flows and is relatively small (~15%) for flood flows, simply using an average standardized duration curve for unit discharge that does not vary with drainage area is unlikely to introduce significant error in sediment routing computations.

The precision of the estimate is also a question. Using the 10 separate estimates computed at each of the 10 HSPF nodes (i.e. the individual triangles in Figure A.7) and assuming no trend with drainage area, it is possible to develop 95% confidence limits for any of the given statistics. These confidence limits are presented in Table C. 3 for a range of flow percentiles and flow bins. This procedure provides confidence limits of between about ±11% and ±35%, depending on the percentile or bin. Most confidence limits are below ±20%, even for the largest flows considered in this analysis. It is unlikely that the HSPF model incorporates all sources of variability into its results, so the confidence limits presented here should not necessarily be considered definitive. However, given the other simplifications in the sediment routing model, this level of variability is unlikely to significantly bias sediment transport computations.

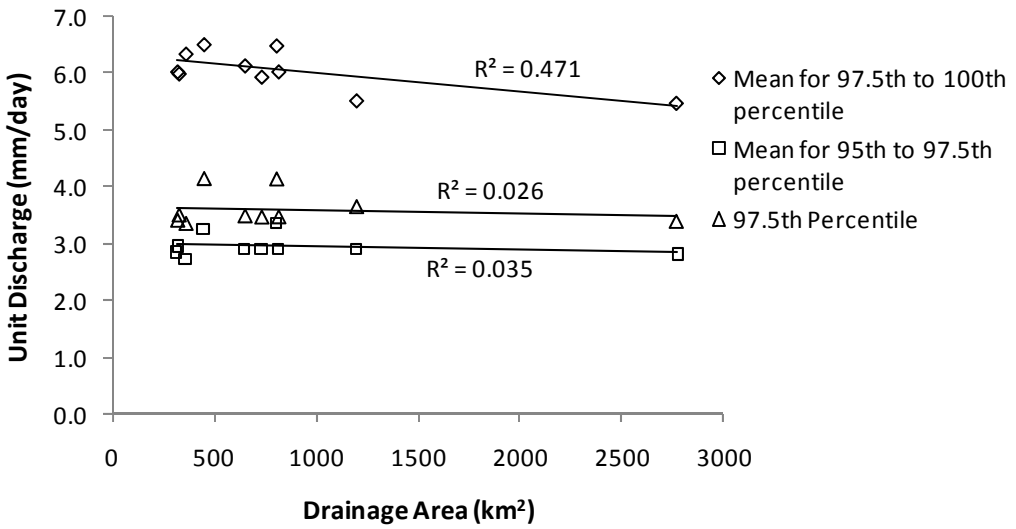

Figure A.7. Trends in geomorphically meaningful unit discharge with drainage area. The 97.5th percentile for unit discharge probably represents unit discharges that result in bankfull or near bankfull conditions. For the 97.5th percentile and for the mean of the 2.5% of unit discharges immediately below this threshold, there are no significant trends. However, there is a statistically significant decrease ($p = 0.028$) in the mean for the upper 2.5% of unit discharges (i.e. those that probably result in out-of-bank flow). The slope of the upper line is -0.00033 mm/day per km².

Table A.3: Confidence limits on various flows computed from results at 10 individual HSPF nodes

unit discharge statistic	average for 10 HSPF nodes (mm/day)	standard deviation for 10 HSPF nodes (mm/day)	95% confidence
Average for entire record	0.60	0.048	±15.5%
Median for entire record	0.20	0.036	±34.8%
95th percentile	2.49	0.143	±11.2%
97.5th percentile	3.61	0.300	±16.3%
99th percentile	5.54	0.331	±11.7%
Average for upper 5%	4.51	0.247	±10.7%
Average for 95th% to 97.5%	2.97	0.198	±13.1%
Average for upper 2.5%	6.06	0.352	±11.4%